12-2018

Modeling, Simulation, and Analysis of Cascading Outages in Power Systems

Wenyun Ju
University of Tennessee, wju1@vols.utk.edu

To the Graduate Council:

I am submitting herewith a dissertation written by Wenyun Ju entitled "Modeling, Simulation, and Analysis of Cascading Outages in Power Systems." I have examined the final electronic copy of this dissertation for form and content and recommend that it be accepted in partial fulfillment of the requirements for the degree of Doctor of Philosophy, with a major in Electrical Engineering.

Kai Sun, Major Professor

We have read this dissertation and recommend its acceptance:

Mingzhou Jin, Fanxing Li, Hairong Qi

Accepted for the Council:
Carolyn R. Hodges

Vice Provost and Dean of the Graduate School

(Original signatures are on file with official student records.)

Modeling, Simulation, and Analysis of Cascading Outages in Power Systems

A Dissertation Presented for the

Doctor of Philosophy

Degree

The University of Tennessee, Knoxville

Wenyun Ju

December 2018

DEDICATION

This dissertation is dedicated to my beloved parents, Chunxi Ju and Jinhua Gong, my elder sisters, Shujuan Gong and Wenxia Ju, whose loves and encouragements make it possible for me to finish this work.

ACKNOWLEDGEMENTS

Time flies in the blink of an eye. I can remember clearly the first day I came to UTK in 2014, before which to pursue a PhD degree in the United States was beyond my imagination. However, the story was happening. As a fruit needs not only sunshine but cold nights and chilling showers to be ripe, a character needs not only joys but trials and difficulties to become mellow. I am becoming more mature and thorough over this intensive period. Today is the day: writing this note of thanks is the finishing touch on my dissertation. It has been a period of intense learning for me, not only in the research area, but also on a personal level. Writing this dissertation has had a big impact on me. I would like to reflect on the people who have supported and helped me so much throughout this period. I would like to express my thanks to those who helped me with various aspects of conducting research and writing this dissertation.

Special mention goes to my advisor, Dr. Kai Sun, for the patient guidance, encouragement and advice he has provided throughout my whole PhD period. I have been extremely lucky to have a supervisor who cared so much about my work, and who responded to my questions and queries so promptly. Without his guidance and persistent help this dissertation would not have been possible.

Similar, profound gratitude goes to Dr. Fangxing “Fran” Li, Dr. Hairong Qi, and Dr. Mingzhou Jin for their times and efforts in serving as the members of my dissertation committee.

I would especially like to thank my dear friends Miss Yajun Wang, Mr. Qingxin Shi, and Miss Siqi Wang. This small group including me is full of energy and passion. Thank you for your company.

I also would like to thank Dr. Weihong Huang, Dr. Fengkai Hu, Dr. Chengxi Liu, Dr. Bin Wang, Dr. Nan Duan, Dr. Junjian Qi, Dr. Lin Zhu, Miss Yinfeng Zhao, Dr. Zheyu Zhang, Mr. Yichen Zhang, and Dr. Wenxuan Yao, who gave much support to my research and PhD life.

Moreover, I would like to express my special thanks to other students and scholars in our group, Dr. Yongli Zhu, Dr. Rui Yao, Mr. Denis Osipov, Mr. Xin Xu, Mr. Yang Liu, Mr. Tianwe Xia, Mr. Guoqiang Zu, Mr. Yichen Guo, and Dr. Dongsheng Cai for being supportive to my research.

In addition, special thanks go to my friends Miss Ling Jiang, Dr. Chongwen Zhao, Mr. Shuoting Zhang, Dr. Bo Liu, and Mr. Ren Ren.

A special thank goes to Angie, you make me realize that life is too short to wait.

Finally, but by no means least, thanks go to the Center for Ultra Wide-Area Resilient Electric Energy Transmission (CURENT) for the support under the Engineering Research Center Program of the National Science Foundation and the Department of Energy under Grant No. EEC-1041877. I would like to express my sincere gratitude for providing excellent materials, logistical and human conditions and creating a loving and friendly atmosphere for conducting research.

Now it is the time to create a new story for my life and start living it.

ABSTRACT

Interconnected power systems are prone to cascading outages leading to large-area blackouts. Modeling, simulation, analysis, and mitigation of cascading outages are still challenges for power system operators and planners.

Firstly, the interaction model and interaction graph proposed by [27] are demonstrated on a realistic Northeastern Power Coordinating Council (NPCC) power system, identifying key links and components that contribute most to the propagation of cascading outages. Then a multi-layer interaction graph for analysis and mitigation of cascading outages is proposed. It provides a practical, comprehensive framework for prediction of outage propagation and decision making on mitigation strategies. It has multiple layers to respectively identify key links and components, which contribute the most to outage propagation. Based on the multi-layer interaction graph, effective mitigation strategies can be further developed. A three-layer interaction graph is constructed and demonstrated on the NPCC power system.

Secondly, this thesis proposes a novel steady-state approach for simulating cascading outages. The approach employs a power flow-based model that considers static power-frequency characteristics of both generators and loads. Thus, the system frequency deviation can be calculated under cascading outages and control actions such as under-frequency load shedding can be simulated. Further, a new AC optimal power flow model considering frequency deviation (AC-OPFf) is proposed to simulate remedial control against system collapse. Case studies on the two-area, IEEE 39-bus, and NPCC power systems show that the proposed approach can more accurately capture the propagation of cascading outages when compared with a conventional approach using the conventional power flow and AC optimal power flow models.

Thirdly, in order to reduce the potential risk caused by cascading outages, an online strategy of critical component-based active islanding is proposed. It is performed when any component belonging to a predefined set of critical

components is involved in the propagation path. The set of critical components whose fail can cause large risk are identified based on the interaction graph. Test results on the NPCC power system show that the cascading outage risk can be reduced significantly by performing the proposed active islanding when compared with the risk of other scenarios without active islanding.

Index Terms—Blackout; cascading outages; multi-layer interaction graph; interaction graph; key link; key component; dynamic load flow; AC-OPA; DC-OPA; AC optimal power flow considering frequency deviation; Northeastern Power Coordinating Council (NPCC) Power System; under-frequency load shedding.

TABLE OF CONTENTS

LIST OF TABLES

LIST OF FIGURES

CHAPTER ONE

INTRODUCTION AND BACKGROUND INFORMATION

1.1 Introduction

Power system is one of the most complex systems in the modern society. The modern power system is approaching to the critical operating limits in the environment of market. With the increasing of load demand, high capacity and long transmission networks are widely used to meet the requirement. With the integration of renewable energies such as wind and solar, the uncertainty, intermittence bring bigger challenge to the operation of power system. Therefore, a random outage or local outage may propagate and thus cause large-scale blackout eventually [1].

Large blackouts, although infrequent, are costly to society with estimates of direct costs up to billions of dollars. For example, a blackout happened in Aug. 14, 2003 in areas of Midwest and Northeast United States, and Ontario in Canada. 50 million people are affected and the total cost of it is around 10 billion dollars [2]. Some other indirect costs such as the failures of communications, natural gas, transportation, water supply and social disruptions are also caused. The influences of large blackouts in the Unites States with more than 50,000 customers or 300 MW load loss are analyzed based on the data sets obtained from North American Electric Reliability Corporation (NERC). It is summarized in Table 1-1.

From Table 1-1, the main reasons of the large blackouts are either extreme natural events (hurricanes, ice storms, etc.) or cascading outages. Table 1.2 gives descriptive statistics for these data with and without the smaller events.

Table 1-1. The 15 Largest North American Blackouts and Their Causes, 1984-2006.

	Date	Location	MW	Customers	Primary cause
1	14-Aug-2003	Eastern U.S., Canada	57,669	15,330,850	Cascading outage
2	13-Mar-1989	Quebec, New York	19,400	5,828,000	Solar flare, cascade
3	18-Apr-1988	Eastern U.S., Canada	18,500	2,800,000	Ice storm
4	10-Aug-1996	Western U.S.	12,500	7,500,000	Cascading outage
5	18-Sep-2003	Southeastern U.S.	10,067	2,590,000	Hurricane Isabel
6	23-Oct-2005	Southeastern U.S.	10,000	3,200,000	Hurricane Wilma
7	27-Sep-1985	Southeastern U.S.	9,956	2,991,139	Hurricane Gloria
8	29-Aug-2005	Southeastern U.S.	9,652	1,091,057	Hurricane Katrina
9	29-Feb-1984	Western U.S.	7,901	3,159,559	Cascading outage
10	4-Dec-2002	Southeastern U.S.	7,200	1,140,000	Ice/wind/rain storm
11	10-Oct-1993	Western U.S.	7,130	2,142,000	Cascading outage
12	14-Dec-2002	Western U.S.	6,990	2,100,000	Winter storm
13	4-Sep-2004	Southeastern U.S.	6,018	1,807,881	Hurricane Frances
14	25-Sep-2004	Southeastern U.S.	6,000	1,700,000	Hurricane Jeanne
15	14-Sep-1999	Southeastern U.S.	5,525	1,660,000	Hurricane Floyd

Table 1-2. Descriptive Statistics for the NERC Disturbance Data, 1984–2006.

	All events ≥0 customers/MW	≥300 MW	≥50k customers	≥300 MW or ≥50k customers
Total number of events	856	278	321	438
Number of blackouts	547	258	304	406
Number after filling missing data	547	307	382	419
Number after adjusting for growth	547	317	373	413
Mean size in MW	524	1508	947	987
Median size in MW	86	634	300	385
Standard deviation in MW	2396	4034	3648	3285
Mean size in customers	164,483	321,984	430,585	317,372
Median size in customers	1323	85,228	149,500	94,643
Standard deviation in customers	689,815	1,106,958	1,075,888	939,638

From the reports of those blackouts [1], [2], and [3], cascading outage is a key factor leading to a large blackout. According to NERC, a cascading outage is "the uncontrolled successive loss of system elements triggered by an incident at any location [4]-[7]." Actually, sometimes the cascading outage is initiated by more than one disturbance. Some cascading outages may stop before they bring large influence to the system, while some of them bring disastrous results. According to N-1 or N-2 criterion, electric power systems are generally designed withstand single or double failure without causing the violation of any operating limit. Nevertheless, other possible outages, such as human errors or hidden failures in protection relays may enlarge the propagation of outages and lead to a cascading outage finally. Generally speaking, the component outages will cause the redistribution of the power flow and then cause the overload of other components even dynamic instability problems.

Cascading outage involves a large amount of complex mechanisms, which makes it more difficult to understand cascading outage fully. This subsection gives an overview on cascading outage from different perspectives and highlights its challenge for the analysis and modeling of cascading outages.

1.1.1 Major Causes of Cascading Outages

Basically, the causes for cascading outages can be divided into four categories [8]:

- Nature disasters: Fire, lighting, wind/rain, ice storm, hurricane, Tornado, earthquake.
- Human activity: Operator error or inappropriate actions, or fail to take actions, inappropriate setting for protection devices, intentional attack.
- Unexpected component failure: Equipment failure or hidden failure.
- System failures: Distance relays trigger the transmission line due to overcurrent or under-voltage, voltage collapse, abnormal excitation in generators, abnormal speed in generators, generators tripped by under-

frequency, generators tripped by under-voltage, generator tripped by out-of-step, insufficient reactive power support, small signal instability.

The first three categories are common outages that initiate the events, whereas the fourth category is failures that commonly enlarge the cascading. It is almost impossible to prevent the happen of the outages in the first and second categories with modern technology. However, most cascading outage blackouts involve the dependent outages in the third and fourth categories.

1.1.2 Procedure of Cascading Outages

According to [9], basically, the procedure of cascading outage can be divided into two phases, which are remarked by slow phase and fast phase.

For the slow cascade phase, the outages propagate slowly and have little influence on the stability of power system. The time interval for this phase ranges from several minutes up to several hours. Most outages in this phase are belonging to common problems and the operators cannot identify them easily. Thus the operators miss the chance to prevent the propagation of outages. Besides, some hidden failures may be exposed during this phase, which trigger some transmission lines and components [10].

During the fast cascade phase, power system becomes unstable. With the redistribution of power flow, the overloaded transmission components are triggered in a short time, they may cause voltage collapse, frequency collapse, and oscillations. Meanwhile, the dynamic instability may trip the generators, which lead to further load and generation imbalance and exaggerate the dynamic instability. It is almost impossible for systems operators to stop the propagation of the cascading during this phase manually. The time interval for this phase ranges milliseconds to tens of seconds [9]. Generally, the overloaded components such as transmission lines can still work for several hours under over-load conditions, and they can be reclosed if no other fault is found. However, when a large power swing happens in power system, the settings of distance relay of zone 2 or zone 3 may trip the transmission line with short time delay, and they will be acting so quickly that the system operator has no time to respond and reclose the line or

stop the cascading. Thus, the cascading starts tripping like a domino and eventually cause a large blackout.

Cascading phenomena are complicated because of the diversity of failures and the many different mechanisms by which failures can interact. There are varying modeling requirements and timescales (milliseconds for electromechanical effects and tens of minutes for voltage support and thermal heating). Combinations of several of types of failures and interactions can typically occur in large blackouts, including cascading overloads, failures of protection equipment, transient instability, forced or unforced initiating outages, reactive power problems and voltage collapse, software, communication, and operational errors. Therefore it is very difficult to analyze it through conventional power system analysis approaches and models. Many models and approaches have been proposed to try to consider those mechanisms [11-94]. Some models and approaches are utilizing complex network theory to investigate the relationship between the propagation of cascading outages and topological structure. Some are using stochastic approaches to consider the uncertainties in a cascading outage. Some are modeling dynamics of system to involve machine, voltage and frequency issues. High-level statistical models have also been proposed to estimate the average cascading outage propagation and blackout distribution sizes, which can provide useful suggestions for power system long-term planning. Interdependent infrastructures are modeled to analyze the interactions between power grids and cyber networks and study the propagation of cascading outage between different networks.

1.2 Modeling, Simulation, and Analysis of Cascading Outages

A large amount of models and approaches has been proposed in order to model, simulate, and analyze the cascading outages [11-94]. However, no existing model or approach can capture all the mechanisms during the cascading outage. Each model or approach can only focus on one or several aspects, while the information of the overall phenomenon is still needed in the simulation. In this

subsection, a brief review and summary of the state-of-art cascading outage analysis models and methodologies will be presented. According to their different perspectives and characteristics, those models and approaches can be divided into six categories:

- High-level statistic approaches
- Stochastic simulation approaches
- Quasi-dynamic and dynamic simulation approaches
- Network theory approaches
- Interdependent approaches
- Other approaches

Note that each model or approach may have characteristics which are involved in other categories. The classification in this thesis is based on its main feature and characteristic. This is just a rough classification and there are other classifications.

1.2.1 High-Level Statistic Approaches

This type of approaches investigated the process of cascading outage without considering the physics of power systems. For example, they may neglect the structure of power systems, times between different outages, and the diversity of power system components and interactions. They are very useful to understand cascading outage in more detailed models.

1) *CASCADE Models*

CASCADE model is an analytically tractable model based on load of the component [11]. It assumes a random initial load on all identical components and a given disturbance load on each component to initiate cascading. Some components may fail when load exceeds a certain threshold, where the load of other components will be redistributed, thus forming a cascading process. The cascading only stops when no overloaded component exists or the whole system fails. The redistributed formulas are much simpler when compared with detailed models that simulate detailed cascading failure mechanisms such as power

flows. It is easier to obtain the total number of component outages as well as the probability distribution of the blackout sizes. The model shows how system loading affects the risk of a cascading failure [12]. When there is low load level, the tail part of component failures is approximately exponential. The probability of a large cascading outage is also low. However, when a critical loading level is exceed, the distribution of the component outages follows the power law and the risk of a large blackout increases significantly. This model is good for understanding the general property of cascading outages but it ignores all physical properties of power systems.

The above model is modified further and applied to analyze several factors related to cascading outages. The cascading motor stall has been analyzed with the CASCADE model in [13]. Reference [14] showed a high risk on voltage collapse when a failure triggered a cascade of motor stalling. [15] has analyzed the power system reliability by using a modified CASCADE model, the time of outage propagation is also considered in [15].

2) *Branching Process Models*

Branching process model can be regarded as an improved CASCADE model and it is widely used in the theory of probability [16]. This model has been used in many areas such as Y chromosome transmission in genetics disappearance of surnames in genealogy. [17] first introduced this model to the analysis of cascading outages. Based on them, some improvements have been made in [18-20], they mentioned the importance for applying the branching process models. More recently, some new applications based on such models can be found in [21], and [22].

Each individual component outage affects the outages in the next stages interdependently according to a given distribution in the branching process model. The results in [23] have shown that the probability distribution of outages from a branching process can match with the simulated CASCADE model as well as the historical data. The computation speed to estimate the propagation and distribution of the size of blackout is faster by using the branching process model.

[24] has investigated the influence of topology on the average propagation of cascading outages in power system with this model. A novel and systematic approach to discretize the data of load shed has been introduced by [25] and the Galton-Watson branching process with a Poisson offspring distribution can be used. Further, a multi-type branching process [26] has been applied to analyze the statistics and interdependencies of cascading outages. The probability distribution of load shed, the isolated buses and their conditional largest possible total outages can be predicted by this model. This model needs few samples of cascading outages to realize relatively accurate estimation but the disadvantage of this model is that it lacks detailed mechanisms of the cascading outages in power systems. It can only estimate the blackout size distribution of cascading outage. From the perspective of operation, real time prediction and mitigation of cascading outages cannot be realized with this model.

3) *Interaction Model*

Reference [27] proposes a power system's interaction model that is constructed based on a database of cascades from either historical events or simulations. That interaction model extracts key information on cascading outages of the power system, quantifying how interactions between component failures influence the risk of cascading outages and capturing general propagation patterns of cascades. Thus, scenarios of cascading outages can be simulated and analyzed quickly and effectively in a time-intensive environment only using that interaction model for prediction of their propagations and mitigation actions without need to conduct time-consuming simulation of the original power system model. Thus, the interaction model if available for a power system can readily fit into real-time operation for operators' situational awareness and decision support.

1.2.2 Stochastic Simulation Approaches

A cascading outage can be described by a sequence of deterministic and stochastic events. For example, based on simulations, the features of cascading

outages can be reproduced basically if we tune the parameters affecting the simulation for well-studied power systems. However, it is another matter entirely to be able to predict or simulate the events of a cascading outage before it happens. However, cascading outage will rarely proceed as you expect. Due to the large uncertainties that initiate and exacerbate the cascading, the stochastic simulation, also known as probabilistic simulation is necessary since it can try to consider all possible factors. Moreover, some factors such as the misoperation because of human error and transmission lines that contact over grown trees due to relatively high current flow are very hard to be modeled in the simulation. It is thus essential to use stochastic approaches to simulate more possible events.

1) *Markov Chain Models*

A Markov chain is a type of stochastic process used to describe a system that follows a chain of linked events [28]. It is utilized to model the stochastic factors in cascading outage of a power grid, such as hidden failure or misoperations. The result of this model can be used as an evaluation of overall probabilities of all states that depicts the cascading outage. The model can normally have a large size.

In reference [29], a stochastic Markov chain model has been introduced. The model was based on power flow redistribution. It took into account the uncertainties in the load setting, generation and line flows. The model also captured the cascading events with regard to real time signals. The critical components have been identified using the metrics provided. Reference [30] presented a network-based Markov chain model to study the propagation dynamics of the entire power networks. Robustness of the power network has been analyzed through the model. An extended Gillespie method was adopted in the model [31]. It also showed that small-world network structure would propagate cascading outage more widely and rapidly compared with a regular power network. A Markovian tree-based multi-timescale cascading outage simulation model has been provided in [32], aiming at risk assessment of cascading outage. The paper also proposed a novel forward-backward

Markovian tree search scheme based on a risk estimation index. In [33], the author introduced a continuous-time Markov chain approach modeling the system dynamics. The model considered loading level, error in transmission-capacity estimation, and constraints in performing load shedding. It also allowed real-time prediction of blackout evolution probability. Recently, an influenced graph model using Markovian chain was described in [34]. Large amounts of data from cascading outage simulations were synthesized into a Markovian network model. The distribution of the cascading outage results achieved from this model matched those from cascading outage simulators. A methodology based on this model has been demonstrated to identify the probability of risk when a component was upgraded in the power system.

2) *PRACTICE Models*

A useful stochastic simulation approach of cascading outages has been proposed in [35]. In this model, “single-path” mode and “multi-path” mode are used. Single-path mode allows uncertainties only relevant to the initial events, after which the system will behave “as expected” during the cascading. Multi-path mode can simulate uncertainties and the response from protection systems, through the whole procedure during the cascading. The hidden failure probabilistic model, the overcurrent relay probabilistic model and the event tree-based probabilistic cascading approaches was adopted in the techniques. The model was tested on Italian EHV transmission grid and a comparison was made with a detailed overload-based dynamic time domain simulator. It showed that the results obtained from the model and the dynamic time domain simulator can match well with each other at least for the slow cascade phase [36].

1.2.3 Quasi-Dynamic and Dynamic Simulation Approaches

Dynamic simulation approaches are similar to conventional methodologies that focus on power system dynamic characteristic analysis, while the difference is that conventional methodologies are hard to simulate interactions under multi-contingency cases during the cascading outage. New dynamic simulation models

perform well on capturing some specific system dynamics during the cascading. In addition, most mechanisms can be included in dynamic simulation models under a variety of outages so that a relatively accurate prediction can be made. However, due to the large amount of details to be taken into consideration, the computation speed will be challenging. Right now, such models will mainly contribute to deeply understanding the cascading outage mechanisms rather than real time prediction and analysis for industrial utilization.

1) *OPA Models*

The researchers from Oak Ridge National Laboratory (ORNL), Power System Engineering Research Center of Wisconsin University (PSerc) and Alaska University (Alaska) proposed this ORNL-PSerc-Alaska (OPA) model [37]. It is DC power flow-based model. This model contains two parts: fast dynamic process and slow dynamic process. Slow dynamic process is utilized to simulate the evolution of power gird such as generation growth, load growth and transmission capacity limits upgrade. The fast dynamic process is often used to simulate outages and cascading overloading. In this model, a re-dispatch model DC-OPF based on linear programing is used to adjust the generation and load. The cost function has been taken into consideration to avoid unnecessary load shedding. This model described a simplified dynamic process of cascading outages and can be used to investigate the self-organization of power systems. This OPA model was validated on a 1553-bus WECC network and the simulation results were compared with historical WECC data with an acceptable approximation [38]. The disadvantage of this model is that it cannot provide an accurate simulation on real outages of power systems and it only focus on the limited parts of cascading outages such as overloading.

An improved OPA model [39] has been proposed to improve the limitations found in the original model. This improved OPA model has considered more important factors such as dispatching, communication, protection relay, planning, and operation mode. Two indices have been proposed to quantify the cascading outage risk from the perspective of statistics, i.e. Value at Risk (VaR)

and Conditional Value at Risk (CVaR). Then this model was validated on the Northeast Power Grid in China.

Another AC OPA model has been proposed by [40]. This model contains two dynamic processes: fast dynamics and slow dynamics. Fast dynamics involve series blackouts. Slow dynamics can reflect the time evolution of power systems. This novel AC OPA model can be used to analyze the voltage stability of power systems and it is tested on the IEEE 118-bus power system and the results showed that the ratio of total load to system transmission capacity can explain SOC of power systems. This model has been modified in [41] further and considered slow process such as tree contact and line outages due to line heating into the simulation of cascading outages. Utility vegetation management was also considered in this model.

2) *Multi-Timescale Quasi-Dynamic Model*

The multi-timescale quasi-dynamic model has been proposed in [42]. This model enabled the consideration of different timescales involved in the process of cascading outages which cannot be simulated by the existing approaches. The simulation of cascading outages with representation of time evolution can be realized. Three categories of timescales: short-term scale, mid-term scale, and long-term scale are modeled. Meanwhile, this model can consider some dynamics such as load variation and generation excitation protection. An improved re-dispatch model has been proposed because that transmission loading relief (TLR) and re-dispatch normally took 10–30 min [43]. The above improvements enabled more accurate simulation of cascading outages. This model was tested on IEEE 30-bus power system to study the role of generation protection. The model was also demonstrated on a reduced 410-bus US-Canada northeast power grid. The results showed that the simulated event can match well with the blackout event happened in 2003.

3) *Manchester Model*

Manchester model was proposed by the University of Manchester [44]. It is based on AC power flow. A wide variety of mechanisms related to cascading outages such as hidden failures, generator instability, under-frequency load shedding (UFLS), emergency load shedding and re-dispatch of active and reactive power were considered in this model. Monte Cardo simulation was used for the risk of assessment of cascading outages with this model. Other research [45-47] extended the Manchester model to study the mitigation strategies for cascading outages and assess the cost of blackout.

4) *TRELSS Model*

Transmission Reliability Evaluation of Large Scale Systems (TRELSS) is another commercial platform for the simulation and analysis of cascading outages [48]. It is developed by EPRI and Southern Company Services. This model can simulate the cascading outage as a sequence of quasi-steady state system conditions based on AC power flow which are triggered by the tripping outages. The actions of breakers have been modeled by the Protection and Control Group (PCG). The model was tested on Western Interconnection power system [49] to identify the most severe initial outages.

5) *ASSESS Model*

ASSESS is developed by Reseau de Transport d'Electricite (RTE) in France and it is a commercial platform for the simulation and analysis of cascading outages [50]. This platform is quite flexible for letting many uncertainties to be considered. Four blocks have been provided by this model such as quasi-steady state simulator that could model dynamics of systems [51], security-constrained AC optimal power flow [52], time-domain simulator that could model many control actions such as governors and zone 3 protection relay [53], and the access to some tools for the statistical analysis of samples of cascading outages. ASSESS provided a wide range of models including sequences of events, protection settings, line ratings, fault clearance time, etc.

The disadvantage of this model is that it requires a large amount of data and the computation speed is still challenge with this platform.

6) *Dynamic PRA Model*

A two-level dynamic probabilistic risk assessment (PRA) model was introduced in [9]. The proposed model divided the process of cascading outage into two phases and two different models were used in the two phases. The influences some factors such as variation of cross-border power flows, maintenance and shut-down of power plants, and the penetration of wind power on cascading outages were investigated. This model was tested on New England Test System (NETS) and New York Power System (NYPS) 69-bus test system. It was found from the results that the thermal effects can contribute to cascading outages.

An improved PRA model was introduced in [54] further. Two decomposition models were used to analyze the fast phase and slow phase of cascading outages, respectively. The frequency and the influence of severe cases can be estimated with this model. The scenarios can be classified with a clustering method so that the dynamic analysis was manageable from a computational perspective. The dynamic models of generators were considered in [55].

7) *COSMIC Model*

A novel nonlinear dynamic model for the simulation of cascading outages has been proposed in [56]. It is called Cascading Outage Simulator with Multiprocess Integration Capabilities (COSMIC). COSMIC was able to simulate power system with a set of hybrid discrete and continuous differential algebraic equations, as well as protection systems and machine dynamics. The model involved a wide variety of mechanisms including rotating machines, exciters, governors, power flows using nonlinear power flow equations, load voltage responses, discrete changes (e.g. components failure and load shedding) and etc. COSMIC used a recursive process to compute the differential algebraic

equations, which represented various mechanisms. Four kinds of loads, i.e. constant power (P), constant current (I), constant impedance (Z), exponential (E), or any combination of them (ZIPE) have been modeled [57]. The results obtained from COSMIC model were compared with that from PowerWorld on IEEE 9-bus power system [58]. Another simulation has been made and the results were compared with a simple dc power-flow QSS model. The cascading processes had good consistency during the early stage between two models, while the simulation was substantially different during later stages.

1.2.4 Complex Network Theory Approaches

Many literature and researches focus on the propagation of cascading outage in complex networks that is partially inspired by the propagation of failures and congestion in Internets [59], [60], [61]. From the statistically results, it is found that power girds have the characteristics of power laws and criticality, which suggests the strong connection between the statistical characteristics of the topology of the network and the dynamics of cascading. The models consider flows of discrete packets that are injected and removed from all nodes and transfer the packets along the shortest distance paths between any two nodes. The criticality of links or nodes can be quantified by the concept of "betweenness". It is proportional to the number of shortest distance paths through the link or node. Based on complex network theory, these models abstract the power grid as undirected network or directed network which is consisting with vertexes and edges to study the statistical characteristics of power grids. These models are very different from the power system models. Cascading phase transitions and the vulnerability of network have been studied in [62], [63], and [64]. It was found that the typical power girds are small-world networks in [65]. Later, some researches have studies power grids based on complex network theory by considering more properties and characteristics of power girds. By considering the electrical distances in power systems, it was found that the power systems have a scale free structure [66]. Topological graph concept has been proposed that was more consistent with the patterns of power

system generation and load [67]. An “influence model” has been introduced in [68]. It is a tree network that representing the influences between idealized components abstractly. Components can be failed or operational according to a Markov model that represents both internal component failure and repair processes and influences between components that cause failure propagation. A Markov model has been proposed for nodal components in [69], it was found that the outages can propagate along the transmission lines of power networks with a fixed probability.

1.2.5 Interdependent Approaches

Analysis of interdependent networks has been done for many years in various areas [70]. With the increased coupling between power grid and cyber or communication network, the risk between the interdependent networks also increases. The possible outages of control systems connecting to the cyber networks such as SCADA can contribute to the propagation of cascading outages between interdependent networks. At the same time, cyber attack is happening frequently in the environment of smart grid [71]. The typical event happened in Ukraine in 2015 [72]. The attack on the cyber network caused the SCADA distribution management system to be controlled remotely and some substations were disconnected for several hours. This attack brought much influence to many areas in Ukraine. With the coupling between power grid and cyber network, one outage in cyber network may propagate to power grid and cause the devices and equipment in power grid to be out of function. Risk assessment for interdependent networks has been studies in some researches [73-77]. It is still a big challenge since many mechanisms are involved from power grid and cyber network.

1) *Complex Network-Based Interdependent Models*

In real world, there are many interdependent infrastructures. We are familiar with some of them such as economic, transportation, and Internet networks. Complex network theory has been widely used in the study of these

areas [78-79]. The coupling between power grid and cyber network has caused much attention [80]. Some researchers begin to investigate the interdependence between power grid and cyber network with complex network theory.

An interdependent model has been introduced in [81], which was used for the analysis of robustness of interdependent networks with the propagation of cascading outages. This model was tested on a power grid and an Internet network involved in Italy blackout happened in 2003. The results showed that by removing a set of critical nodes, the cascading outage would be triggered in the two interdependent networks and caused a complete fragmentation finally. An analytic solution can be obtained with this model. An improved interdependent model was proposed in [82], it was used to analyze the robustness of power gird with random multiple support-dependence relations. The test results showed that the similar conclusion can be obtained from the interdependent networks when compared with that from the single networks. An interdependent model was introduced in [83], it was used for designing some strategies to mitigate the propagation of cascading outages in interdependent networks. The model was tested on a power grid and an Internet network involved in Italy blackout happened in 2003. It was found that the cascading outage in interdependent networks can be suppressed by selecting a small number of autonomous nodes. The above models are useful to study the general and overview property of interdependent networks but they fail to consider properties of power gird such as Kirchhoff laws. Some electrical properties have been considered in the coupling model proposed in [84], and the model considered power grid and the supporting Control and Communication Network (CCN). For power gird, substation and generator were considered. For CCN, the router was considered. The minimum number of nodes from both networks was calculated whose fail can totally destroy the interdependent networks. A new interdependent model was proposed to involve there networks, i.e. power grid, communication network, and interdependency network [85]. A sensitivity analysis was performed to evaluate the mitigating method in the model. More recently, a more

comprehensive model has been proposed in [86]. The model used a mesh network that considered power system characteristics. Moreover, bidirectional links including data uploading and command downloading channels were modeled. These links were supposed to connect all cyber network nodes as well as a corresponding physical node in power grids. The fragility of the coupling model has been studied under various cyber-attacks, such as denial-of-service (DoS) attacks, replay attacks and false data injection attacks. Load shedding and relay protection have been involved in the model.

2) *Flocking-Based Hierarchical Cyber-Physical Models*

A hierarchical cyber-physical multi-agent model of smart grid based on flocking theory has been presented in [87-88]. The model considered dynamic nodes (generators in this model), PMU and local cyber-controller. The frequency, phase angle and other related parameters were involved in the generators which were regarded as physical parts. PMU and local cyber-controller served as cyber elements. The model concentrated on control strategies for robustness and resilience of a coupling system. The potential performance improvement has been tested using New England 39-bus power system with various faults and communication delays.

3) *Inter-Dependent Markov Chain Models*

A probabilistic cascading outage analysis framework was provided by the Inter-Dependent Markov Chain (IDMC) model to study the effects of interdependencies among power grid and physical networks. The IDMC was introduced by [89] and it demonstrated that interdependencies between two systems can affect each other on distribution sizes of outages significantly. The results also showed that systems with exponentially distributed outages sizes tend to be less robust as evidenced by the power-law distributed outage sizes for the two networks. It assumed that the communication network was more vulnerable when an outage occurred, which would increase the probability of

outage in power grid. It was also found that when power system components failed, it may trigger cyber networks as well with a given probability.

1.2.6 Other Approaches

1) *Potential Cascading Models*

Physical and Operational Margins (POM) is based on AC power flow. The Potential Cascading Models (PCM) is an integrated function of POM [90]. With the initial events, the following events can be simulated with this model. For selecting the initial events, cluster approach was used to select the N-1 or N-2 contingencies. This model was tested on US 2007 Eastern Interconnection model with summer peak load. The previous manually analysis was consistent with the result obtained. And some unidentified potentially cascading-initiating possibilities were found. The model used the same data to test remedial actions in [91]. The remedial actions such as active and reactive power dispatch, phase-shifter adjustment, and transformer tap change, emergency load shedding, line switching, and reactor and capacitor switching were applied at each stage during the process of cascading outage until the propagation of cascading outage has been fully mitigated [92]. It showed that all identified potential cascading outage can be stopped using the proposed remedial actions.

2) *Historical Data-Based Models*

The main purpose of historical data-based models was to reproduce the history blackout events with accurate approximation. The models can be modified if there is obvious mismatch between the real disturbance data and reproduced results. This model would be very helpful for deeply understanding the blackout and cascading outages. An event was simulated and reproduced by using Electric Power Research Institute (EPRI) ETMSP models [93]. The tested event happened on August 10, 1996, the location is in western North America. Around 7.49 million people were affected with loss of 30,390 MW of load. In this study, the standard WSCC dynamic data was used to reproduce the simulation result for this event, however, the result was far away from the real data. Some

modifications were made on the data and models and then the simulation results could match well with the real data. Many factors that contribute to cascading outages need to be considered in the simulation and analysis of cascading outages. However, historical data-based models may not be the best models to analyze the cascading outage.

3) *Hidden Failure Models*

Hidden Failure model has been proposed in [94] and hidden failure plays important role to the propagation of cascading outages. With the propagation of outages, there will be overloaded line in the power system and the lines connecting to the overloaded line are exposed to the unexpected tripping. Generally, hidden failure model is based on DC power flow. The influences of critical factors such as hidden failure probability function, spinning reserve capacity, system load level, and power flow distribution were investigated. Critical protection relays in the power system can be identified by fast simulation and random search. The model was tested on WSCC 179-bus power system with mitigation approaches and risk assessments being studied.

The comparisons between different models and approaches are summarized by Table 1-3 [95].

Table 1-3. Comparison of the Models and Approaches of Cascading Outages.

	Models	**Advantages**	**Disadvantages**
High-Level Statistic Approaches	CASCADE Models	Failure probability is related to load level.	Ignores all details of cascading.
	Branching Process Models	Can be regarded as an improved CASCADE model. Consider each failure component from	
	Interaction Model	Quantify how interactions between component failures. Probabilistic method to generate new samples of cascading outages.	
Stochastic Simulation Approaches	PRACTICE Models	"Single-path" mode and "multi-path" mode introduced. Event-tree-based approach adopted.	Fail to consider dynamic instability and cascading details.
	Markov Chain Models	Non-locally propagation illustrated. Enable quantitative risk assessment. Simple and tractable.	

Table 1-3. Continued.

	Models	Advantages	Disadvantages
Quasi-Dynamic and Dynamic Simulation Approaches	OPA Models	Take into consideration the effects of dispatching, automation, communication, relay protection, operation mode and planning. Tree contact, failure of lines due to line heating, and UVM modeled.	Slow simulation. Detailed power system data required.
	Multi-timescale Quasi-Dynamic Model	Employ quasi-dynamic approach. Approximate time evolution considered. Improved re-dispatch simulation.	
	Manchester Models	AC power flow adopted. Monte Carlo methods are applied to risk assessment.	
	TRELSS Model	Take into account actions of breakers. Voltage problems modeled using quasi-steady state AC power flow.	
	ASSESS Model	Security-constrained AC optimal power flow provided. Using quasi-steady state simulator to model dynamics of system. Modeling controls in system through full time-domain simulator.	
	Dynamic PRA Model	Two levels of cascading outage simulated using two different models.	
	COSMIC Model	Consider non-linear dynamic mechanisms. Various load and relay modeled.	
Complex Network Theory Approaches	Topological Models	Quickly discover the unexpected emergence of collective behavior.	Lack of electrical features of power systems.
Interdependent Approaches	Complex Network-Based Interdependent Models	Interdependencies depicted. Computer and cyber risks considered.	Difficult to validate. Detailed mechanisms ignored.
	Flocking-Based Hierarchical Cyber-Physical	Frequency, phase angle, and other related parameters involved. Control strategies provided.	
	Inter-Dependent Markov Chain Models	Enable a system-level prediction with tractable details of the system. Dynamic nodes, PMU and local cyber-controller modeled.	
Other Approaches	Potential Cascading Models	"Cluster" approach employed. Aim at predicting potential cascading outages.	Focus only part of cascading outage mechanisms.
	Historical Data-Based Models	Accurately reproduce history events. Complementary to existing models.	
	Hidden Failure Models	Hidden Failure and generator re-dispatch considered.	

1.3 Contributions of this Work

The main challenges for the modeling, simulation and analysis of cascading outages are:

1) The detailed process of cascading outages in a power system cannot be captured accurately by existing steady-state approaches due to ignoring dynamics under outages and control actions. Although dynamic simulation can provide more detailed dynamic information but its major drawback is intense time consumption for large system models. Also, existing power system models are not validated well for mid-term or long-term power system simulations over an extended time period of tens of minutes to several hours, which, however, are the typical time spans for the whole process of cascading outages. Thus, power flow based steady-state or quasi-dynamic simulation models are acceptable for representing the cascading process at least for the early stage of cascading outages since transient behaviors of a power system fade away and system often reaches its steady state quickly. Therefore this thesis focuses on the development of steady-state approaches for the modeling, simulation, and analysis of cascading outages that are able to provide important insights on dynamic behaviors of the system under outages and control. The existing steady-state approaches for cascading outages are mainly for offline analysis. This thesis will target at online simulation and analysis of cascading outages for proactive mitigation control against a power blackout.

2) Frequency is an important indicator of the real-time balance between active powers of the generation and load in a power system, especially during cascading outages. Abnormal frequency may trigger under-frequency load shedding (UFLS) and generator frequency protection, causing a large amount of loss in generation and load, so it is a significant contributing factor of cascading outages and blackouts. However, frequency is seldom considered yet in existing steady-state approaches for the simulation and analysis of cascading outages.

This thesis introduces the system frequency deviation into the power flow model so that frequency-related outages and control actions can be simulated.

3) Various remedial and emergency actions, including load and generator tripping, excitation controls, and intentional islanding, are deployed to prevent cascading blackouts. The intentional or active islanding method is a good way for mitigation of cascading outages. The computational efficiency of these methods is the remaining challenge.

The main focus of this thesis is for the three challenges mentioned above. The contributions of this thesis are summarized by:

1) The framework of a multi-layer interaction graph is proposed for the monitoring and mitigation of cascading outages. This multi-layer interaction graph can be constructed offline based on a large number of samples of cascades with detailed stated-state models. It can be used online for monitoring and mitigating cascading outages.

2) A novel steady-state approach for the simulation of cascading outages is proposed considering frequency. By using this approach, the propagation of cascading outages can be captured more accurately.

3) An online strategy of critical component-based active islanding is proposed that isolates outages within a designed area so as to reduce the cascading outage risk of the system.

CHAPTER TWO
MULTI-LAYER INTERACTION GRAPH FOR SIMULATION AND ANALYSIS OF CASCADING OUTAGES

2.1 Introduction

The high computational complexity for simulation of cascading outages cannot meet the requirements for online applications. Thus, an advisable approach for online analysis and mitigation of cascading outages would be utilization of a high-level model that is established offline directly from a comprehensive database on historical or simulated cascading events. The "influence model" which is a tree network is proposed to quantify the influences between the components of network [68]. Similar to this general idea, [96] quantifies the interactions between transmission lines by line interaction graph in order to analyze cascading failures. Ref. [27] constructs an interaction network from a database of cascade outages to capture key components and key links between component outages that play critical roles in outage propagation. The interaction network is useful for understanding the general patterns of outage propagation and has potentials in online applications. Then this interaction network can be combined with online monitoring and mitigation of cascading outages. The valuable information extracted from the samples of cascading outages includes the outage components involved, propagation paths of outages, amounts of load shedding, geographic distances between two outages, etc., which if presented together can provide system operators with a comprehensive picture on the propagation patterns of outages and take effective control actions.

This chapter first demonstrates the application of the interaction model and interaction graph to a realistic Northeastern Power Coordinating Council (NPCC) power system in Section 2.2 [97]. Then this chapter proposes a multi-layer interaction graph [98] as the extension and generalization of the single-layer interaction network in [27]. Different from that interaction network, this multi-

layer interaction graph integrates multiple layers that respectively identify the key intra-layer links and components in each layer contributing the most to outage propagation from various perspectives, e.g. the number of line outages, the amount of load shedding and the electrical distance on outage propagation. Besides, key inter-layer links that connect components from different layers are also defined to model the transition from one type of consequences to another type. All the key intra-layer links and components and key inter-layer links and components together provide comprehensive information on the dominant outage propagation patterns, based on which effective mitigation measures can be further developed. Section 2.3 introduces the proposed multi-layer interaction graph and the method for identifying key intra- and inter-layer links and components. Section 2.4 proposes multiple strategies to mitigate the propagation of cascading outages and validates the proposed multi-layer interaction graph. Section 2.5 proposes a method to determine the minimum number of samples of cascading outages needed for constructing a reliable multi-layer interaction graph. Section 2.6 demonstrates the multi-layer interaction graph obtained from a simulated database of cascading outages on a Northeastern Power Coordinating Council (NPCC) 48-machine 140-bus system. Finally conclusions are drawn in Section 2.7.

2.2 Demonstration of Interaction Graph and Interaction Model on the NPCC Power System

2.2.1 Original Cascades and Simulated Cascades

In this chapter, “original cascades” are the cascading outage sequences from utilities or generated by detailed cascading outage models while “simulated cascades” are the cascading outages sequences produced directly by the interaction model that is built from “original cascades”.

2.2.2 Interaction Matrix and Interaction Graph

The interaction matrix ***B*** determines how components (e.g. lines) interact with each other based on the original cascades. The nonzero element b_{ij} of ***B*** is the empirical probability that the failure of component *i* triggers the failure of component *j*. The interaction matrix can be represented by the interaction network or graph $\varsigma(C,L)$, for which each link corresponds to one nonzero element in ***B*** and represents that a failure of the source vertex component causes the failure of the destination vertex component with nonzero probability. The vertex set *C* represents all components of the system.

2.2.3 Identification of Key Links and Components

In [27] the link weight I_l is defined to indicate the contribution of a link *l* to the propagation of cascading outages. The link weight is actually the expected value of the number of failures that are propagated through the link. Then, the set of key links L^{key} can be obtained by

$$L^{key} = \{l \mid I_l \geq \varepsilon_l I_l^{\max}\} \tag{2.1}$$

where ε_l >0 is a constant to identify the key links with large link weight, $I_l^{\max}$ is the largest link weight of all links.

The vertex out-strength of the interaction network indicating how much a component *i* influences another is

$$S_i^{out} = \sum_{l \in L^{out}(i)} I_l \tag{2.2}$$

where $L^{out}(i)$ is the set of links starting from vertex *i*. The set of key components C^{key} which contribute mostly to the propagation of cascading outages can be obtained by

$$C^{key} = \{i \mid S_i^{out} \geq \varepsilon_s S_i^{out,\max}\} \tag{2.3}$$

where ε_s >0 is a constant to identify key components with large out-strengths, and $S_i^{out,\max}$ is the largest value of all components.

2.2.4 Interaction Model

As in [27], an interaction model can be used to efficiently simulate cascades based on the initial tripping probability of each component and the interaction matrix ***B***. All components are assumed to be initially operating and each component fails with a small probability. The component failures then cause other component failures independently according to the empirical probability in interaction matrix ***B***.

2.2.5 Mitigation Strategies of Cascading outages

Since key links contribute much to propagation of cascading outages, which may be mitigated by weakening the corresponding element in interaction matrix ***B***. Thus, mitigation strategies may be suggested, e.g. blocking relays on the destination vertices and even controlled islanding [99] to break some key lines and isolate cascades. A random mitigation strategy means weakening elements in ***B*** randomly while an intentional mitigation strategy chooses key links in matrix ***B*** to weaken. Subsection 2.2.7 will investigate effectiveness of mitigation strategies in reducing risks of cascading outages.

2.2.6 Determining The Line Flow Limits

In order to apply the interaction model to the NPCC test bed, we first generate original cascades by using the fast dynamic process of AC-OPA model for which reasonable line flow limits as important parameters are needed. In [40], the line flow limits are determined by running the fast dynamics of OPA and the slow dynamics of OPA on a base load level that together emulate a long-term power system planning process to selectively upgrade lines in response to their involvements in daily failures starting from initial guesses of the limits. Then the line flow limits at an expected load level (either the base load level or a future level) are determined by

$$Limit_i^{DC} = Limit_i^k / \lambda^m \tag{2.4}$$

where $Limit_i^{DC}$ represents the line flow limit of component *i* at the expected load level, $Limit_i^k$ is the line flow limit of component *i* on the *k*-th simulation day, λ>1 is

a constant, representing mean load daily growth factor, and $m \leq k$. The line flow limits to be determined are for the base load level if $m=k$, or a targeting future load level if $m<k$. In this chapter, satisfaction to the N-1 criterion on each simulation day is not required. However, the OPA algorithm can easily be modified to consider the N-1 criterion. For example, [100] extended the OPA simulation to address the N-1 criterion.

Fig. 2-1 describes an OPA-based method for obtaining the line flow limits. The advantage of using DC-OPA is fast and easy to solve. However, such a DC-OPA method when determining line flow limits does not consider the influence of reactive power. In contrast, the fast dynamic process of AC- OPA to produce a database of original cascades does consider reactive power and voltage variations. That cause some limits from DC-OPA to be violated at high probabilities for lines carrying heavy reactive power flows, e.g. those supporting load center areas.

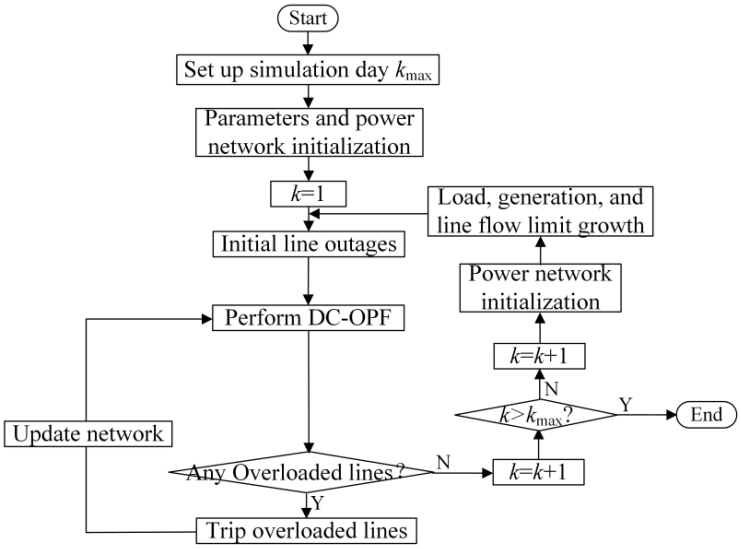

Figure 2-1. Flow chart of the DC-OPA method for line flow limits.

Here we have to mention that for a power system, if each bus has a high power factor (>0.76 for the IEEE 118-bus system studied in [20] and [27]), the impact of reactive power on violations of the line flow limits from the DC-OPA

method during the fast dynamic process of AC-OPA is minor. In that case, the limits from the DC-OPA method can directly be used. However, for the NPCC test bed, there are a few load buses with very low power factors, e.g. buses 3, 92, 95 and 114 since in those areas, there are a few lines carrying heavy reactive power flows to support voltage. The limits from the DC-OPA method will be violated in the fast dynamic process of AC-OPA. Therefore, for some power system like the NPCC test bed, we need to revise the line flow limits obtained by DC-OPA based method using (2.5) to give considerations to the impact from reactive power, where $Limit_i^{AC}$ and $Limit_i^{DC}$ are respectively a corrected line flow limit and the limit obtained from the original DC-OPA method, and Q_i is the planned reactive power flow of component *i* at the expected load level, which may approximately be estimated by, e.g., the reactive power flow at the base load level multiplied by λ^{k-m} if there is no better knowledge on it.

$$Limit_i^{AC} = \sqrt{(Limit_i^{DC})^2 + Q_i^2} \tag{2.5}$$

Alternatively, an AC-OPA method may substitute AC OPF for DC OPF in the procedure of Fig. 2-1 for more accurate limits addressing reactive power. However, that will cause greatly increased computation burdens but the limits obtained will have similar statistical properties with the limits obtained by the aforementioned modified DC-OPA method.

2.2.7 Simulation Results

1) *Determining Line Flow Limits for the NPCC Test Bed*

The original NPCC 140-bus, 48-machine, 233-branch model comes from the Power System Toolbox [101] and represents the backbone transmission of the northeast region of the Eastern Interconnection, which was involved in the 2003 blackout event. The base load level of the model is 28GW. We use constant P/Q load models. The first task is to obtain a set of reasonable line flow limits for that base load level such that a test bed is developed for cascading outages simulation.

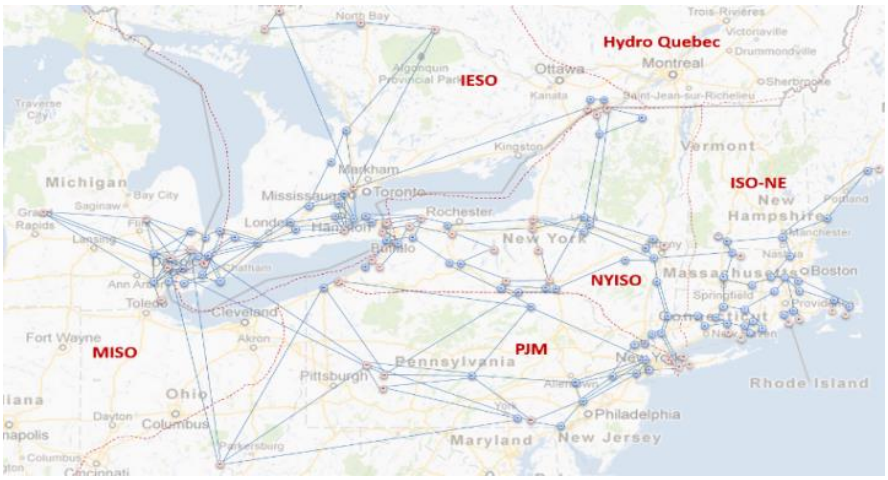

Figure 2-2. NPCC power system test bed.

Table 2-1. Information of Parameters.

Parameter	DC-OPA	AC-OPA	Remark
No. of days	64000	10000	Simulation days
λ	1.0005	-	Daily load and generation growth factor
μ	1.005	-	Line improvement factor
γ	1.67	1.67	Load variability
p_0	0.0001	0.0001	Probability of initial line outage

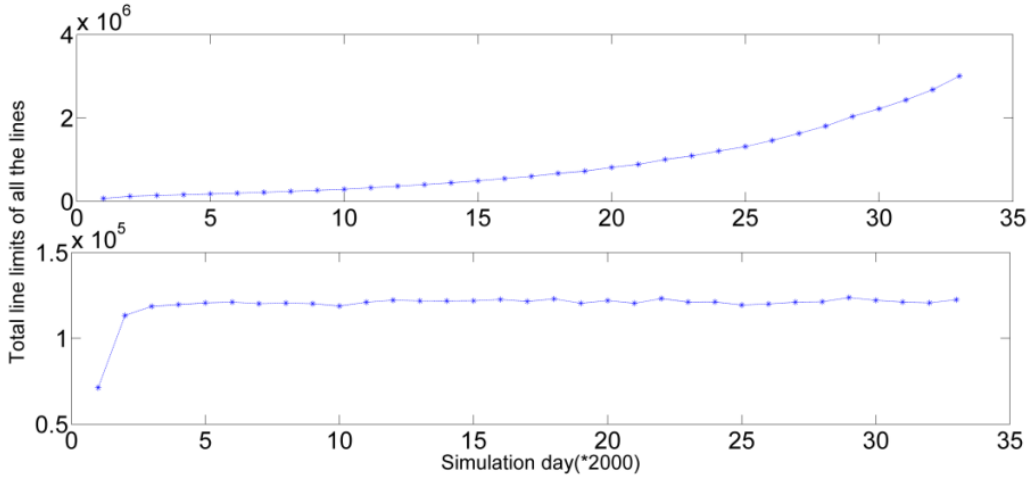

Figure 2-3. Simulation results of total line flow limits (the upper one is the total line flow limits for the current load level, and the bottom one is the total line flow limits after converting to the basic load level).

The 2nd column of Table 2-1 gives main parameters of the original DC-OPA method. Each initial line flow limit takes double of the base line flow. After a set of line flow limits $Limit_i^{DC}$ is obtained. The final line flow limits $Limit_i^{AC}$ are calculated from (2.5). Then, the test bed is simulated by an AC-OPA based fast dynamic process to generate the original cascades, whose parameters are given in the 3rd column.

Fig. 2-3 gives the total line flow limit from the original DC-OPA method. From it, a conclusion is that the total line flow limit is stable after the number of simulation days reaches 10000 when two strengths, the load growth to trigger cascades and the line upgrading to reduce the risk of cascades, reach their balance, i.e. the equilibrium of the slow dynamic process. We compared the average variation of each line limit between two stages, i.e. the 10000-th day and the 64000-th day. The variation is as small as 6.9% so that we may ignore the fluctuation of the total line limit after the 10000-th day and adopt the set of line flow limits on that day as the initial limits.

Table 2-2. Line Flow Limits for Original DC-OPA Method.

Line No.	MW and MVar flows at base load level	Line flow limit by DC-OPA	Updated limit
4	3.99MW,43.83Mvar	24.93MVA	50.42MVA
5	5.07MW,45.91Mvar	24.17MVA	51.88MVA
223	51.44MW,163.09Mvar	126.09MVA	206.15MVA

Reactive powers of lines 4, 5 and 223 are found larger than the line flow limits from the original DC-OPA method. Table 2-2 gives those limits, their updated values by using (2.5), and the real and reactive power flows of those lines at the base load level for purpose. The updated line flow limits will be used in simulation to create original cascades.

2) *Building the Interaction Model*

Table 2-3. Key Links of NPCC Test Bed.

$i \rightarrow j$	Line pairs	l_j
199 → 198	(126,125)→(126,124)	4156.7
38 → 6	(33,32)→(4,1)	3005.5
112 → 105	(81,78)→(75,76)	2041.7
19 → 24	(13,12)→(15,14)	1549.7
38 → 8	(33,32)→(5,31)	1377.1
6 → 36	(4,1)→(31,30)	1330.9
21 → 6	(14,13)→(4,1)	1278.2
198 → 201	(126,124)→(127,126)	1277.7
198 → 204	(126,124)→(128,126)	1254.8
198 → 225	(126,124)→(138,126)	1253.2
112 → 197	(81,78)→(125,124)	1186.6
38 → 42	(33,32)→(35,34)	928.6
38 → 40	(33,32)→(34,33)	893.5
18 → 24	(12,7)→(15,14)	832.6
24 → 29	(15,14)→(18,17)	816.4
19 → 21	(13,12)→(14,13)	784.0
105 → 215	(75,76)→(134,132)	780.3
19 → 23	(13,12)→(15,7)	749.6
38 → 7	(33,32)→(5,4)	735.1
32 → 31	(20,19)→(20,17)	721.9
114 → 166	(83,112)→(113,112)	672.9
197 → 198	(125,124)→(126,124)	669.1
162 → 163	(111,108)→(111,109)	650.4
6 → 35	(4,1)→(30,29)	643.7
197 → 203	(125,124)→(128,125)	631.0

Table 2-4. Key Components of NPCC Test Bed.

Key component	Line	S_i^{out}
38	(33,32)	8822.2
6	(4,1)	7339.7
199	(126,125)	5914.4
112	(81,78)	5586.7
105	(75,76)	4473.7
198	(126,124)	4097.9
19	(13,12)	3664.8
24	(15,14)	3302.1
166	(113,112)	2974.0
21	(14,13)	2610.3
8	(5,31)	1994.5
18	(12,7)	1892.9
197	(125,124)	1583.9
215	(134,132)	1580.8
35	(30,29)	1470.1

Following the algorithm of the interaction model, key links and components that play important roles in the propagation of cascading outages are identified. Those identified key links are actually line pairs in the NPCC test bed, and their weights I_l for the original cascades are listed in Table 2-3.

Complementary cumulative probability distribution of link weight of all links is displayed in Fig. 2-4. Both ε_l and ε_s take 0.15. Key links only take 0.7% of all links of the system but the sum of their weights cover 38.5% of the total weights of all links. These very few links contribute quite a lot to the propagation of cascading outages and together capture highly concentrated key information on cascading outages of the NPCC test bed. The identified key components are listed in Table 2-4. Failures of these components are the most involved ones in cascades. System operators should pay more attentions to those components. The number of key components is 15, i.e. 6.43% of all components for the original cascades. However, the sum of the out-strengths of key components is 68.8% of that for all involved components.

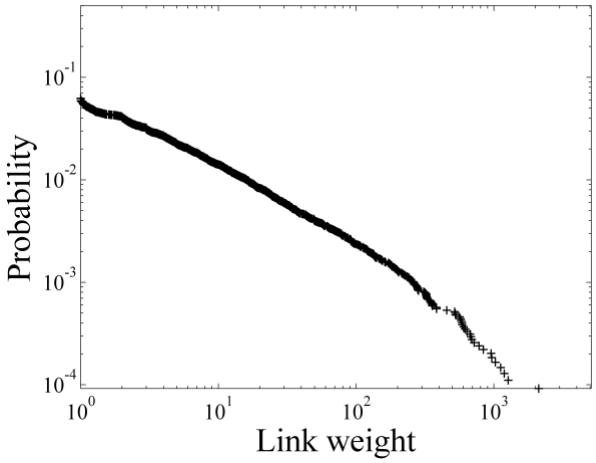

Figure 2-4. Complementary cumulative probability distribution of link weight.

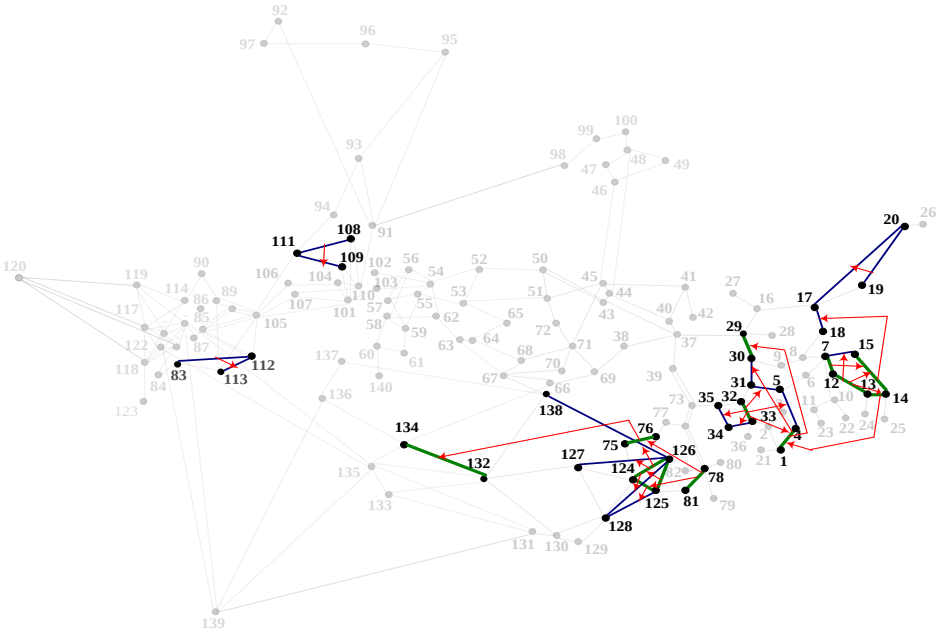

Figure 2-5. Key links (red arrows), key components (green lines), and other involved components (blue lines) with the rest of the system (faded).

Fig. 2-5 highlights the key links (red arrows), key components (green lines) and other involved components (blue lines), which together determine the areas that are most vulnerable to cascading outages. Actually, those areas match very well the geographical locations of load center areas in the actual NPCC system such as the Connecticut load center and New York City load center. From those identified links and components, propagation paths of cascading outages are indicated, e.g. the path (75, 76) → (134, 132), (13, 14) → (4, 1) and (15, 14) → (18, 17). Observations from Fig. 2-5 on the propagation paths are: first, the source and destination vertices of most key links, e.g. at an earlier stage of a propagation path, are lines geographically close to each other, which indicates that cascading outages often initiate from local problems; second, however, at the later stage of a path, some key links may have source and destination vertices far away from each other, which means that, at a later stage, cascading outages develop to a wider-area or even system-wide problem. The second observation indicates that the power system exhibits more nonlinear "butterflyeffect" behaviors in a later stage of cascading outages, which are

captured by the AC-OPA based fast dynamic process for creating the original cascades and consequently can be captured by the interaction model. This property is similar to the discussion in [27]. Those observations suggest that mitigation strategies should be taken before cascading outages develop to a system-wide problem.

3) *Comparison between Original and Simulated Cascades*

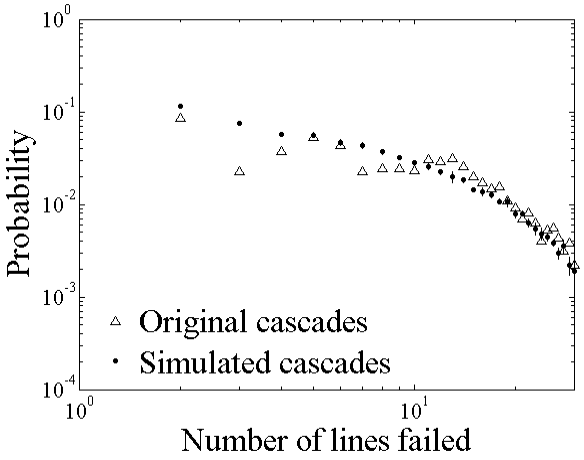

Figure 2-6. Probability distributions of the total number of line failed for original and simulated cascades.

The probability distributions of the total number of line outages respectively for original cascades and simulated cascades are shown in Fig. 2-6. We simulate 20 times and obtain the average probability distribution and the standard deviations (vertical axis) for the simulated cascades. It is found that those two distributions basically match especially for bigger cascades (with >10 lines failed). The standard deviations for the simulated cascades are small. It indicates that the interaction model authentically captures the statistical properties of the original cascades.

4) *Mitigation Strategies for Cascading Outages*

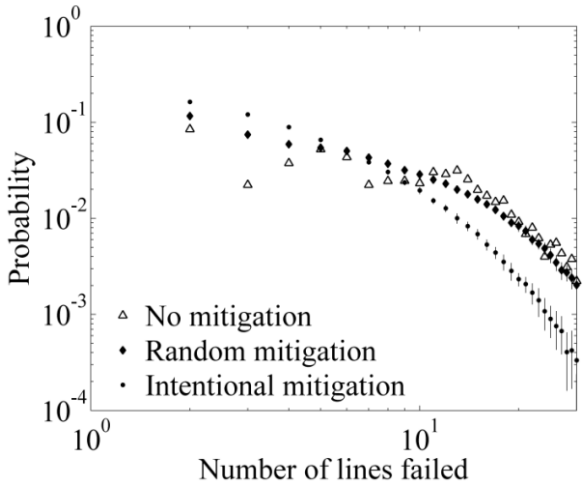

Figure 2-7. Probability distributions of the total number of line failed for original and simulated cascades under different mitigation strategies.

Intentional mitigation strategies that block some relays suggested from the interaction model are tested and compared with random relay blocking strategies. From Fig. 2-7, the risk of large-scale cascades is greatly reduced with the intentional strategies while that for the random strategies is not obvious, which suggests the identified key links indeed play important roles in the propagation of cascading outages.

2.3 Multi-Layer Interaction Graph

The schematic diagram of the multi-layer interaction graph is illustrated in Fig. 2-8, which has three layers respectively in terms of the number of line outages, the amount of load shedding and the electrical distance of outage propagation. In each layer of Fig. 2-8, the key intra-layer links and components for one power grid are highlighted respectively by thick arrows and lines. Note that the number of key intra-layer links and components can vary based on different selection thresholds, which will be discussed later.

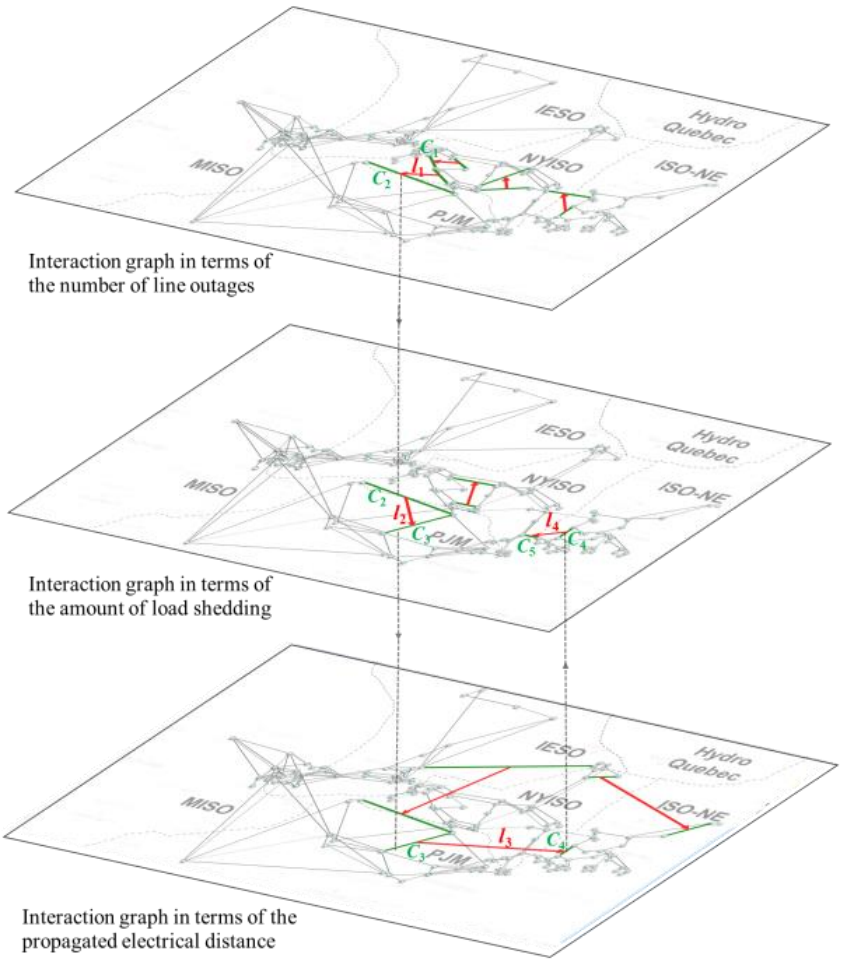

Figure 2-8. Schematic diagram on how a scenario of cascade outages propagates in and across multiple layers of the interaction graph for the NPCC power system. (thick red arrows and green lines are key intra-layer links and key intra-layer components; broken lines with arrows indicate transitions between layers)

$$C_1 \xrightarrow{l_1} C_2 \xrightarrow{l_2} C_3 \xrightarrow{l_3} C_4 \xrightarrow{l_4} C_5$$

Figure 2-9. Path of a sample scenario of cascade outages.

Fig. 2-8 presents a simple scenario on the propagation of cascading outages within and across layers. As shown in Fig. 2-9, the path of that scenario involves five components C_1, C_2,..., and C_5 connected by four directed intra-layer links l_1, l_2, l_3, and l_4, which respectively belong to the first, second, third and second layers. This entire process of cascading outages can only be observed from the multi-layer interaction graph while any single-layer can only provide partial information for the entire process. The multi-layer interaction graph generated offline provides a big picture on propagation patterns of cascading outages, which is valuable for the system operators to take effective control actions.

In this section, three control strategies that weaken key intra-layer links located in each layer are studied to mitigate cascading outages respectively from three perspectives, i.e. the number of line outages, the amount of load shedding, and the propagated electrical distance. Besides, integrated mitigation strategies involving key intra-layer links from different layers can be applied.

2.3.1 Database of Cascades and Links

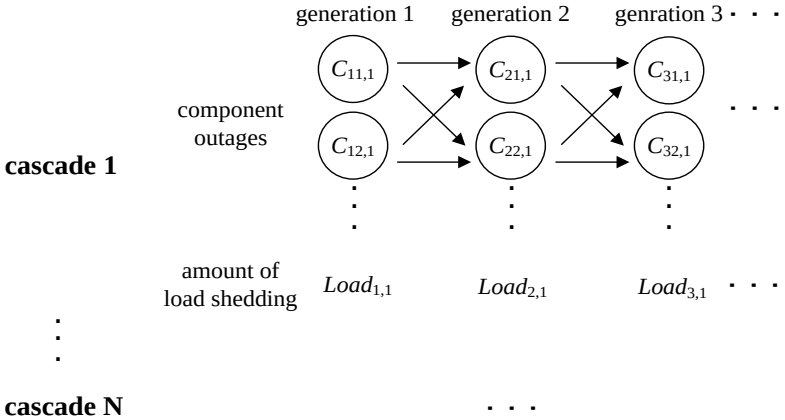

Figure 2-10. Schematic diagram of the cascades.

Typically, the transmission lines or transformers can be considered as components. For simplicity, “cascade” in the rest of the chapter means one sample of cascading outages, whose outages are clustered into multiple

generations by time or sequence of outages. Each cascade starts with initial component outages in generation 1 and continues to generate outages in the following generations until there is no outage or the system collapses as illustrated by Fig. 2-10. Here $C_{ij,m}$ is the j-th component outage in generation i of the m-th cascade, and $Load_{i,j}$ is the amount of load shedding at the i-th generation of the m-th cascade.

Following the same structure as Fig. 2-10, a large number of independent cascades triggered by different initial component outages comprise the database of cascades. The component outages in one generation are considered to happen almost at the same time, whose sequence can be ignored. Thus, some causality between any two component outages respectively from two consecutive generations is hypothesized. A component outage $C_{ij,m}$ may potentially be caused by several component outages by going through all of the cascades, among which the one occurring the most times in the database is assumed to be the true cause of $C_{ij,m}$ in ref. [27]. Other links connecting the remaining component outages and $C_{ij,m}$ are regarded as the redundant links. Finally, the set of links is obtained and denoted by L_{total}.

2.3.2 Link Weights for Different Layers

Different link weights are defined for the three layers:

- The link weight applied in the first layer is the empirical probability (denoted by P_l) of the source component outage causing the destination component outage [27].
- The link weight in the second layer is the average amount of load shedding (denoted by W_l) triggered by the link.
- The link weight of the third layer is the electrical distance (denoted by Z_l) in terms of equivalent impedance between the source and destination component outages.

1) *Link Weight in Terms of the Number of Line Outages*

The link weight is calculated by

$$P_l = \frac{N_{l:i\to j}}{N_i} \tag{2.6}$$

where $N_{l:i\to j}$ is the number of occurrences for link *l* and N_i is the number of times of outages of the source component *i* over the entire database.

2) *Link Weight in Terms of the Amount of Load Shedding*

In each cascade, the initial outages propagate to subsequent outages in the following generations. For the *m*-th cascade in the database, the component outages in generation *g*-1 can produce subsequent outages in generation *g* resulting in $Load_{g,m}$ of load shedding, which can be assigned to the links connecting the component outages in generation *g*-1 and *g*. The average amount of load shedding for link *l* in the *m*-th cascade is defined as

$$d_l^m = \frac{Load_{g,m}}{N_{(g-1,g),m}} \tag{2.7}$$

where $Load_{g,m}$ represents the amount of load shedding at generation *g* of the *m*-th cascade and $N_{(g-1,g),m}$ is the total number of links connecting generations *g*-1 and *g*. From all of the cascades which involve link *l*, the average amount of load shedding caused by link *l* is defined as

$$W_l = \frac{\sum_{m=1}^{N_l} d_l^m}{N_l} \tag{2.8}$$

If the true causalities between consecutive generations are unknown, for simplicity, we may assume that those $N_{(g-1,g),m}$ links connecting generations *g*-1 and *g* have the same amount of load shedding as shown by (2.7) and hence have uniform weights in one cascade. An alternative method may adopt non-uniform link weights and calculate the link weight by

$$d_{l:i\to j}^m = \frac{Load_{g,m}}{N_{(g-1,g),m}} \frac{F_i}{\sum_{i\in C(i)} F_i} \tag{2.9}$$

where the source component *i* outage and destination component *j* outage are respectively in generations *g*-1 and *g*. F_i is the power flow of component *i* before

its outage and $C(i)$ is the set of component outages at generation g-1. An interpretation of (2.9) is that the links starting from source component i which have large power flows before its outage will be assigned large link weights in that cascade, which is reasonable since the outage of component i may cause power flow redistribution of some heavily loaded lines nearby.

3) *Link Weight in Terms of Propagated Electrical Distance*

The NERC blackout report [2] shows that outages may propagate to next outages either near or far in the network and become widespread in a later stage of cascading outages. The statistical characterization of how cascading outages typically spread on the network is analyzed in [21] based on standard utility data. In this chapter, the links' spatial spreading is quantified by the electrical distance defined by [102-103], which originally quantifies the distance between two buses in power systems. Here, we adapt it to quantify the electrical distance between two components (i.e. lines) as

$$\begin{aligned} Z_{i(i_s,i_d)\to j(j_s,j_d)} &= \min\{Z^{equ}_{i_s j_s}, Z^{equ}_{i_s j_d}, Z^{equ}_{i_d j_s}, Z^{equ}_{i_d j_d}\} \\ Z^{equ}_{\alpha,\beta} &= Z_{\alpha\alpha} - 2Z_{\alpha\beta} + Z_{\beta\beta} \quad \alpha \in \{i_s, i_d\}, \beta \in \{j_s, j_d\} \end{aligned} \tag{2.10}$$

Where $Z_{i(i_s,i_d)\to j(j_s,j_d)}$ is the electrical distance for the link $i \to j$ with source component i and destination component j, $Z^{equ}_{i_s j_s}$, $Z^{equ}_{i_s j_d}$, $Z^{equ}_{i_d j_s}$, and $Z^{equ}_{i_d j_d}$ are four equivalent impedances which each start from a bus of the source component and end at a bus of the destination component as calculated by the above formula. $Z_{\alpha\beta}$ is the α-th row β-th column entry of the network impedance matrix, and $Z_{\alpha\alpha}$ and $Z_{\beta\beta}$ are the α-th and β-th diagonal elements, respectively.

2.3.3 Construction of Multi-Layer Interaction Graph

The proposed multi-layer interaction graph has three layers. Each layer is comprised of key intra-layer links and components which contribute the most to outage propagation from one specific perspective, i.e. the number of line outages, the amount of load shedding, and the propagated electrical distance.

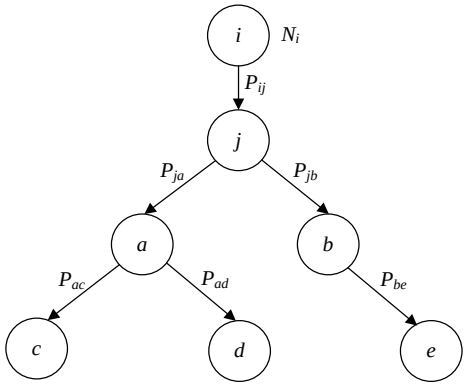

Figure 2-11. Subgraph influenced by a link in the first layer.

For the first layer, a directed acyclic subgraph starting from the link $i \rightarrow j$ can be extracted from L_{total} as shown in Fig. 2-11, and this subgraph (denoted by $C(i \rightarrow j)$) is unique and comprised of all the components influenced by link $i \rightarrow j$. To identify the key links, an index called the Cascading Outage Contribution (COC) is proposed to quantify the contribution of a link to propagation of outages in terms of the number of line outages. Given N_i times of component i outage, the expectation of the number of component j outages is

$$E_j = N_i P_{ij} \tag{2.11}$$

where P_{ij} is the empirical probability that the outage of component i causes the outage of component j. For any component $c \in C(i \rightarrow j), c \neq j$, the expectation of the number of outages given the times of its source component outage is

$$E_c = E_{c_s} P_{c_s j} \tag{2.12}$$

where c_s is the source outage of component c. Then define

$$COC^I_{i \rightarrow j} = \sum_{c \in C(i \rightarrow j)} E_c \tag{2.13}$$

which quantifies the total expected value of component outages that propagate through link $i \rightarrow j$. It can characterize the extent of the outage propagation in terms of the number of line outages. The larger $COC^I_{i \rightarrow j}$, the more critical the link. The set of key links can be obtained from those having the largest weights, e.g.

$$L^I_{key} = \left\{ l \mid COC^I_l \geq \lambda_I COC^I_{l\max} \right\} \tag{2.14}$$

where $COC^I_{l\max}$ is the largest value of COC^I for all links in the database and 1> λ_I ≥0 is the threshold.

To quantify the contribution of component *i* to the propagation of outages, define the out-strength index (*OS*) as

$$OS_i^I = \sum_{l \in \varsigma(i)} COC_l^I \tag{2.15}$$

where $\varsigma(i)$ is the set of links starting from component *i*. The out-strength of a component quantifies how much a component influences the others components. The components with large OS^I can cause great consequences and thus play crucial roles in the propagation of outages. The set of key components is obtained by selecting those components having the largest OS^I's as

$$C_{key}^I = \left\{ i \middle| OS_i^I \geq \beta_I OS_{i\max}^I \right\} \tag{2.16}$$

where $OS^I_{i\max}$ is the largest OS^I for all components and 1> β_I ≥0 is the threshold.

Note that if an isolated key component exists in one layer that is not involved in any key link, it should be removed from C^I_{key} since it is not very useful to analyze the propagation of outages. The same handling is applied to C^{II}_{key} and C^{III}_{key} defined later.

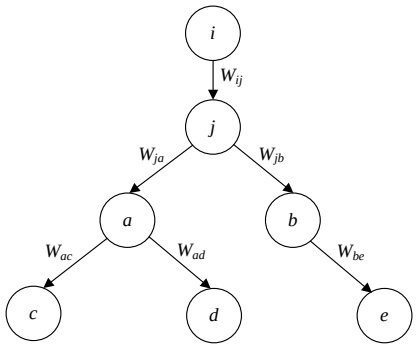

Figure 2-12. Subgraph influenced by a link in the second layer.

Using directed acyclic subgraph shown in Fig 2-12, the key links in the second layer can be identified by means of the COC of link *i*→*j* defined in (2.17)

to quantify the consequence with propagation of outages in terms of the amount of load shedding.

$$COC_{i\to j}^{II} = \sum_{l\in C(i\to j)} W_l \tag{2.17}$$

where W_l is the average amount of load shedding triggered by link l.

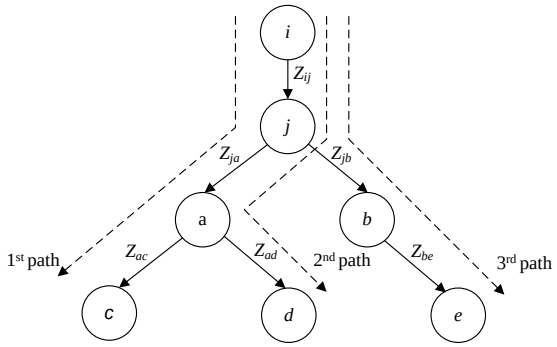

Figure 2-13. Subgraph influenced by a link in the third layer.

Similarly, using the subgraph in Fig. 2-13, the key links in the third layer are identified by the COC of link $i\to j$ defined in (2.18), where D_t^{path} is the total electrical distance for the t-th path starting from link $i\to j$, N_{path} is the number of paths starting from component j, G_t is the number of links along the t-th path, and Z_k is the electrical distance for the k-th link along the t-th path. $COC_{i\to j}^{III}$ can quantify the average distance of outage propagation starting from link $i\to j$.

$$COC_{i\to j}^{III} = \frac{\sum_{t=1}^{N_{path}} D_t^{path}}{N_{path}}, \quad \text{where} \quad D_t^{path} = \sum_{k=1}^{G_t} Z_k \tag{2.18}$$

The key links and components in the second and third layers can be identified by a method similar to (2.14)-(2.16). Their sets of key links and key components are denoted by L_{key}^{II}, C_{key}^{II}, L_{key}^{III}, and C_{key}^{III}, respectively. Note that the key links and key components within a single layer are called key intra-layer links and components in order to distinguish them with the following inter-layer links and inter-layer components.

In real-world power systems, for example, consider how the transmission line outages spread in the August 10 1996 Western interconnection blackout in [104]. Occurrences of early outages did not cause obviously severe consequences on the system but did cause some transitions underneath to increase vulnerability of the system. In this chapter, inter-layer links are also proposed in order to understand the transitioning of the outage propagation across different layers.

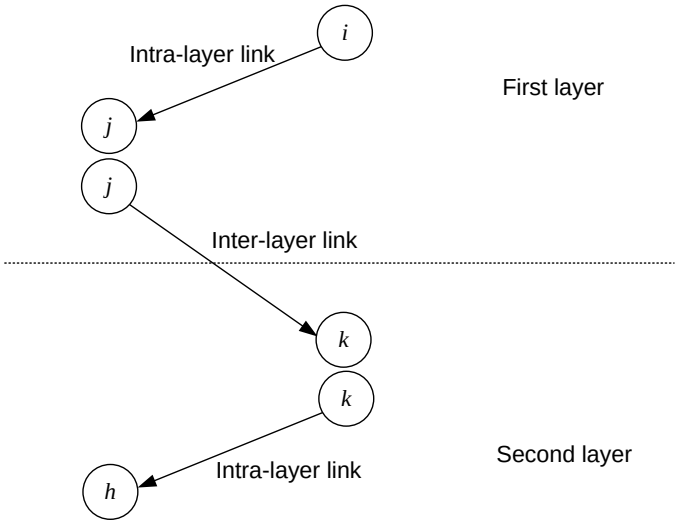

Figure 2-14. An inter-layer link between the first and second layers.

Fig. 2-14 illustrates an inter-layer link connecting the first and second layers, where link $i \rightarrow j$ is an intra-layer link in the first layer and link $k \rightarrow h$ is an intra-layer link of the second layer. Link $j \rightarrow k$ is an inter-layer link starting with the destination component outage of the first link and ending at the source component outage of the second link. The total number of candidate inter-layer links between any two layers equals the product of the number of their key intra-layer links. The following two steps can identify the key inter-layer links on the most frequent inter-layer transitions and the key inter-layer components involved in those transitions: 1) for any two layers *s* and *d*, select the top γ % links from $L_{total} - L_{key}^{s} \cup L_{key}^{d}$ as the key inter-layer links; 2) all components involved in the

source component outages of those key inter-layer links are defined as key inter-layer components.

2.4 Mitigation Strategies

2.4.1 Weakening of Key Intra-Layer Links

The propagation of cascading outages could be mitigated by weakening key intra-layer links [27]. When the source component of a key intra-layer link is tripped and causes the overloading of its destination component, that destination component will be tripped at a reduced probability to simulate intentional relay blocking as mitigation of outage propagation. In this way, cascades can be generated by simulations with that mitigation strategy.

In this chapter, the following six mitigation strategies that weaken a number (denoted by *K*, e.g. 20-100) of intra-layer links from different perspectives are compared:

- *Strategy-LO*: Weaken the top-K key intra-layer links in the first layer in terms of the number of line outages.
- *Strategy-LS*: Weaken the top-K key intra-layer links in the second layer in terms of the amount of load shedding.
- *Strategy-ED*: Weaken the top-K key intra-layer links in the third layer in terms of the propagated electrical distance.
- *Strategy-3L*: Weaken the top-K/3 key intra-layer links of the three layers.
- *Strategy-LOLS*: Weaken the top-K/2 key intra-layer links in the first layer and the top-K/2 key intra-layer links in the second layer in different stages of cascades.
- *Strategy-R*: Weakening randomly selected K intra-layer links for comparison purposes.

Strategy-LO, *Strategy-LS,* and *Strategy-ED* are single-layer mitigation strategies. *Strategy-3L* is an integrated mitigation strategy in which the key intra-layer links are from the three layers. *Strategy-LOLS* is an integrated mitigation

strategy in which the key intra-layer links are from the first and second layers. The key intra-layer links from the two layers are weakened in different stages of cascading outages. The key intra-layer links in the first layer are weakened in the early stage (generation 1 to 2) of cascading outages, and the key intra-layer links from the second layer are weakened in the later stage (generations 2 to 3) of cascading outages.

2.4.2 Validation of Mitigation Strategies

To validate a mitigation strategy, simulation of cascading outages is performed with each of the above strategies to generate a new database of cascades. Then, compared to the original database without mitigation, each mitigation strategy is evaluated by the reduced proportion of the average number of line outages, the average amount of load shedding, or the average electrical distance of outage propagation for each cascade. More specifically, the propagated electrical distance for one cascade is

$$ED_{cascade} = \sum_{g=1}^{N_{gen}-1} \max\{ED_{g,g+1}\} \tag{2.19}$$

where max{$ED_{g,g+1}$} is the maximal electrical distance between generation g and g+1 by going through all of links connecting these two generations, and N_{gen} is the number of generations for one cascade.

In general, a mitigation strategy that weakens the key intra-layer links from one layer can significantly mitigate the problem concerned by that layer compared to the random intra-layer link weakening and the key intra-layer link weakening for a different layer. It is anticipated that *Strategy-LO* can reduce the number of line outages much more effectively than *Strategy-R*, *Strategy-LS,* and *Strategy-ED*. Thus, the multi-layer interaction graph provides a way to choose the most effective strategy mitigating the most critical type of problems in cascading outages.

2.5 Number of Cascades Needed for a Database

More cascades tend to contain more information about the property of cascading outages. As a result, the number of identified links will increase and the COCs and the rankings of links can change. However, the rankings of the top-T_L key intra-layer links will stay unchanged after the number of cascades exceeds a threshold M^{min}. M^{min} can be determined by a procedure similar to the methods in [26] and [27]: gradually increasing the number of cascades, recording the set of top-T_L key intra-layer links, and finding the smallest number of cascades beyond which the top key intra-layer links do not change. Specifically, for the multi-layer interaction graph, the following steps are taken to determine M^{min} that make every layer have stable top-T_L key intra-layer links. Because the set of inter-layer links depend on the components of the key intra-layer links, the resulting the set of inter-layer links are also stable.

Let M_i, i=1, 2,…, T_M be a series of numbers gradually increased by ΔM as candidate numbers of cascades to be included into the database. $S_{T_L}(M_i)$ is the set of top-T_L key intra-layer links from M_i cascades. Define

$$R(M_i) = \left| S_{T_L}(M_{i-1}) \cap S_{T_L}(M_i) \right| / T_L \tag{2.20}$$

which gives the ratio between the number of common key intra-layer links from two consecutive numbers of cascades and T_L. Then we calculate the standard deviation σ_i of $R(M_i)$ around M_i as (2.21). Then M^{min} is determined as the smallest M_i with σ_i less than a given tolerance τ .

$$\sigma_i = \sigma([R(M_{i-2}), \quad R(M_{i-1}), \quad R(M_i)]), \ \ i \geq 2 \tag{2.21}$$

The number of cascades needed is the maximum value among the M^{min}s for the three layers.

2.6 Case Studies

A database of 10000 independent cascades is produced by simulations in MATLAB using the improved DC OPA model in [39] on an NPCC 140-bus system shown in Fig. 2-15. The total time cost is about 13800 seconds on a desktop PC with Intel Core i7-3770K 3.40GHz and 4GB RAM.

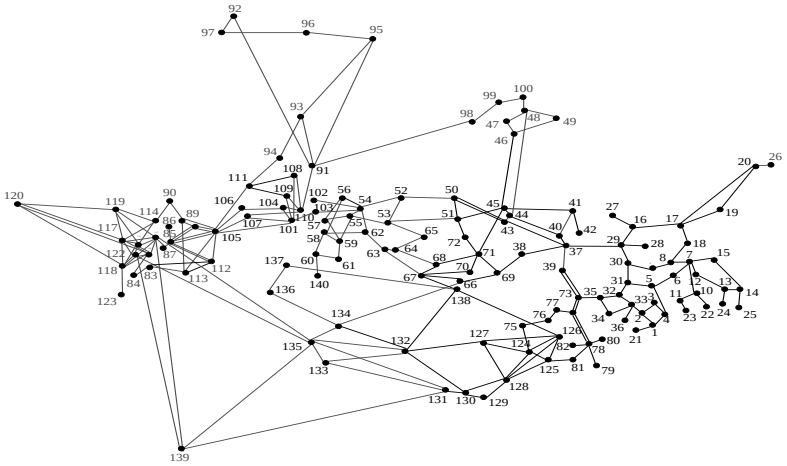

Figure 2-15. NPCC 140-bus system.

Line flow limits are critical parameters in the simulation of cascading outages. Here, the “N-1” security criterion is applied to the system and there is no overloaded line after any “N-1” contingency. Therefore the initial outages for simulations are selected from “N-k” (k≥2) contingencies in the NYISO area. The load variation at each load bus is assumed to follow uniform distribution in [0.95, 1.05]. The probability of the line tripping depends on its loading according to Table 2-5 from [90].

Table 2-5. Probability of Tripping with Line Loading.

Line Loading (% of Limit)	Probability of Tripping
100	0.10
110	0.30
120	0.60
130	0.80
140	0.95
150	1.00

In the real-time operation environment, if initial outages have occurred and tend to spread to a wide area, the system operator needs to make an immediate decision to evaluate and mitigate the outages. It would be time consuming to simulate a single cascade in time domain using detailed and accurate models on all power system components, so it is impossible to online simulate many possible cascades starting from the same initial outages in order to predict how

the cascading outages might propagate. For example, for the NPCC 140-bus system, the time costs for even the powerflow-based DC OPA model and AC OPA model to simulate 100 cascades are 128s and 504s on a desktop PC. For a utility-scale power system having tens of thousands of buses, simulations on even powerflow-based models also become unacceptably slow. Thus, it is more reasonable to utilize the proposed interaction graph constructed based on a database of offline simulated cascades. The models to be used in offline simulation can be detailed sufficiently to consider protective actions and system dynamics over a wide range from transient dynamics to mid-term or long-term dynamics to ensure the credibility of the database. Thus, online simulation can be avoided and the real-time application of this interaction graph constructed from the database for real-time prediction will be fast and practical.

2.6.1 A Multi-Layer Interaction Graph

A multi-layer interaction graph with three layers is visualized in Figs. 2-16-2-18. Each layer contains top-100 key intra-layer links and top-20 key intra-layer components. All components (i.e. transmission lines) of the NPCC system are represented by gray nodes (each located at the middle of the line), key intra-layer components are highlighted as green dots and key intra-layer links are represented by red arrows.

Note that the multi-layer interaction graph may vary with changes on the system topology and load level. If the changes are large, e.g. global load variations on the whole system, the set of key intra-layer links and component in each layer can vary significantly. Subsection 2.6.3 compares the interaction graphs respectively from the original database and a new database of cascades considering global load variations on the whole system.

Note that if the changes are small, e.g. slight load variations in a local area, most of key intra-layer links and components in other areas are still valid and important predictors on how outages may propagate. Thus, only some key intra-layer links and components in that local area need to be updated using the database having new cascades included. It will be investigated in the future work.

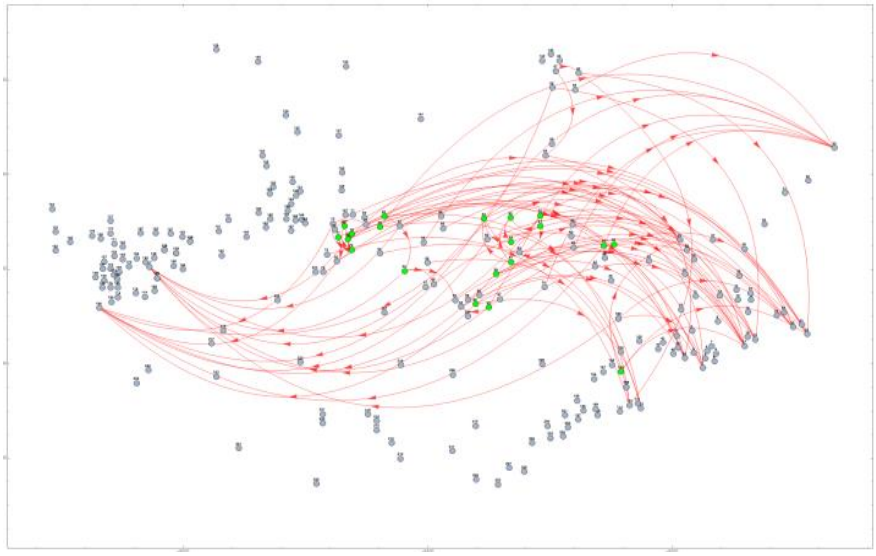

Figure 2-16. Top-100 key intra-layer links and top-20 key intra-layer components in terms of the number of line outages.

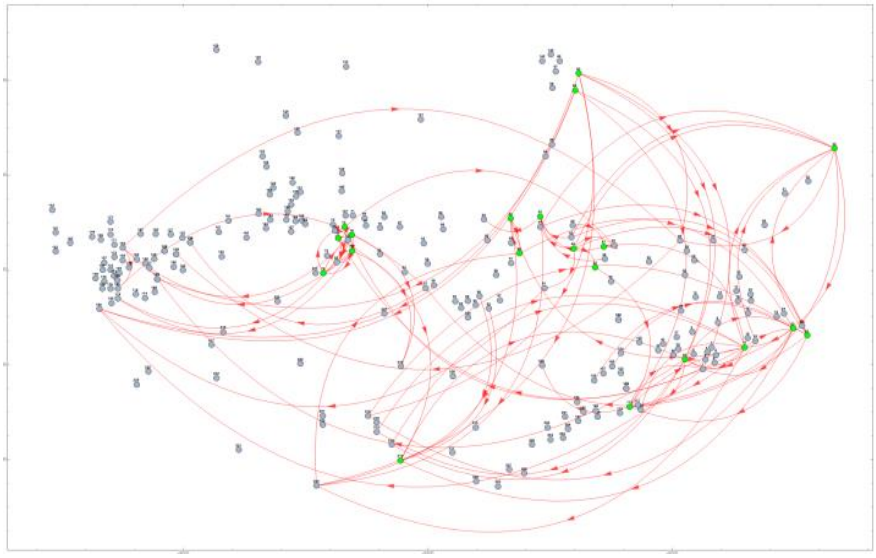

Figure 2-17. Top-100 key intra-layer links and top-20 key intra-layer components in terms of the amount of load shedding (excluding 2 isolated components).

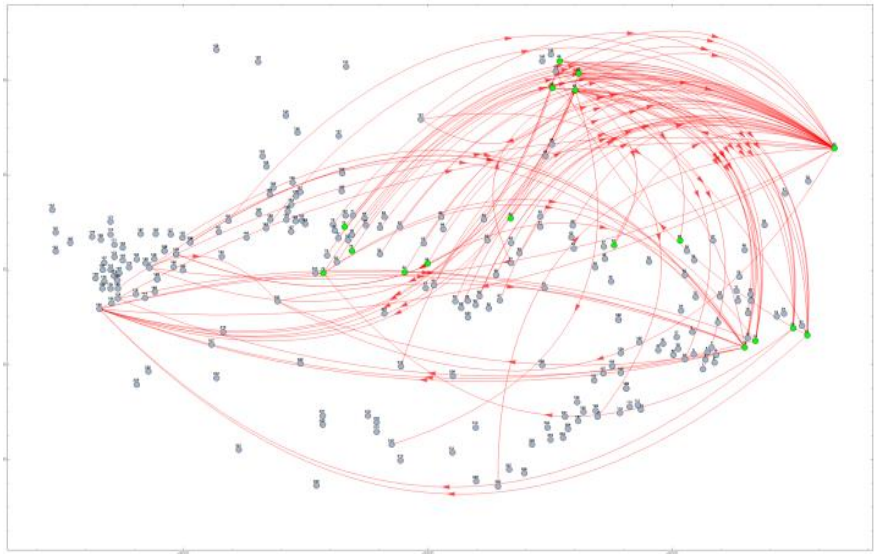

Figure 2-18. Top-100 key intra-layer links and top-20 key intra-layer components in terms of the propagated electrical distance (excluding 3 isolated components).

The overlapped links between different layers are very few as listed in Table 2-6, indicating the independency of the three types of key intra-layer links.

Table 2-6. Numbers of Overlapped Links between Different Layers.

Number of Key Intra-layer Links in Each Layer	Number of Overlapped Links between Two layers		
	1st and 2nd Layers	1st and 3rd Layers	2nd and 3rd Layers
20	0	0	0
50	1	4	0
100	4	7	7

The numbers of occurrences for the top-100 key intra-layer links in different layers are given by Fig. 2-19. The key intra-layer links in the first layer has much more occurrences than the key intra-layer links in the second layer. It indicates that the links with large occurrences have high probabilities to be identified as the key intra-layer links of the first layer, which is reasonable from the definitions (2.11)-(2.13). Those links with a large number of occurrences have high probabilities to be identified as the key intra-layer links in the first layer. However, these links may not be identified as the key intra-layer links in terms of

the amount of load shedding. For the key intra-layer links in the second layer, although they occur much less often than those of the first and third layers, they contribute the most to the amount of load shedding. For the key intra-layer links in the third layer, the number of occurrences is distributed more dispersedly.

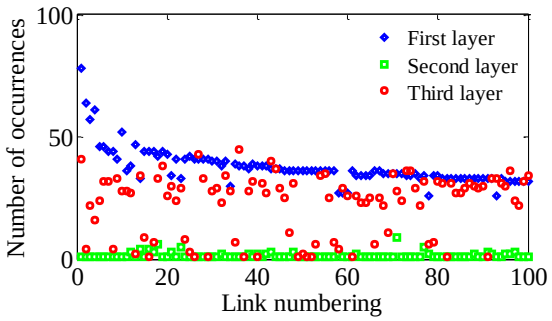

Figure 2-19. Numbers of occurrences for key intra-layer links in different layers.

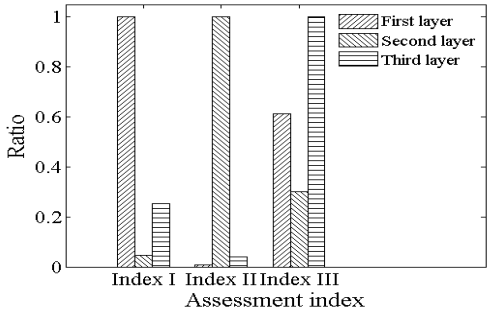

Figure 2-20. Comparison for the assessment indices for the top-100 key intra-layer links in different layers (Index I - average number of line outages; Index II - average amount of load shedding; Index III- average propagated electrical distance).

For a further comparison, the average number of line outages, the average amount of load shedding and the average propagated electrical distance are calculated as Indices I, II and III, respectively for the top-100 key links from different layers and then are normalized to [0,1] as shown in Fig. 2-20. The comparison confirms the distinct focuses of three layers; i.e. the index matching the focus of the layer has the highest value.

2.6.2 Key Inter-Layer Links and Components

Cascading outages may propagate within a single layer of the interaction graph or may cross to a different layer directly or through an inter-layer link. It is important for the system operators to monitor the inter-layer transitioning since it indicates the consequences of outages becoming less monotype. Here the numbers of inter-layer links between different layers for different numbers of key intra-layer links are shown in Fig. 2-21. The number of inter-layer links increases a lot with the increase of the number of key intra-layer links.

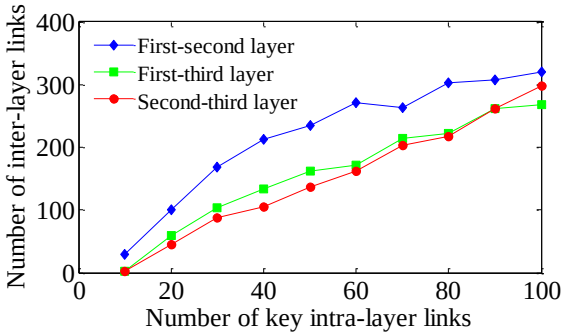

Figure 2-21. Numbers of inter-layer links for different numbers of key intra-layer links.

Fig. 2-22 shows only the top-15 key intra-layer links in each layer and the key inter-layer links between different layers. The number of inter-layer links between the first and second layers, the first and third layers, and the second and third layers are 65, 22, and 16, respectively. The sets of key inter-layer links between different layers can be selected from the top γ=50% of candidate inter-layer links. The number of key inter-layers between the first and second layers, the first and third layers, and the second and third layers are determined as 12, 6, and 4, respectively. The numbers of key inter-layer components involved in the key inter-layer links between the first and second layers, the first and third layers, and the second and third layers are 7, 5, and 3, respectively, as highlighted in Fig. 2-22.

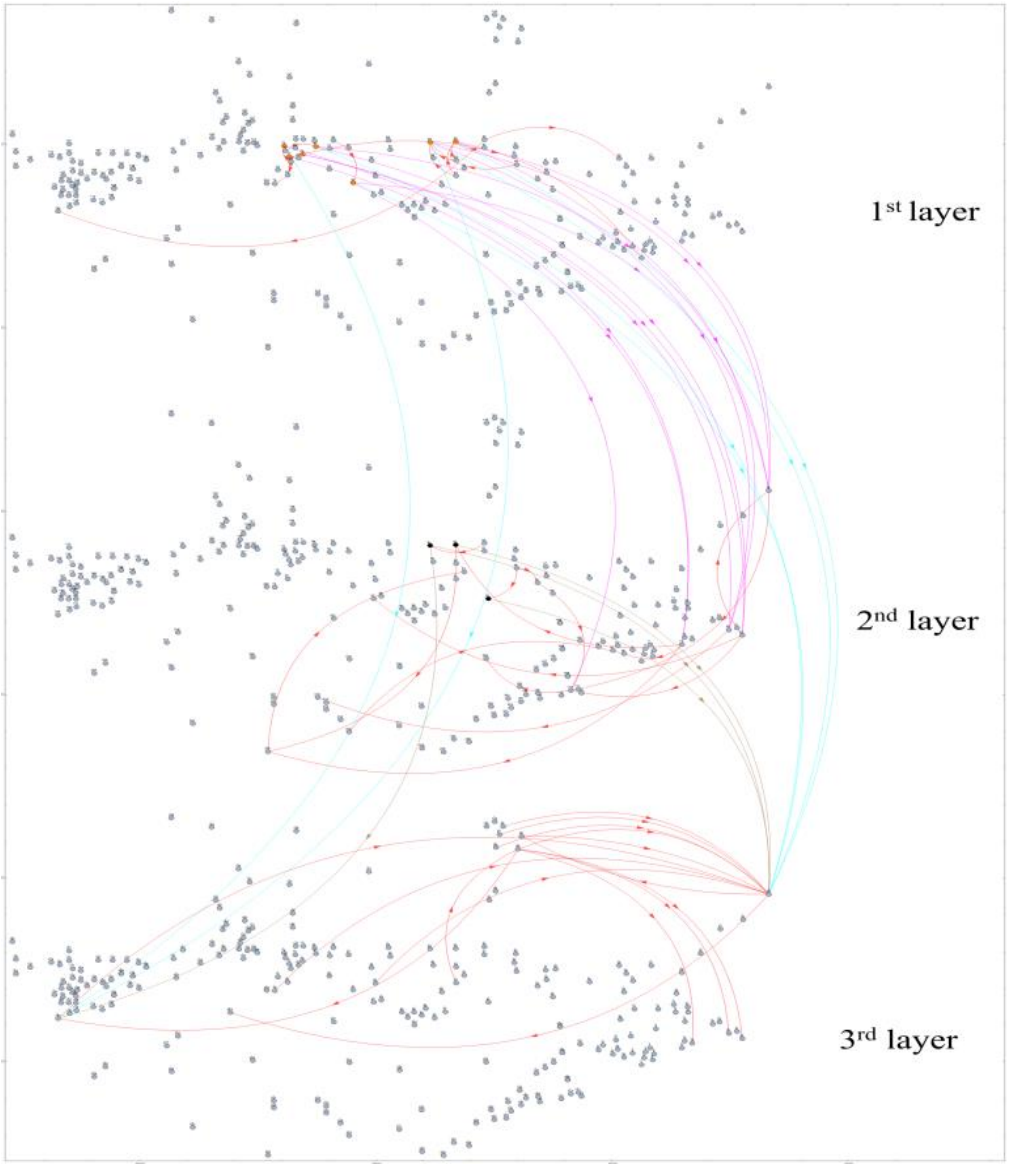

Figure 2-22. Schematic diagram of key inter-layer links, key inter-layer components, and key intra-layer links (key inter-layer links between the 1st and 2nd layers, between the 1st and 3rd layers, and between the 2nd and 3rd layers are magenta, brown and cyan arrows, respectively; intra-layer links in each layer are red arrows; key inter-layer components involved in the key inter-layer links between the 1st and 2nd layers, between the 1st and 3rd layers, and between the 2nd and 3rd layers are orange, pink and black dots; key inter-layer components involved in the key inter-layer links between the 1st and 3rd layers are also located in the 1st layer).

Note that the set of key inter-layers links depends on the selection of the key intra-layer links. An inter-layer link could become an intra-layer link in another case and vice versa. From the number of inter-layer links and key inter-layer links between different layers, we can find that the correlation between the first and second layers is tighter than any other two layers. Many inter-layer links connect the key intra-layer links in the first layer to those in the second layer. This observation can help to propose an integrated mitigation strategy by combing the key intra-layer links from the two layers and weaken them in different stages of cascading outages.

2.6.3 Multi-Layer Interaction Graph for Increased System Load

The variation of system topology, unit commitments and system load level will definitely affect the multi-layer interaction graph. Here the influence of the load variation on the multi-layer interaction graph is analyzed. Under this case, the load level of the system is scaled up by 10% which is uniformly added to each load bus of the system. The new database with the same number of cascades as the original database is generated for the new system load level. The three layers with key intra-layer links and components are shown by Figs. 2-23-2-25.

The identified key intra-layer links in each layer with 110% and 100% load levels of the system are compared. The numbers of overlapped links by comparing different numbers of key intra-layer links are shown in Fig. 2-26. From a sensitivity study on the number of overlapped links, the key intra-layer links in the first and second layers are more sensitive to the global load variation of the system than those in the third layer.

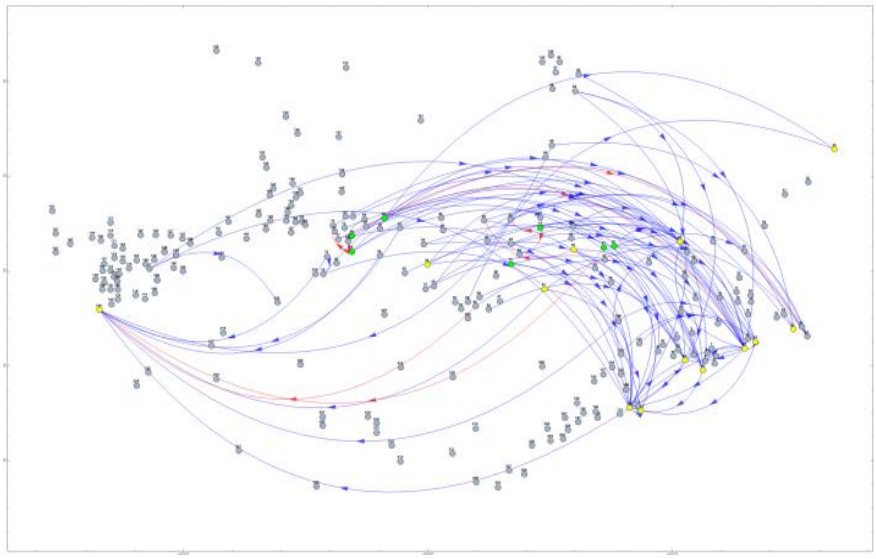

Figure 2-23. Top-100 key intra-layer links and top-20 key intra-layer components in terms of the number of line outages at 110% system load (red/blue arrows are overlapped/different links compared to 100% system load; green/yellow dots are overlapped/different components compared to 100% system load).

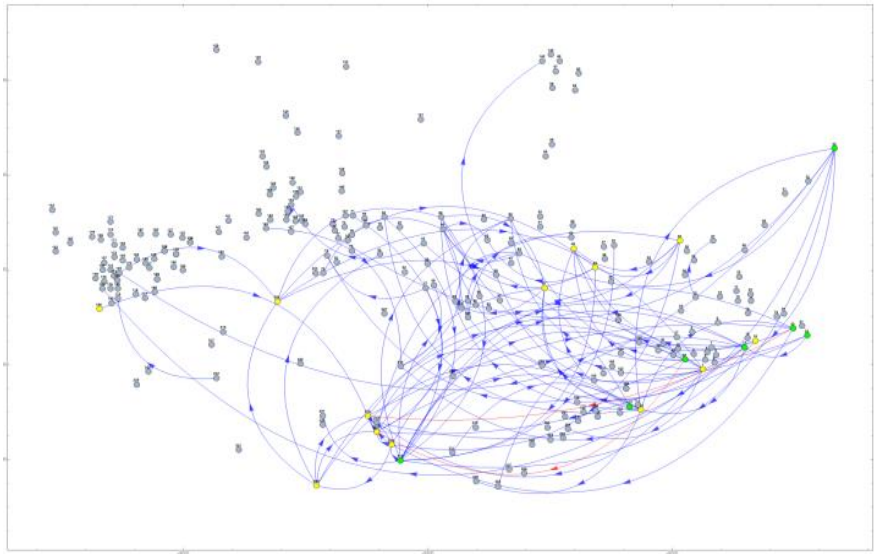

Figure 2-24. Top-100 key intra-layer links and top-20 key intra-layer components in terms of the amount of load shedding with 110% system load.

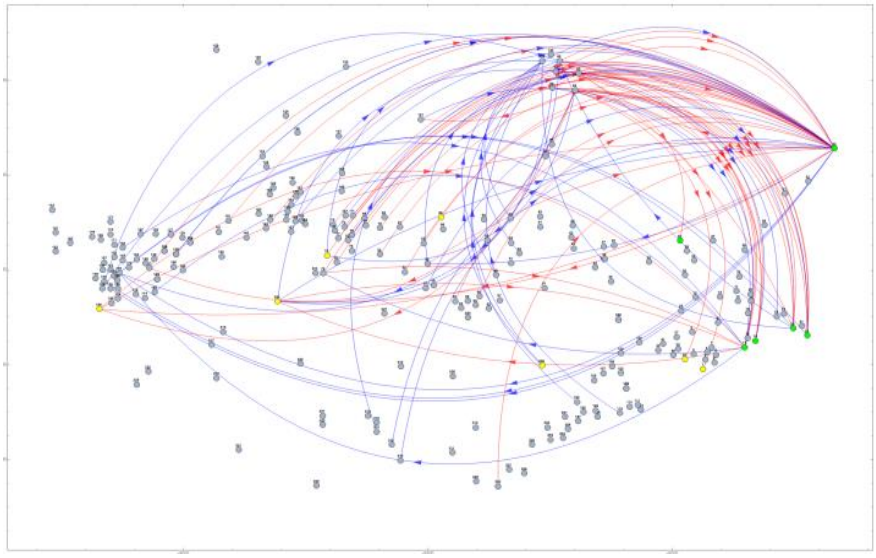

Figure 2-25. Top-100 key intra-layer links and top-20 key intra-layer components in terms of the propagated electrical distance with 110% system load (excluding 7 isolated components).

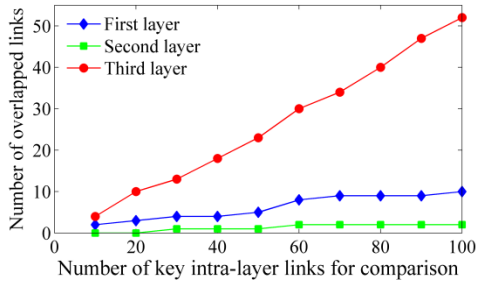

Figure 2-26. Numbers of overlapped links for different numbers of key intra-layer links.

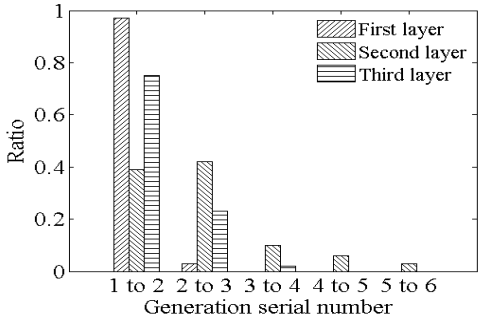

Figure 2-27. Distribution of key intra-layer links in transitions of generations.

2.6.4 Distribution of Key Intra-Layer Links among Generations

A key intra-layer link in a specific layer may connect two consecutive generations in either early or later stages of a cascade. For each of the three layers, the distribution of the top-100 key intra-layer links in transitions between generations is shown in Fig. 2-27. The maximum number of generations involved in the links is 6.

The majority of the key intra-layer links of the first layer connect generations 1 and 2, and also the majority of the key intra-layer links in the third layer connect generations 1 and 2. These observations suggest that reducing line outages to limit the spreading of outages should have a high priority in the early stage of cascading outages, and the system operators should pay more attention to the first and third layers of the interaction graph. The key intra-layer links in terms of load shedding are more dispersed and mainly connect generations 1, 2, and 3. The increased percentage of key links from generations 2 to 3 indicates that load shedding is the main problem in later stages. It is reasonable to have more load shedding in later stages of a cascading outage.

These observations enlighten us to propose the *Strategy-LOLS* mentioned in Section 2.4.1, i.e. an integrated mitigation strategy to weaken the key intra-layer links in the first layer in the early stage (generations 1 to 2) of cascading outages and key intra-layer links in the second layer in the later stage of cascading outage (generations 2 to 3). In fact, the majority of cascades in the database contain 3 generations and the average number of generations is 3.14.

2.6.5 Validation of Mitigation Strategies

When the source component of a key intra-layer link fails, the destination component may become overloaded and can be tripped by protective relays. Each mitigation strategy considered here reduces the probability of the relay tripping to 10%. The number (i.e. K) of intra-layer links to be weakened is set up as 20 for all the mitigation strategies. For *Strategy-3L,* the numbers of key intra-layer links in the first, second, and third layers are set up as 7, 7, and 6,

respectively. The case for *Strategy-R* is simulated for 20 times. These mitigation strategies are compared in terms of three assessment indices as shown in Table 2-7.

Strategy-LO can significantly reduce the average number of line outages by 24.36%. *Strategy-ED* can reduce the average number of line outage but not significantly because the first and third layers show relevant properties from Fig. 2-19 and Fig. 2-20. *Strategy-LS* and *Strategy-R* may even increase the number.

Similarly, *Strategy-LS* significantly reduces the average amount of load shedding by 69.21%. However, *Strategy-ED* and *Strategy-LO* reduce it slightly and *Strategy-R* even increases it for some cascades.

The average propagated electrical distance can be reduced by 18.87% by *Strategy-ED*. *Strategy-LO* only reduces it slightly and *Strategy-LS and Strategy-R* may even increase the propagation.

The results validate that a specific problem, e.g. number of line outages, amount of load shedding, and propagated electrical distance, can be effectively mitigated by a strategy that weakens key intra-layer links from a matched layer.

Strategy-R may even increase the average number of line outages, load shedding and average electrical distance, which indicates the ineffectiveness of the random mitigation strategy.

Strategy-LS increases the average number of line outages and the average propagated electrical distance. This is because the mitigation strategy is not to stop the propagation of outages but change the direction of propagation. Weakening key links of a wrong type may even bring negative impacts.

Strategy-3L reduces the average number of line outages, the average amount of load shedding, and the average propagated electrical distance by 26.54%, 65.31%, and 15.65%. It is obvious since the key intra-layer links are combined from the three layers.

Strategy-LOLS is applied to different stages of cascading outages with the key intra-layer links from the two layers. A link will be weakened if it is between generations 1 and 2 and belongs to the top-10 key links of the first layer, or if it is

between generations 2 and 3 and belongs to the top-10 key links of the second layer. It reduces the average number of line outages and average amount of load shedding by 25.78% and 56.46%, respectively. This validates that the key links in the first layer are highly relevant to early stages of outages and key links in the second layer are more involved in later stages of outages.

In general, for each link, the number of its mitigation under *Strategy-3L* is larger than that under *Strategy-LOLS*. That is because a link may appear in different stages of outages varying from different cascades. *Strategy-3L* will weaken it wherever it appears. However, *Strategy-LOLS* only weaken it when it appears in a pre-determined stage of cascading outages.

Table 2-7. Influences of Different Mitigation Strategies on Different Assessment Indices.

Mitigation Strategies	Average Number of Line Outages	Average Amount of Load Shedding	Average Propagated Electrical Distance
Strategy-LO	-24.36%	-3.29%	-6.44%
Strategy-LS	+3.67%	-69.21%	+4.52%
Strategy-ED	-8.15%	-4.73%	-18.87%
Strategy-3L	-26.54%	-65.31%	-15.65%
Strategy-LOLS	-25.78%	-56.46%	-9.11%
Strategy-R	-3.23% to +4.21%	-6.59% to +7.94%	-1.66% to +2.79%

It is suggested that the system operators can monitor the propagation of outages based on the first and third layers of the interaction graph during the early stage of outages. With the spread of cascading outages, more attentions should be paid to the second layer. Then the strategy of weakening key intra-layer links of the corresponding layer can be applied, which is shown by *Strategy-LOLS* as one example. Incomplete information from a single layer interaction graph could mislead the system operators to take inappropriate control actions and may enlarge the propagation of outages undesignedly. The multi-layer interaction graph can provide comprehensive information helpful for online monitoring and mitigation of cascading outages.

2.6.6 Determining the Number of Cascades

As an example, the number of cascades for identifying top-100 key intra-layer links in the second layer is presented here. The number of cascades in other layers can be determined by the same approach.

Set T_M =100, M_1=100, ΔM =100, and τ =0.01. Fig. 2-28 shows how $R(M_i)$ and its standard deviation σ_i change with the number of cascades. They become flat when cascades reach a specific number M^{min}, which is around 3600, meaning that the top-100 key links in the second layer can be identified using 3600 cascades. The number of cascades needed for a database can be determined as 5200, which is the maximum value among all M^{min}'s for three layers. The number of cascades used in this chapter, i.e. 10000, is large enough.

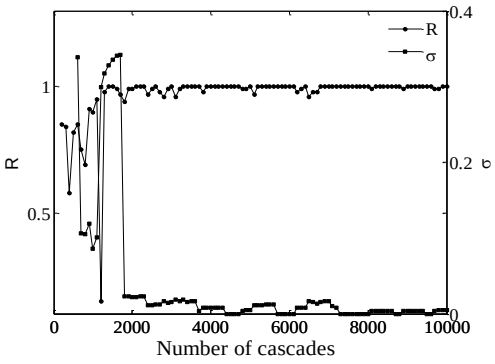

Figure 2-28. R and σ for different numbers of cascades.

2.7 Conclusions of this Chapter

This chapter first extends the interaction network and interaction model proposed in [27] to the NPCC power system to identify the key links and components that play important roles to the propagation of cascading outages. Then it proposes a multi-layer interaction graph on cascading outages of power systems as an extension of the single layer interaction network proposed in [27]. It intends to assist the system operators in predicting propagation of outages and making decisions on mitigation actions. The multi-layer interaction graph can be obtained offline from a database of simulated or historical cascades and then applied online. The graph comprises multiple layers respectively depicting key

components and key links that contribute the most to outage propagation from different perspectives, i.e. the number of line outages, the amount of load shedding and the electrical distance of outage propagation. Two types of key links, i.e. key intra-layer link and key inter-layer link and their corresponding key components are proposed and defined. They together provide comprehensive information for the monitoring and mitigation of cascading outages. Meanwhile, key intra-layer link based mitigation strategies corresponding to each layer and two integrated mitigation strategies are also proposed and validated on the NPCC 140-bus system.

CHAPTER THREE
SIMULATION OF CASCADING OUTAGES USING A POWER-FLOW MODEL CONSIDERING FREQUENCY

3.1 Introduction

Many models and approaches for the simulation of cascading outages mentioned in Chapter 1 can be categorized as steady-state models, quasi-dynamic models and dynamic models basically. For instance, the CASCADE, DCSIMSEP, branching process, OPA, Hidden failure, and Interaction model can be characterized as steady-state models. The multi-timescale quasi-dynamic model considers system steady-state behaviors in different timescales. And the COSMIC and Hybrid models are uses dynamic simulation to simulate cascading outages.

The major drawback of dynamic simulation is its intense time consumption in large system models. Also as mentioned by [42], although nonlinear transients are often prominent in fast cascade stages, in other cases the transients fade away and system reaches steady state quickly, so the power flow based steady-state or quasi-dynamic models are sufficient for representing the cascading process instead of dynamic simulation.

Frequency is an important indicator of the real-time balance between active power of generation and load, especially during cascading outages. Abnormal frequency deviation may trigger under-frequency load shedding (UFLS) [105][106] and generator frequency protection, causing large amount of loss in generation and load, so it is a significant contributing factor of cascading outages and blackouts [107]. A conventional power flow model assumes the system frequency to be always constant by means of one or multiple swing buses to eliminate any active power imbalance. However, ideal swing buses with infinite capability of power balancing and frequency regulation do not exist in real power systems. In practice, frequency is regulated in a distributed way: first,

governors of generators regulate their speeds and active power outputs following their designed regulation strategies; second, frequency-sensitive loads in a system also vary their actual power consumptions with the frequency deviation. Therefore, it is important to consider frequency-related system behaviors and operations in the simulation of cascading outages.

Since the 1970's, efforts have been made to include frequency deviation in power flow models [108]. In ref. [109] published in 1986, a "dynamic load flow" (DLF) algorithm in which the unbalanced active power is allocated among all generators with speed controllers was proposed, but such a model cannot obtain the frequency. In ref. [110], the frequency is taken as an unknown variable in DLF calculation. In recent decades, for the purposes of fast simulation or analysis with large power systems, many power flow models considering frequency have been proposed [111]-[121], which mainly incorporate power-frequency characteristics into a power-flow model and consider power-frequency characteristics with loads, speed governors of generators or automatic generation control (AGC). Refs. [112] and [113] consider power-frequency and voltage dependent characteristics of loads and speed governors of generators in power flow models with dispatcher training simulators. Ref. [114] considers power-frequency and voltage dependent characteristics with loads, voltage-reactive power characteristic of generators, speed governors of generators in power flow models for security assessment of power systems. Refs. [115]-[117] incorporate power-frequency characteristics of active loads and speed governors of generators into power flow models for risk assessment. Other fields to apply such power-flow models include microgrid control [118][119] and analyses involving wind generation [120][121]. Analysis and simulation of cascading outages can also apply such models. Refs. [122] and [123] incorporate frequency deviation into cascading outage simulation based on a DC power flow model, in which frequency deviation is calculated directly from power-frequency characteristics of generators and loads.

This chapter proposes a novel steady-state approach for simulation of

cascading outages with frequency-related system characteristics and operation actions such as frequency deviation, power-frequency characteristics of generators and loads, UFLS scheme, and generator frequency protection [124]. The contributions of this chapter are mainly in these three aspects. First, the proposed approach integrates calculation of frequency deviation into a power flow model like [109] (called “DLF model” in the rest of the chapter since it is developed and inspired from the DLF algorithm in [108]-[116]). Thus, power flow results are able to reflect active power imbalance and address power-frequency characteristics of generators and loads. Second, an AC optimal power flow model considering frequency deviation (for short, AC-OPFf) is proposed, which determines remedial control against system collapse indicated by divergent power flow calculation. Thanks to the consideration of frequency deviation, the DLF and AC-OPFf models enable more credible steady-state simulation on a power system under cascading outages. Third, the proposed approach enables the UFLS scheme and generator frequency protection to be modeled, which is critical but has not yet been addressed by existing steady-state approaches for simulation of cascading outages.

The rest of this chapter is organized as follows. Section 3.2 presents the proposed simulation approach for cascading outages. It first introduces the DLF model employed in the proposed approach, proposes the novel AC-OPFf model, and then presents the UFLS scheme as well as generator frequency and line protection models used in the proposed approach, and finally compares the procedure of the proposed approach with a conventional approach for simulation of cascading outages. Comprehensive case studies are presented in Section 3.3, which first benchmarks the results of the DLF model with that of time-domain simulation on a two-area system, and then tests the proposed approach using many cascading outage scenarios on the IEEE 39-bus system and NPCC 48-machine, 140-bus systems. The simulated cascading outages are analyzed and compared with those from the conventional approach. Finally, Section 3.4 draws the conclusions.

3.2 Proposed Simulation Approach for Cascading Outages

This section first briefly introduces the DLF model and proposes the AC-OPFf model, which is compared with a conventional AC-OPF model. Then, the section presents the UFLS scheme, as well as the generator and line protection models to be used in the proposed simulation approach.

3.2.1 DLF Model

The static power-frequency characteristics (SPFCs) of a load at bus *i* can be approximated by

$$P_{Di} = P_{D0i}(1 + D_i f_d), \quad f_d = f - f_n \tag{3.1}$$

where f is the system frequency, f_n is the nominal frequency, f_d is the frequency deviation, P_{D0i} is the active power load at f_n, and constant D_i quantifies frequency-sensitivity of the load, showing how active the load changes with frequency deviation.

When active power balance of the system cannot be maintained at the nominal frequency, a frequency deviation exists. The speed governor of a generator at bus *i* can automatically regulate its steady-state output P_{Gi} according to its regulation factor R_i:

$$P_{Gi} = P_{G0i} - f_d / R_i, \quad P_{Gi,\min} \le P_{Gi} \le P_{Gi,\max} \tag{3.2}$$

where P_{G0i} is its active power output at f_n, and $P_{Gi.min}$ and $P_{Gi.max}$ are the lower and upper limits of active power output.

Consider an *n*-bus power system having *m* PQ buses (numbered from 1 to *m*), *n*-*m*-1 PV buses (numbered from *m*+1 to *n*-1), and a slack bus with No. *n*. The DPF calculation targets at eliminating active power mismatches at all *n* buses and reactive power mismatches at *m* PQ buses.

$$\Delta P_i = P_{Gi} - P_{Di} - V_i \sum_{j \in i} V_j (G_{ij} \cos\theta_{ij} + B_{ij} \sin\theta_{ij}) \quad i = 1, ..., n \tag{3.3}$$

$$\Delta Q_i = Q_{Gi} - Q_{Di} - V_i \sum_{j \in i} V_j (G_{ij} \sin\theta_{ij} - B_{ij} \cos\theta_{ij}) \quad i = 1, ..., m \tag{3.4}$$

where P_{Gi} and P_{Di} are calculated from (3.1)-(3.2), Q_{Gi} and Q_{Di} are the reactive power of generation and load at bus *i*, which are assumed frequency-independent. V_i is the voltage magnitude at bus *i*, $\theta_{ij}=\theta_i-\theta_j$ is the phase angle difference between buses *i* and *j*, and G_{ij} and B_{ij} are the real and imaginary elements in the bus admittance matrix.

Mismatches ΔP_i and ΔQ_i make up an *n*-vector $\Delta\mathbf{P}_{n\times1}$ for all buses and an *m*-vector $\Delta\mathbf{Q}_{m\times1}$ for all PQ buses. Note that there are *n*+*m* unknown variables including frequency deviation f_d, *n*-1 voltage angles and *m* voltage magnitudes. The DPF problem can be solved using the Newton-Raphson method by solving the corrections:

$$\begin{bmatrix}\Delta\mathbf{P}_{n\times1}\\ \Delta\mathbf{Q}_{m\times1}\end{bmatrix}=\begin{bmatrix}\Delta\mathbf{P}_{(n-1)\times1}\\ \Delta P_n\\ \Delta\mathbf{Q}_{m\times1}\end{bmatrix}=\mathbf{J}\begin{bmatrix}\Delta\boldsymbol{\theta}_{(n-1)\times1}\\ \Delta f_d\\ \mathbf{V}^{-1}_{m\times m}\Delta\mathbf{V}_{m\times1}\end{bmatrix} \tag{3.5}$$

where $$\mathbf{J}=\begin{bmatrix}\mathbf{J_1}_{\,(n-1)\times(n-1)} & \dfrac{\partial\Delta\mathbf{P}}{\partial f_d}_{\,(n-1)\times1} & \mathbf{J_2}_{\,(n-1)\times m}\\ \dfrac{\partial\Delta P_n}{\partial\boldsymbol{\theta}}_{\,1\times(n-1)} & \dfrac{\partial\Delta P_n}{\partial f_d} & \mathbf{N}_{1\times m}\\ \mathbf{J_3}_{\,m\times(n-1)} & \mathbf{0} & \mathbf{J_4}_{\,m\times m}\end{bmatrix}$$

In (3.5), ΔP_n is the active power mismatch of the slack bus, which will be eliminated unlike that in conventional power flow calculation, $\Delta\mathbf{P}_{(n-1)\times1}$ includes active power mismatches of the other buses, $\Delta\boldsymbol{\theta}_{(n-1)\times1}$ is the vector of angle corrections for all buses except for the slack bus, Δf_d is the correction of system frequency deviation, $\mathbf{V}^{-1}_{m\times m}$ is a diagonal matrix made of the reciprocals of V_i's of *m* PQ buses, and $\Delta\mathbf{V}_{m\times1}$ is the vector of corrections of V_i's for all PQ buses.

The Jacobian matrix **J** is an (*n*+*m*)-dimensional square matrix containing partial derivatives of the active and reactive power injections with respect to voltage angles, magnitudes and f_d. The elements of $\mathbf{J_1}$, $\mathbf{J_2}$, $\mathbf{J_3}$ and $\mathbf{J_4}$ in the *i*-th

row and *j*-th column are $\frac{\partial P_i}{\partial \theta_j}$, $\frac{\partial P_i}{\partial V_j}V_j$, $\frac{\partial Q_i}{\partial \theta_j}$, and $\frac{\partial Q_i}{\partial V_j}V_j$, i.e. the same as the corresponding elements in the Jacobian matrix of conventional power flow model. Let the bus angle θ_n of the slack bus be zero. The other elements of **J** are:

$$\left(\frac{\partial \Delta \mathbf{P}}{\partial f_d}\right)_i = \frac{\partial \Delta P_i}{\partial f_d} = \begin{cases} -P_{D0i}D_i & \text{for PQ buses} \\ -(P_{D0i}D_i + \frac{1}{R_i}) & \text{for PV and slack buses} \end{cases}, i = 1,...,n \tag{3.6}$$

$$\left(\frac{\partial \Delta P_n}{\partial \boldsymbol{\theta}}\right)_j = \frac{\partial \Delta P_n}{\partial \theta_j} = -V_n V_j (G_{nj}\sin\theta_j + B_{nj}\cos\theta_j),\ j = 1,...,n-1 \tag{3.7}$$

$$\left(\mathbf{N}\right)_j = \frac{\partial \Delta P_n}{\partial V_j}V_j = -V_n V_j (G_{nj}\cos\theta_j - B_{nj}\sin\theta_j),\ \ j = 1,...,m \tag{3.8}$$

Solving the DLF model by the N-R method does not bring much more computational burden than solving a conventional power flow model because only one unknown variable and one equation are added. Note that by considering the active power generation limits, constraint $P_{Gi,\min} \le P_{G0i} - f_d / R_i \le P_{Gi,\max}$ is checked with updated f_d at each iteration of the N-R method. If the constraint is violated, freeze P_{Gi} at the limit.

From (3.5), the Jacobian matrix **J** with the DLF model has the similar sparsity to that with the conventional power flow model, but has more nonzero elements because of the introduced frequency deviation f_d. **J** with the DLF model has at most 2*n*+*m*-1 more nonzero elements than that of the conventional power flow model. Consider the total number of elements of the **J** is $(n+m-1)^2$ for a conventional power flow model or to be $(n+m)^2$ for the DLF model, the ratio of $2n+m-1$ to $(n+m-1)^2$ or $(n+m)^2$ is very small for a large power system. Therefore, the **J** with the DLF model is still quite sparse. For example, the ratio $(2n+m-1)/(n+m-1)^2$ is just equal to 0.007 for the NPCC 48-machine, 140-bus power system.

Finally, there are the following remarks on the DLF model used in the proposed approach:

Remarks:

1) In industry practices, AGC is usually disabled in simulation of cascading outages, so this chapter does not consider AGC or secondary frequency regulation in the proposed approach.

2) Reactive power loads are less sensitive to a frequency deviation than active power loads, and are often assumed frequency-independent in refs. [115]-[117], which is also assumed so in this chapter.

3) In a conventional power flow model, buses are categorized into PQ buses, PV buses and swing buses. The DLF model may inherit those bus types [125], which indicate the quantities that are basically unchanged. For instance, P_{D0i} in (3.1) and P_{G0i} in (3.2) respectively correspond to "P" components in PQ and PV buses. In fact, P_{D0i} and P_{G0i} slightly vary with frequency deviation around certain constant values. Strictly speaking, PV and PQ buses in a DLF model only maintain constant voltage magnitudes and reactive power injections. Finally, only one swing bus is needed for the DLF model, which is mainly used as a reference bus for voltage angles.

3.2.2 Dynamic Load Flow Model

During cascading outage simulation, calculation with the DLF model described by (3.1)-(3.8) may diverge, indicating a significantly stressed condition or event system collapse, which can be mitigated by remedial control such as generation redispatch and load shedding. The proposed AC-OPFf model is presented as (3.9) in Table 3-1 to model a centralized remedial control scheme. It is compared with a conventional AC-OPF model (3.10) side by side about the objective function and constraints.

In the AC-OPFf model, the objective function is to keep the largest remaining active power load after remedial control. The weighting factor λ_i quantifies the importance of load at bus i. The control variables of AC-OPFf

model are P_{Gi}, P_{Di}, Q_{Gi}, Q_{Di}, V_i, θ_i, and f_d, respectively. Here P_{Gi} and P_{Di} are corresponding to equations (3.1) and (3.2). First two constraints are power flow equations (3.9*a* and 3.9*b*). The rest of constraints are about power generations (3.9*c* and *3.*9*d*), bus voltage magnitudes (3.9*e* and 3.9*f*), loads (3.9*g* and 3.9*h*), branch flows (3.9*i*), constant power factor (3.9*j*), and frequency deviation (3.9*k*). Note that in the AC-OPFf model, one equality constraint (3.9a) and three inequality constraints, (3.9*c*), (3.9*g*), and (3.9*k*), involve frequency deviation, so the final calculated frequency deviation may not meet its upper or lower limit in (3.9k) if a limit in (3.9*c*) or (3.9*g*) is met.

Table 3-1. AC-OPFf and AC-OPF Models.

AC-OPFf	**AC-OPF**
$\min\ -\sum_i \lambda_i P_{Di}$	$\min\ -\sum_i \lambda_i P_{Di}$
s.t.	*s.t.*
$\Delta P_i = P_{Gi} - P_{Di}$	$\Delta P_i = P_{Gi} - P_{Di}$
$-V_i \sum_j V_j (G_{ij} \cos\theta_{ij} + B_{ij} \sin\theta_{ij}) = 0 \quad (3.9a)$	$-V_i \sum_j V_j (G_{ij} \cos\theta_{ij} + B_{ij} \sin\theta_{ij}) = 0 \quad (3.10a)$
$\Delta Q_i = Q_{Gi} - Q_{Di}$	$\Delta Q_i = Q_{Gi} - Q_{Di}$
$-V_i \sum_j V_j (G_{ij} \sin\theta_{ij} - B_{ij} \cos\theta_{ij}) = 0 \quad (3.9b)$	$-V_i \sum_j V_j (G_{ij} \sin\theta_{ij} - B_{ij} \cos\theta_{ij}) = 0 \quad (3.10b)$
$P_{Gi,\min} \le P_{Gi} \le P_{Gi,\max} \quad (3.9c)$	$P_{Gi,\min} \le P_{Gi} \le P_{Gi,\max} \quad (3.10c)$
$Q_{Gi,\min} \le Q_{Gi} \le Q_{Gi,\max} \quad (3.9d)$	$Q_{Gi,\min} \le Q_{Gi} \le Q_{Gi,\max} \quad (3.10d)$
$V_{i,\min} \le V_i \le V_{i,\max} \quad (3.9e)$	$V_{i,\min} \le V_i \le V_{i,\max} \quad (3.10e)$
$-\frac{\pi}{2} \le \theta_i \le \frac{\pi}{2} \quad (3.9f)$	$-\frac{\pi}{2} \le \theta_i \le \frac{\pi}{2} \quad (3.10f)$
$0 \le P_{Di} \le P_{D0i} \quad (3.9g)$	$0 \le P_{Di} \le P_{D0i} \quad (3.10g)$
$0 \le Q_{Di} \le Q_{D0i} \quad (3.9h)$	$0 \le Q_{Di} \le Q_{D0i} \quad (3.10h)$
$\lvert S_{ij} \rvert \le S_{ij,\max} \quad (3.9i)$	$\lvert S_{ij} \rvert \le S_{ij,\max} \quad (3.10i)$
$Q_{Di} P_{D0i} = \frac{P_{Di} Q_{D0i}}{(1 + D_i f_d)} \quad (3.9j)$	$Q_{Di} P_{D0i} = P_{Di} Q_{D0i} \quad (3.10j)$
$f_{d\min} \le f_d \le f_{d\max} \quad (3.9k)$	

In the conventional AC-OPF model, the objective function is also to keep the largest remaining active power load after control. The control variables of AC-OPF model are P_{Gi}, P_{Di}, Q_{Gi}, Q_{Di}, V_i, and θ_i, respectively. The constraints shown

by (3.10a)-(3.10j) are similar to those of the AC-OPFf model except that frequency deviation is not considered.

Compared with the AC-OPF model, the AC-OPFf model is more general with consideration of frequency deviation. In fact, the AC-OPF model can be regarded as a special case of the AC-OPFf model with f_d equals zero.

The optimality of the final AC-OPF or AC-OPFf solution depends on what algorithm is used and how much gap to the true global optimum is acceptable. In the simulation of cascading outages, introduction of the AC-OPF or AC-OPFf model does not aim at finding the best control strategy; rather, the mainly purpose is to mimic remedial control by the central control room like the OPF module in OPA models [39,40,126]. Therefore, the AC-OPF or AC-OPFf model aims to find a new feasible power flow solution when system collapse happens. In reality, if the proposed simulation approach is applied by power companies, they may easily replace the AC-OPF or AC-OPFf model by their central remedial control strategies.

3.2.3 Under-Frequency Load Shedding Scheme

The inclusion of frequency deviation in the DLF model also enables UFLS to be simulated when there is a substantial, unacceptable frequency decline. A practical UFLS scheme is typically designed to shed 25-30% of the system load in steps with pre-designated loads in each reliability coordinator region when frequency drops to a low threshold [2]. In addition, more load will be progressively shed if frequency decline continues.

As given in Table 3-2, this chapter adopts an UFLS scheme in the simulation of cascading outages for the proposed approach based on the NERC UFLS reliability standard “PRC-006 NPCC” [127] for NPCC region.

Table 3-2. UFLS Scheme of NPCC for Different Load Buses.

100MW or More Load		50 MW or more and less than 100 MW		25 MW or more and less than 50 MW	
f_t (Hz)	L_p(%)	f_t (Hz)	L_p (%)	f_t (Hz)	L_p (%)
59.5	6.5	59.5	14	59.5	28
59.3	6.5	59.1	14	-	-
59.1	6.5	-	-	-	-
58.9	6.5	-	-	-	-

Note: f_t and L_p stand for frequency threshold and percentage of load shed.

In general, shedding active power load $\Delta P_{Di,UFLS}$ also cause curtailment of an amount of reactive power load $\Delta Q_{Di,UFLS}$. If the UFLS scheme is triggered, the percentage of active power load to be shed is determined by frequency thresholds in Table 3-2. Then the change in reactive power load is calculated by (3.11) assuming a constant power factor to be maintained.

$$\frac{\Delta Q_{Di,UFLS}}{\Delta P_{Di,UFLS}} = \frac{Q_{Di}}{P_{Di}} \tag{3.11}$$

3.2.4 Generator Frequency and Transmission Line Protections

Protective actions with generators and transmission lines may introduce additonal failures and uncertainties to system operations under cascading outages [128], [129]. Utilization of the DLF model enables simulatons of some frequency-related protecitve actions. Generator frequency and transmission line protections are modeled in the proposed approach.

As illustrated by Fig. 3-1, according to the characteristics of the turbine and power plant auxiliaries, the frequency span of a generator can be divided into three types of ranges [129]: (1) the normal operation range bounded by f_1 and f_2, (2) two restricted time operation ranges outside the normal range bounded by a lower limit f_L and an upper limit f_U, i.e. intervals [f_L, f_1] and [f_2, f_U], and (3) prohibited ranges lower than f_L or higher than f_U.

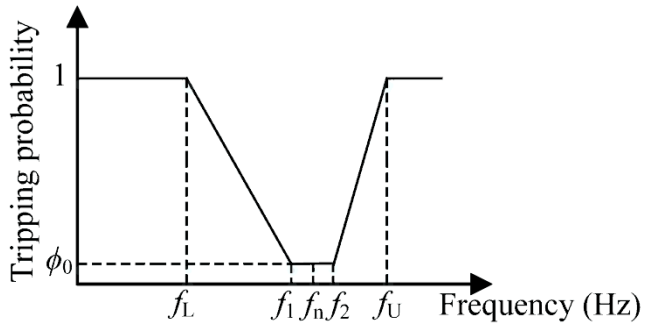

Figure 3-1. Relationship between generator trip probability and frequency.

The tripping probability $\phi(f)$ of generator i as a function of its frequency relay is shown in Fig. 3-1 and (3.12), where ϕ_0 is the unexpected action probability of generator frequency relay.

$$\phi(f)=\begin{cases}1 & f<f_L \text{ or } f>f_U \\ \dfrac{(\phi_0-1)f+f_1-\phi_0 f_1}{f-f_L} & f_L\le f\le f_1 \\ \phi_0 & f_1<f<f_2 \\ \dfrac{(1-\phi_0)f+\phi_0 f_U-f_2}{f_U-f_2} & f_2\le f\le f_U\end{cases} \tag{3.12}$$

The proposed approach models both the UFLS scheme and generator frequency protection, whose relay actions are in different timeframes. For example, the typical time delay of a UFLS scheme is 0.1s for the Eastern Interconnection [127] while the time delays of generator frequency relays vary from 0.1s to several hundreds of seconds depending on the severity of frequency deviation. Accordingly, the proposed simulation approach uses a module shown in Fig. 3-2 to coordinate the UFLS scheme and generator frequency protection, which performs UFLS for a higher priority than generator frequency protection as long as the criterion of triggering UFLS is satisfied. Only if UFLS is not triggered, generator frequency protection might be triggered at probability $\phi(f)$ defined by (3.12). This module is embedded into the proposed approach shown by Fig. 3-3 and represented by the block “UFLS and generator frequency protection module”.

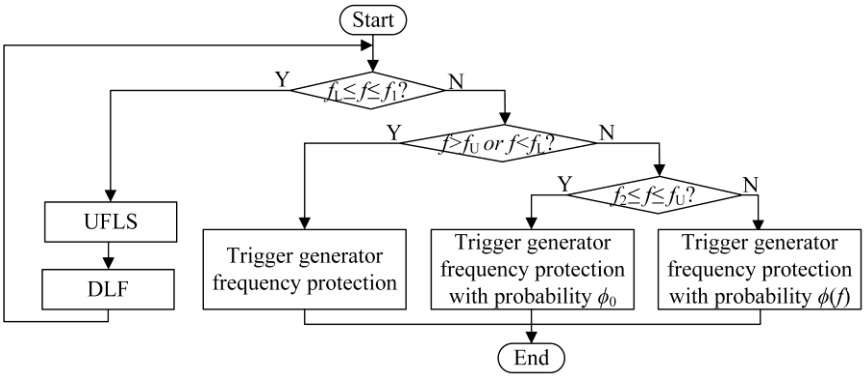

Figure 3-2. UFLS and generator frequency protection module.

With the propagation of cascading outages, a transmission line *i-j* is overloaded if its apparent power S_{ij} exceeds transmission capacity $S_{ij,max}$. Each overloaded line is tripped at a probability denoted by β and the probability of tripping the rest of lines is assumed to be $\varepsilon \times \left| \frac{S_{ij}}{S_{ij,\max}} \right|^{\tau}$. Here, ε is a base probability of any unwanted protection operation and should increase with the loading ratio of the line [39].

Remark**:** the proposed approach is based on a steady-state power flow model, so there is no explicit time evolution information. Unlike time-domain simulation, the tripping sequence and dynamic process on generators are not modeled in detail. In simulation by the proposed approach, once a generator is tripped, it will not be recovered until the end of simulation.

3.2.5 Simulation Procedure of the Proposed Approach

The proposed approach for the simulation of cascading outages is shown in Fig. 3-3. For comparison, a conventional approach for simulating cascading outages is shown in Fig. 3-4, which replaces the DLF and AC-OPFf models by the conventional power flow and AC-OPF models and does not consider the UFLS scheme and generator frequency protection. The block “Parameters and power network initialization” in both Fig. 3-3 and Fig. 3-4 performs conventional power flow calculation to obtain a base operating condition with nominal system frequency at 60Hz before the initial line outage is added at the next step.

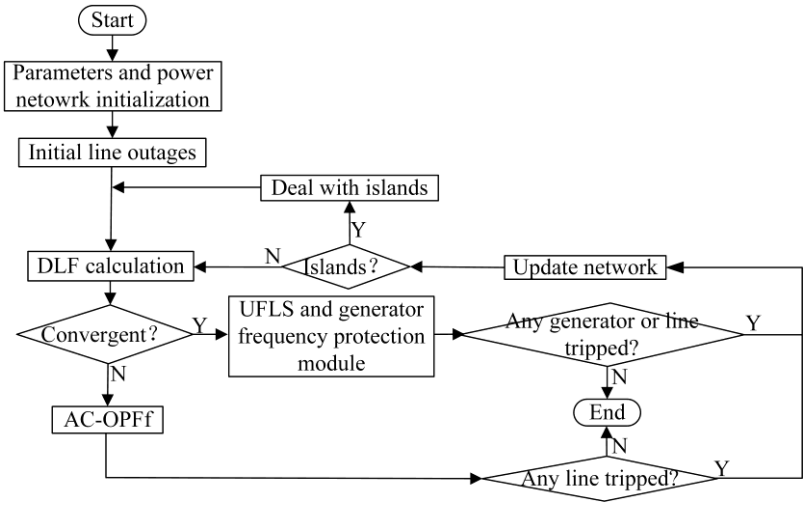

Figure 3-3. Simulation procedure of the proposed approach.

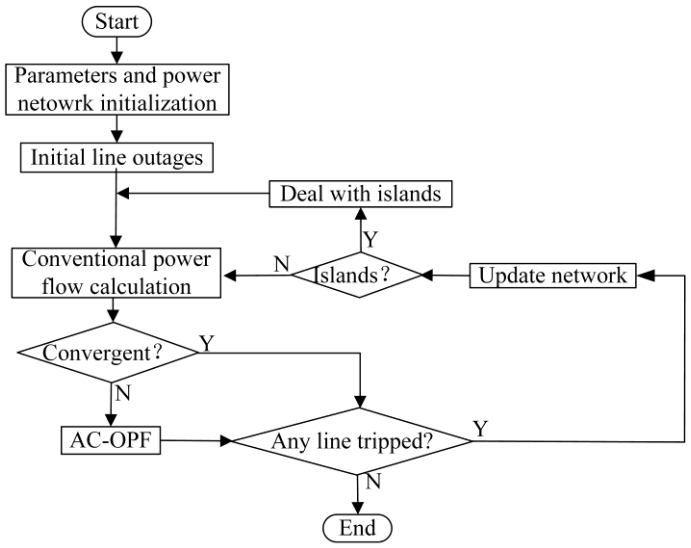

Figure 3-4. Simulation procedure of a conventional approach for comparison.

If the system separates into islands during cascading outages, the bus with the largest active power generation limit in each island can be chosen as the swing bus for that island according to the suggestions from [130]. For the DLF model, the function of the swing bus in each island is not to eliminate active power imbalance by itself; rather, it and other PV buses will compensate the active power imbalance depending on their power-frequency characteristics. The swing bus is then used as a reference bus for voltage angles in each island. If divergence is caused by a large imbalance in real power of any, the AC-OPFf or AC-OPF model will be performed to search for a new solution.

3.3 Case Studies

This section first uses Kundur's two-area, 4-machine power system [131] to benchmark the frequency calculated by the DLF model with the steady-state frequency obtained from time-domain simulation. Then, the section compares the simulation results from the proposed and conventional simulation approaches on the IEEE 39-bus power system and NPCC 48-machine, 140-bus power system [97], [132]. Both simulation approaches are implemented in MATLAB. Time-domain simulations are performed by TSAT of Powertech Labs. Parameters in test cases are following.

3.3.1 Selection of Parameters

In the DLF model, let D_i = 1 pu for all loads in (3.1), and R_i = 0.0056 pu in (3.2) for all generators, which is based on the system base (100 MVA) after the conversion from the value of R in Table III based on the generator base. Let λ_i =1 for all loads in AC-OPFf and AC-OPF models. Assume a maximum 0.5 Hz frequency deviation in constraint (3.9k), i.e. f_{dmin}=-0.5 Hz, f_{dmax}=0.5 Hz. The threshold to trigger the UFLS scheme is 59.5 Hz.

For generator frequency protection, set ϕ_0, f_L , f_1, f_n, f_2, and f_U as 0.002, 57 Hz, 59.5Hz, 60Hz, 60.5Hz, 61.7Hz, respectively in (3.12). For transmission line protection, let β=0.999, ε =0.001, and τ =10, the same as [39].

Table 3-3. Parameters for the Turbine-Governor Model.

Parameter	Value	Unit
Speed regulation factor R	0.05	pu
Turbine damping coefficient D_t	0	pu
Main steam control valve max limit V_{max}	1	pu
Main steam control valve min limit V_{min}	0.3	pu
Governor time constant T_1	0.5	s
Steam chest time constant T_2	1.0	s
Reheater time constant T_3	1.0	s

For time-domain simulation on the two-area system as a benchmark for frequency, all generators use the 2nd order classic model equipped with steam turbine-governor model "TGOV1" [133].

For the time-domain simulation on the NPCC power system, 24 generators are represented by a detailed round rotor model "GENROU" with an exciter model "ESDC1A" with PSS/E v32. [134] and the other 24 generators use the classic model. All generators are equipped with the "TGOV1" governor model using the same parameters in Table 3-3. All loads are modeled as frequency-dependent loads, i.e. "IEELBL" in PSS/E v32 and reactive powers of loads are assumed to be constant.

Transmission capacity limit $S_{ij,max}$ of each line of the IEEE 39-bus system is from the data with MATPOWER 6.0 toolbox. For the NPCC power system, $S_{ij,max}$ of each line is generated by two steps: 1) finding initial limits to make sure no overloading after any N-1 contingency; 2) increasing all limits by 20% to ensure some reliability margin.

3.3.2 Tests on the Two-area System

The two-area system has loads at buses 7 and 9. To compare steady-state system frequencies from the DLF model and time-domain simulation, three scenarios of load changes are tested: a) shedding the load on bus 7; b) shedding loads on both buses; c) increasing loads on both buses.

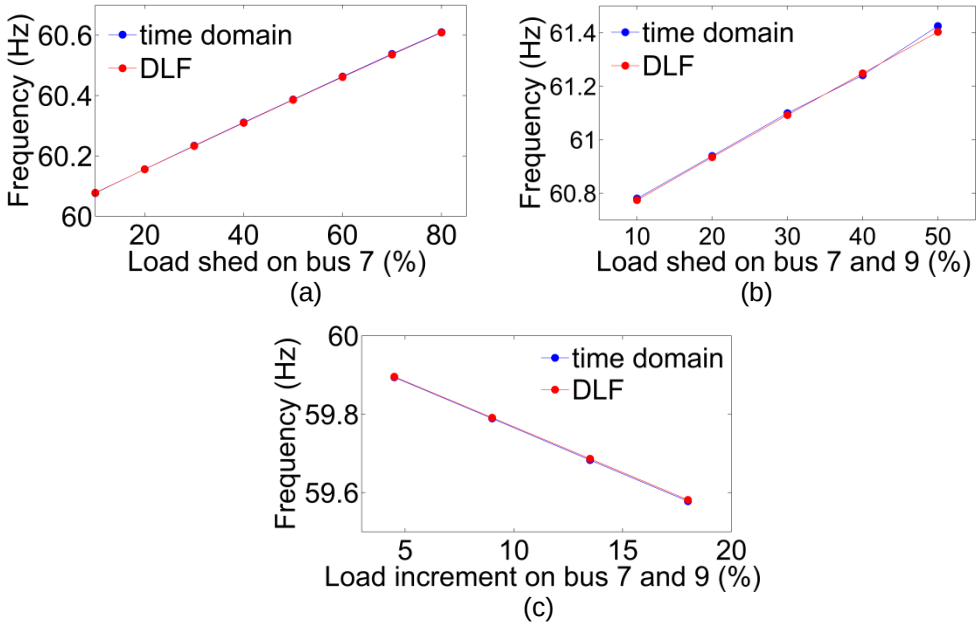

Figure 3-5. Frequency variations from the DPF model and time-domain simulation.

From Fig. 3-5, the steady-state frequencies from the DLF model in all three scenarios match well the time-domain simulation results, which verifies the accuracy of the steady-state frequency calculated from the DLF model.

3.3.3 Tests on the IEEE 39-bus System

The following four groups of tests are performed on the IEEE 39-bus system, whose purposes are provided:

1) Verifying the accuracy of steady-state frequency and the convergence characteristics with the DLF model. Two scenarios are designed, i.e. Scenarios 1 and 2.

2) Testing the UFLS and generator frequency protection module and the influence of SPFCs of loads on frequency. One scenario is used, i.e. Scenario 3.

3) Studying the influence of active power generation limits on frequency. Scenario 4 is designed to intentionally make the active power outputs of some generators reach their generation limits after the line outages.

4) Comparing the simulated cascading outages from the proposed approach based on Fig. 3-3 and conventional approach based on Fig. 3-4 statistically. Scenarios starting from all N-2 initial outages are considered.

Scenarios 1, 2, 3, and 4 of the above 1)-3) are shown on the IEEE 39-bus system in Fig. 3-6, distinguished in color.

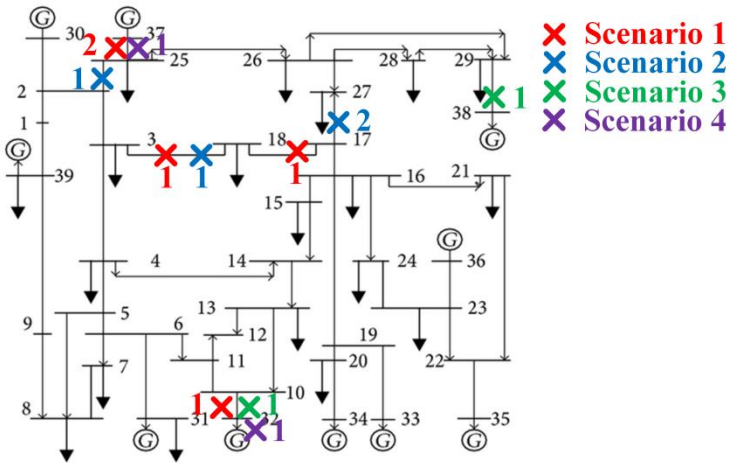

Figure 3-6. Scenarios 1, 2, 3, and 4 on the IEEE 39-bus system (outages are marked with crosses and labeled with stages).

1) *Verification of Steady-state Frequency*

Scenario 1 represents the line outages without causing system separation, and Scenario 2 represents the line outages that cause the system to separate into islands. Those two typical scenarios both introduce major disturbances, i.e. line outages, to cause large power imbalances and significant frequency deviations. The steady-state values of frequencies following the line outages are obtained from both the DLF model and time-domain simulation, and the results are compared.

Scenario 1: trip line 10-32, line 17-18, and line 3-18 in stage 1 and then trip line 25-37 in stage 2.

In time-domain simulation, two stages are intentionally separated by 100 seconds to make sure that the frequency can reach its steady-state before the next outage. Frequencies from time-domain and the DLF model for all stages are shown in Fig. 3-7. Only steady-state frequencies are compared. Generator 32 is tripped at stage 2 and then generator 37 is tripped at stage 3. The frequencies

calculated by the DLF model for the remaining system at stages 2 and 3 are close to those from time-domain so as to verify the accuracy of frequency calculated by the DLF model. The slight mismatch for the frequencies between them is because the power flow results of them are not exactly the same.

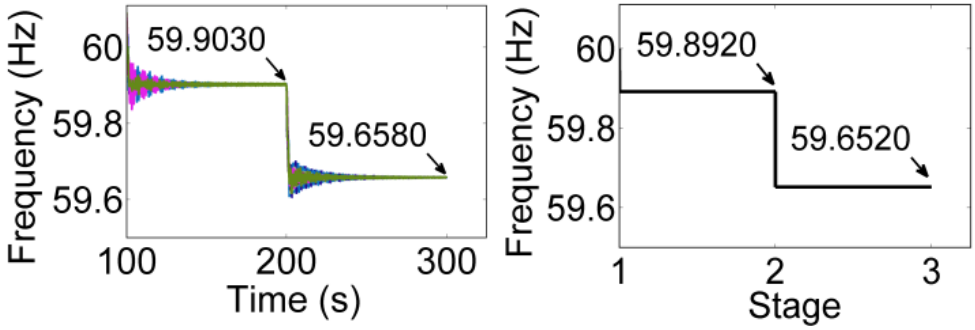

(a) From time-domain simulation (b) From the DPF model

Figure 3-7. Frequency variations of scenario 1.

Scenario 2: trip lines 2-25, 3-18 in stage 1 and trip line 17-27 in stage 2.

The system separates into two islands after line outages in stage 2, including a main island with 8 generators and a smaller island with generators 37 and 38 indicated by a dashed box in Fig. 3-8. The steady-state frequencies from the DLF model in stages 1 and 2 are very close to those from simulation as compared in Fig. 3-8.

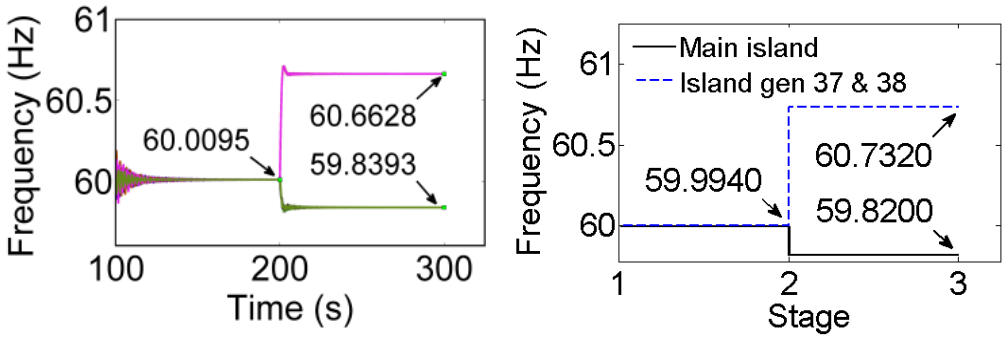

(a) From time-domain (b) From the DPF model

Figure 3-8. Frequency variations of scenario 2.

The convergence of N-R method in the DLF model is tested for Scenarios 1 and 2. Fig. 3-9 shows how mismatches of equations in solving the DLF model changed with iterations for the two stages of outages. Mismatches drop below the tolerance of 10^{-9} (pu) and power flows converge after 3 or 4 iterations. The mismatch (y-axis) takes the largest value among all ΔP_i and ΔQ_i at each iteration.

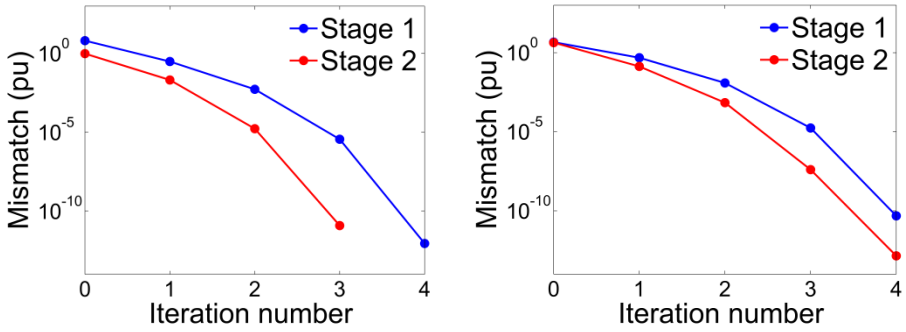

(a) From Scenario 1 (b) From Scenario 2

Figure 3-9. Convergence of N-R method with the DLF model.

Table 3-4. Estimation of Convergence Rate of DLF Calculation.

Scenarios		ρ_k		
		***k*=0**	***k*=1**	***k*=2**
Scenario 1	Stage 1	0.040	0.325	0.380
	Stage 2	0.829	1.353	0.000
Scenario 2	Stage 1	0.027	0.468	0.394
	Stage 2	0.460	0.341	0.413

Iterations with the N-R method converge at a quadratic rate to the solution when the initial guess is sufficiently close to the solution. For a series $\{x_k\}$ converging to x^* with a quadratic rate, eq. (3.13) should be satisfied [135][136].

$$\frac{|x_{k+1}-x^*|}{|x_k-x^*|^2} \le M \qquad if\ M > \frac{|h''(x^*)|}{2|h'(x^*)|} \tag{3.13}$$

For the DLF model or a conventional power flow model, function *h* in (3.13) represents (3.3) and (3.4) and *h'* and *h"* are the first derivate and second derivate of *h.* Treat the power flow results at the last iteration on the DLF as the

solution x^*. Table 3-4 calculates $\rho_k = \frac{|x_{k+1} - x^*|}{|x_k - x^*|^2}$ at each iteration step *k* of the N-R method on the DLF model. From the results, the values of ρ_k for different *k*'s are basically of the same scale, which demonstrates quadratic convergence of the N-R method in solving the DLF model.

2) *Tests on UFLS and Generator Frequency Protection Module and Influence of SPFCs of Load on Frequency*

In the proposed approach for simulation of cascading outages, the UFLS and generator frequency protection module in Fig. 3-2 will be activated together with some scenarios. Here Scenario 3 tripping lines 32-10 and 38-29 is illustrated.

After tripping lines 32-10 and 38-29, the DLF model gives frequency *f*=59.39Hz, which falls into the range of 57Hz to 59.5Hz. Then, the UFLS scheme is triggered to shed 384.07MW load and then *f* increases to 59.55Hz. Since the new frequency *f* after DLF falls into the range of 59.5Hz to 60.5Hz, generator frequency protections are triggered at a probability of 0.002. Finally, in this scenario, no generator is tripped.

Additionally, the influence of SPFCs of loads on frequency is analyzed in Scenario 3. Fig. 3-10 shows that the larger the parameter *D*, the smaller is the frequency deviation.

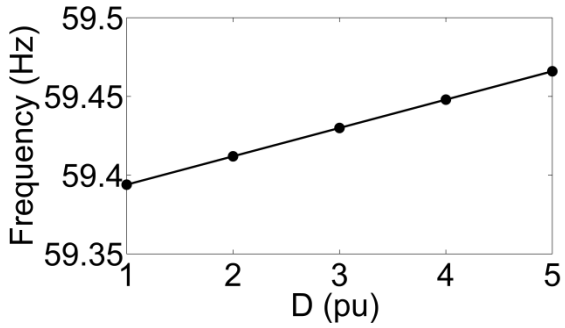

Figure 3-10. Frequency vs *D* of Scenario 3.

3) *Influence of Active Power Generation Limits on Frequency*

Active power generation limits are considered in the DLF model. Here, the impact of active power generation limits on frequency is studied on Scenario 4. Table V compares active power outputs of generators and system frequencies after tripping lines 10-32 and 25-37 with and without considering active power generation limits, respectively.

From Table 3-5, the frequency deviation of -1.29Hz considering active power generation limits is larger than the deviation of -0.49Hz without considering active power generation limits. If some generators reach their active power generation limits, their active power outputs will be fixed at the limits while the other generators such as generator 31 with sufficient margin will continue increasing active power. If active power generation limits are omitted, the frequency deviation may be underestimated.

Table 3-5. Generator Power Outputs and System Frequencies.

Generator	P_{Gmax} (MW)	Without limits		With limits	
		P_G (MW)	f_d (Hz)	P_G (MW)	f_d(Hz)
30	350.00	395.66	-0.49	350.00	-1.29
31	1145.60	507.88		749.74	
33	732.00	777.66		732.00	
34	608.00	653.66		608.00	
35	750.00	795.66		750.00	
36	660.00	705.66		660.00	
38	930.00	975.66		930.00	
39	1100.00	1145.66		1100.00	
32	750.00	-	-	-	-
37	640.00	-	-	-	-

4) *Statistical Comparison of Two Simulation Approaches*

Some indices evaluating the severity of cascading outages can be used to compare the scenarios of cascading outages generated by the two approaches based on Figs. 3-3 and 3-4, such as the number of line outages and amount of

load shed. The cascading outage simulations of the two approaches are tested and compared on cascading outage scenarios starting from all N-2 initial outages. Note that the system is N-1 secure, or in other words, it has no overloaded line after any N-1 line outage. Of all the 1035 pairs of cascading outage scenarios derived by the two approaches, the ones which do not propagate beyond the initial outages for both approaches are excluded from comparison. Totally K=1028 scenarios for each approach are compared here.

Define the following two indices to compare the cascading outages simulated by the two approaches.

$$R_{i,path} = \frac{|A_i|}{|B_i|}, R_{i,load} = \frac{Load_{A_i}}{Load_{B_i}}, i = 1,2,..,K \tag{3.14}$$

where A_i and $Load_{Ai}$ are the set of line outages and amount of load shed on scenario i of cascading outages from the conventional approach; B_i and $Load_{Bi}$ are the set of line outages and amount of load shed on scenario i from the proposed approach; $|\cdot|$ represents the number of elements in a set.

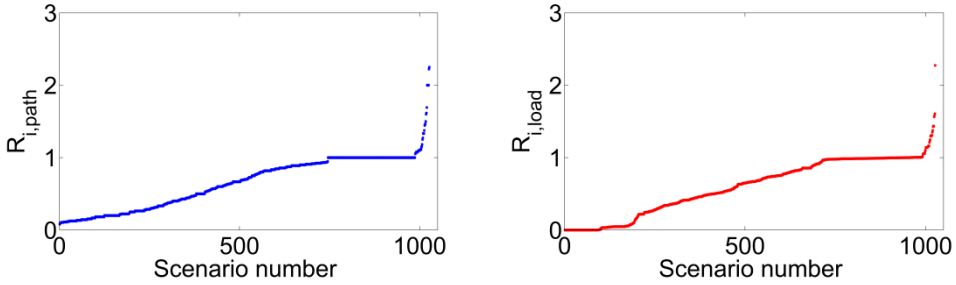

(a) Length of cascading outage (b) Load shed of cascading outage

Figure 3-11. Ratios between two approaches.

Fig. 3-11(a) shows that for most scenarios, $R_{i,path}$<1, indicating that line outages propagate more as simulated by the proposed approach than the conventional approach. From Fig. 3-11(b) and Table 3-6, the proposed approach tends to have more load shed than the conventional approach due to the consideration of the UFLS scheme and generator frequency protection. It can be inferred that the conventional approach underestimates the extent of outage propagation due to ignoring frequency variations, frequency-related remedial

actions and protections. The proposed approach better captures the propagation of outages and losses of load due to frequency-related factors.

Furthermore, the overlaps between the sets of line outages of cascading outages generated by two approaches are evaluated to compare the simulated cascading outage paths. Define the average overlap ratio R_{avg} [56] for the sets of line outages of cascading outages between two approaches as

$$R_{avg} = \frac{1}{K}\sum_{i=1}^{K} R_{i,overlap}\ ,\ R_{i,overlap} = \frac{|A_i \cap B_i|}{|A_i \cup B_i|} \tag{3.15}$$

R_{avg} is 0.61, indicating distinct characteristics of outage propagations simulated by the two approaches.

Table 3-6. Statistical Comparison of the Two Approaches with 1028 Samples.

Approaches	Average No. of line outages	Average amount of load shed (MW)
Conventional	7.76	1848.9
Proposed	12.89	3376.5

UFLS is triggered in 255 of the 1028 scenarios. The average, maximum, and minimum amounts of load shed by UFLS scheme are 282.23MW, 599.60MW and 40.85MW, respectively. This study shows that if impacts of frequency deviation and the UFLS scheme are ignored in simulation, the risk of cascading outages will be underestimated.

3.3.4 Tests on the NPCC System

1) *Verification of Steady-state Frequency*

The steady-state frequency calculated by the DLF model is also verified on the NPCC 48-machine, 140-bus power system.

Two scenarios (numbered Scenarios 5 and 6 below) of cascading outages are selected for verifying the frequencies calculated by the DLF model. The scenarios cause large active power imbalances leading to over- and under-frequency conditions. Note that the purpose of the tests here is only to verify the

calculated steady-state frequency, so the AC-OPFf model, the UFLS scheme and generator frequency protection module are deactivated in the two scenarios.

Scenario 5 has two stages of outages as listed in Table 3-7. The steady-state frequencies obtained from the DLF model and time-domain simulation are compared in Table 3-8. Scenario 6 has three stages of outages shown by Table 3-9. The frequencies are compared in Table 3-10. From the comparisons, the results derived from the DLF model is very close to the benchmarking results, which verifies the accuracy for capturing the steady-state frequency by the DLF model.

Table 3-7. Propagation Path of Cascading Outages in Scenario 5.

Stages	Line Outages
1	130-131, 131-133, 131-135, 131-139
2	124-128, 125-128, 126-128, 127-128, 128-130

Table 3-8. Comparison of Steady-state Frequencies for Scenario 5.

Approaches	Frequency (Hz)	
	Stage 1	Stage 2
DPF	60.137	60.244
Time-domain	60.147	60.268

Table 3-9. Propagation Path of Cascading Outages in Scenario 6.

Stages	Line Outages
1	85-86, 85-105
2	78-79
3	131-133, 132-133, 133-135

Table 3-10. Comparison of Steady-state Frequencies for Scenario 6.

Approaches	Frequency (Hz)		
	Stage 1	Stage 2	Stage 3
DPF	59.779	59.622	59.498
Time-domain	59.802	59.649	59.532

Note: three generators are tripped one by one after stages 1, 2 and 3.

2) *Detailed Comparison of Two Simulation Approaches*

This section conducts detailed comparisons between the proposed approach and conventional approaches on two more scenarios numbered 7 and

8. Figs. 3-12-3-13 show the outage paths, amounts of load shed and frequency variations of two scenarios.

For Scenario 7, the outage propagation paths from the same initial outages simulated by two approaches are the same (in Fig. 3-12), and the frequency deviation is not significant. After stage 2, the frequency only deviates by -0.033Hz. After the line outages in stage 3, power flow calculations by the DLF model and conventional power flow model both diverge, indicating system stress, and then AC-OPF and AC-OPFf are invoked to find new operating points, respectively. The system frequency after AC-OPFf is 60.498 Hz, which is within the normal range, so the UFLS scheme is not triggered. After AC-OPF and AC-OPFf, there are no other lines tripped and outages stop for both approaches. The comparison on Scenario 7 indicates that the two approaches behave similarly with small frequency deviation. However, with the proposed approach, the operators can monitor the variation of system frequency, which is more practical than the conventional approach.

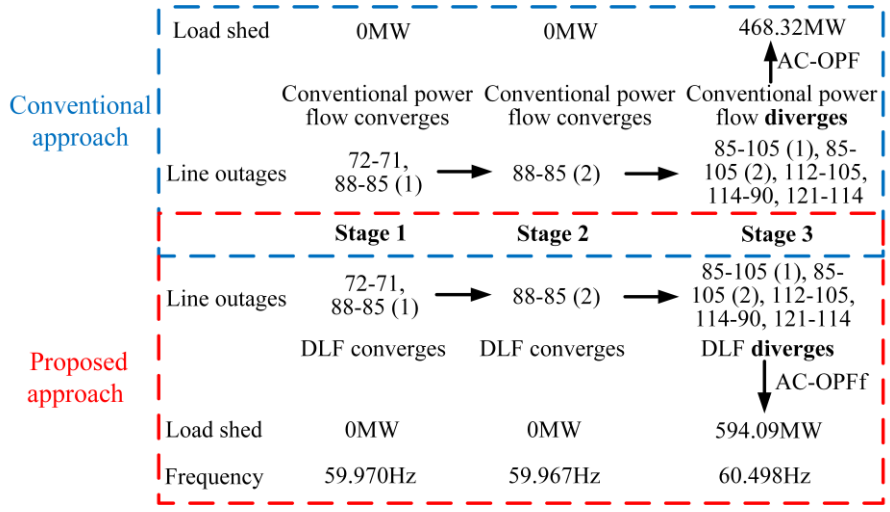

Figure 3-12. Comparison of two approaches on Scenario 7.

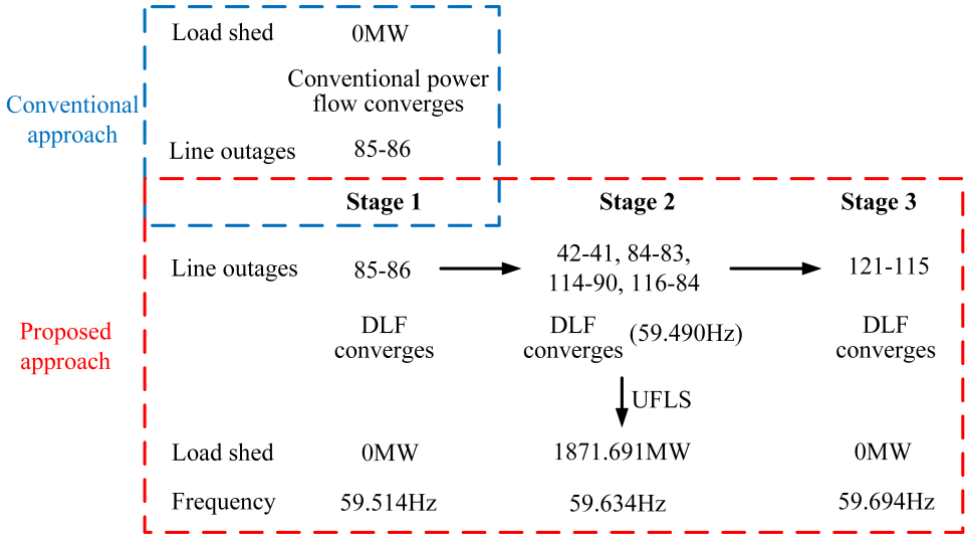

Figure 3-13. Comparison of two approaches on Scenario 8.

For Scenario 8, the outage propagation paths simulated by two approaches from the same initial outage coincide at the first stage and then differ from stage 2 (Fig. 3-13). In the simulation with the proposed approach, after line outages at stage 2, the frequency deviation for the remaining system hits -0.51 Hz, so UFLS is triggered to shed load and recover the system frequency to 59.634 Hz. The frequency for the remaining system after stage 3 is 59.694 Hz and UFLS is not further triggered. The outage propagations and the resulting power flow profiles from the two approaches are relatively close in the first stage and then become distinct from stage 2. This indicates that variations of system frequency cannot be ignored during the propagation of cascading outage, especially for the later stages of outages. Otherwise, the impacts of cascading outages may be significantly underestimated.

3) *Detailed Comparison of Two Simulation Approaches*

A large number of cascading outage scenarios are simulated on the NPCC system using the proposed and conventional approaches to further compare the outage propagation patterns. Each scenario starts from an “N-2” contingency.

For the two approaches, Table 3-11 compares the average numbers of line outages, the average amounts of load shed by remedial actions, and the average amounts of load shed by the UFLS scheme in 10000 independent scenarios. Cascading outages with the proposed approach tend to propagate more and are more severe than those from the conventional approach. This again indicates the significance of considering frequency variations and frequency-related actions in the simulation of cascading outages.

Table 3-11. Statistical Comparison of the Two approaches with 10000 Samples.

Approaches	Average No. of line outages	Average load shed (MW)	Average load shed by UFLS (MW)
Conventional	8.79	222.45	0
Proposed	14.27	985.02	146.97

The time performances of two approaches are tested on a desktop computer with Intel Core i7-3770K 3.40GHz and 4GB RAM. The total time costs for the same number of scenarios created by two approaches are compared in Table 3-12. The proposed approach takes about 16% more time than the conventional approach because for a number of scenarios with large frequency deviations, the cascading outages simulated by the proposed approach propagate for more stages and hence require more N-R computations.

Table 3-12. Comparison in Time Performance

Number of scenarios	Conventional approach	Proposed approach
10000	14.50 hours	16.78 hours

3.4 Conclusion of this Chapter

In this chapter, a novel steady-state cascading outage simulation approach is proposed, which integrates a DLF model and a novel AC-OPFf model considering frequency deviation. The chapter discusses the significance of considering frequency variations in simulation of cascading outages. The proposed approach can accurately capture the steady-state frequency. Also, the proposed AC-OPFf model considering frequency deviation can simulate the

control actions against system collapse. Thus, the proposed approach is able to model loss of load due to both frequency insecurity and voltage collapse, and hence can better match practical grid operations than the conventional steady-state approach that ignores the variation of frequency. The proposed approach enables the modeling of frequency related remedial actions and protections such as UFLS scheme and generator frequency protection. The frequency calculated by the DLF model has been benchmarked with time-domain simulation results on both small and large systems. Detailed and statistical comparisons between the proposed and conventional approaches have been conducted to demonstrate the merits of the proposed approach. The proposed approach only focuses on capturing steady-state frequency variations in the simulation of cascading outages and is unable to provide detailed dynamic behaviors of frequency following each disturbance.

CHAPTER FOUR
CRITICAL COMPONENT-BASED ACTIVE ISLANDING FOR REDUCING CASCADING OUTAGE RISK

4.1 Introduction

According to [9], basically, the procedure of cascading outage can be divided into two phases, which are remarked by slow phase and fast phase. If the cascading outage propagates to the fast phase, a fast transient instability process unfolds resulting in a collapse of the entire system [137]. However, it is possible for the system operators to evaluate the system status and take some remedial and control actions to prevent the propagation of cascading outages.

Many remedial actions have been reported in [138]. These remedial actions include generator excitation, re-dispatch of generation, load shedding, generator tripping, and Intentional controlled islanding (ICI).

Intentional controlled islanding (ICI) has been proposed as an effective remedial action [139, 140] for systems under emergency status [139–143]. After a severe contingency, ICI intentionally separates the power system into several self-sustaining isolated islands. Generally, to obtain an islanding solution, ICI can be formulated as a constrained optimization problem. However, to solve this optimization problem in real-time or within a limited timeframe such as a few seconds is extremely complicated and the complexity increases exponentially with the system size [144–149]. To search for the set of lines splitting the system, multiple constraints need to be considered. Some typical constraints include load-generation balance, coherency generator, thermal limits, voltage and transient stability. It is very complicated obtain a solution with a limited timeframe with considering all the constraints. It is practical to consider only part of the constraints [151]. Among these constraints, the constraint generator coherency is crucial for successful controlled islanding since it enhances the transient stability of the islands [146, 147, 152]. The existing ICI approaches can be classified as

two classes. The objective of the first class is to minimize power imbalance [143–149]. The objective of second class is to minimize power flow disruption [150, 151, 153]. These approaches may obtain different islanding solutions but they can be regarded as ‘NP-hard’ searching problems [154]. For these problems, there is no general ‘polynomial time’ algorithm to find the optimal solution [155]. More efficient methods should be investigated in order to realize fast searching for the islanding solution [146–148].

For the second class approaches, Spectral clustering-based methods have been proposed [156], belonging to graph theoretic techniques. The eigenvalues and eigenvectors of a matrix representing the power system can be calculated to determine the islanding solution within ‘polynomial time’. Even though this method requires less computation burden, it does not include the generator coherency constraint. Later, a spectral clustering controlled islanding (SCCI) algorithm has been introduced in [151]. The SCCI algorithm minimizes the power flow disruption, while ensuring that each island contains only coherent generators. However, an islanding solution can only be directly determined when the number of islands is two.

In this chapter, the perspective for studying active islanding is quite different with the existing researches. It is assumed that the set of lines that splitting the power system into islands are predefined. It is a reasonable since the tie lines connecting to the remaining system for an area operated by the *ISO* are always under monitoring and the strategy for isolating this area is also predesigned. The focus of this chapter is to investigate the effective stage to perform active islanding during the propagation of cascading outages. A critical component-based active islanding for reducing the cascading outage risk is proposed. Critical components whose fail can cause large cascading outage risk are identified based on the interaction graph. With the propagation of outages, if any component belonging to the critical components is involved in this cascade, active islanding will be performed in real time to change the propagation path of outages in order to reduce the cascading outage risk. The remaining sections are

organized as follows. Section 4.2 presents the proposed strategy of active islanding in detail. Section 4.3 tests the proposed strategy of active islanding on an NPCC power system and validates it. Conclusion is drawn in Section 4.4.

4.2 Proposed Strategy of Active Islanding

4.2.1 Illustration of Active Islanding

Here one scenario of cascading outage on the NPCC power system is used to illustrate the procedure for performing active islanding. This scenario contains twelve line outages involved in four stages.

Stage 1: Lines 1-2 and 1-21.

Stage 2: Line 6-7.

Stage 3: Lines 7-8, 9-30, and 30-31.

Stage 4: Lines 32-35, 35-39(double lines), 37-39, 50-52 and 52-54.

A simulator for the simulation of cascading outage is shown by Fig. 4-1.

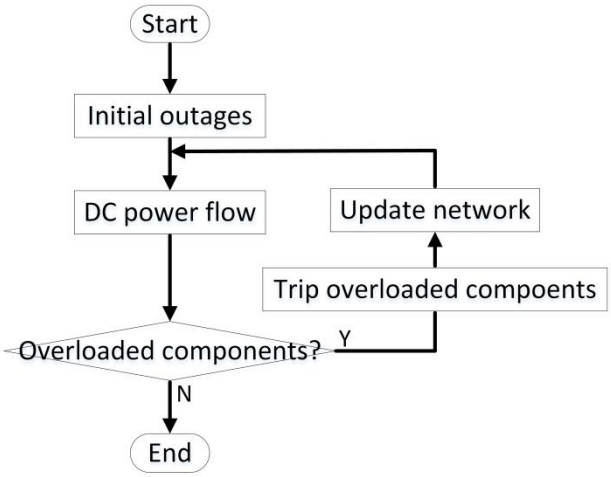

Figure 4-1. Simulation procedure of cascading outage without active islanding.

The DC power flow results show that there are no overloaded lines after line outages in stage 4. The propagation of cascading outage stops. These line outages are remarked by colors in Fig. 4-2.

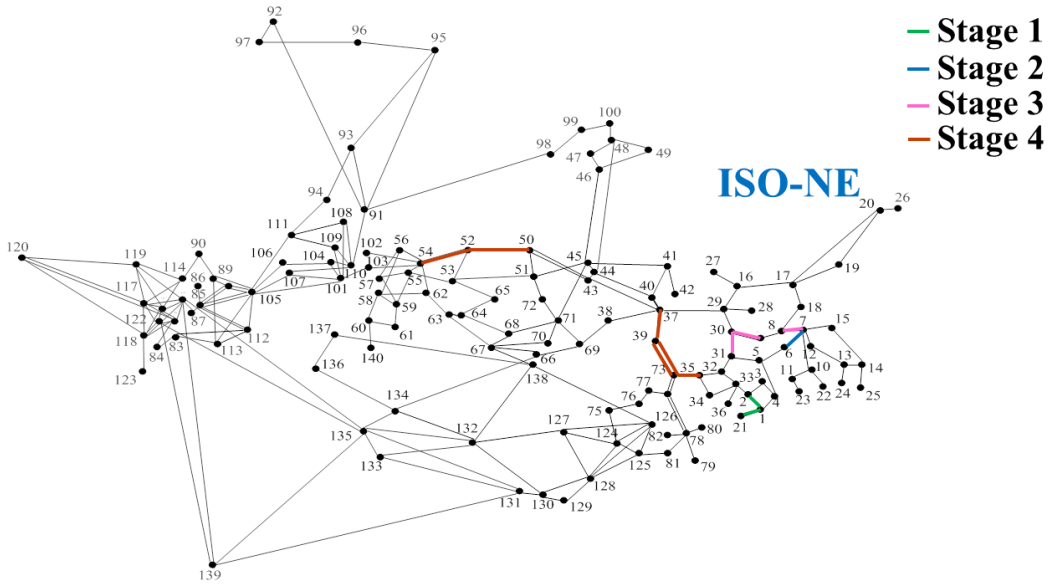

Figure 4-2. One scenario of cascading outage without active islanding.

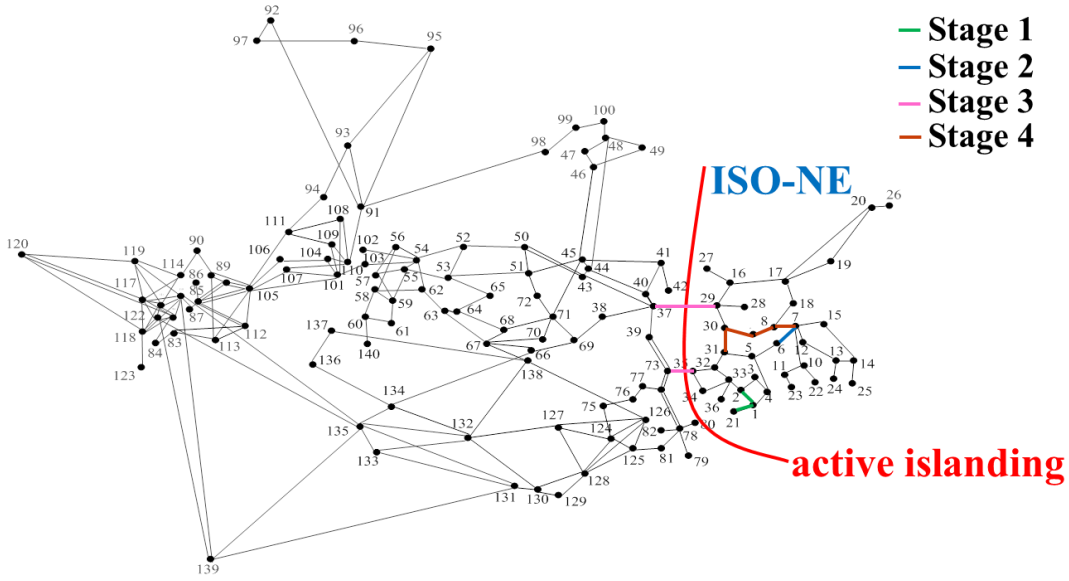

Figure 4-3. One scenario of cascading outage with active islanding.

As comparison, when line 7-6 becomes overloaded with the propagation of outages following the same initial line outages, rather than tripping it, active islanding is performed to isolate ISO New England area, then lines 29-37 and 35-73 are tripped intentionally. After performing active islanding, the DC power flow results show that lines 7-8, 8-9, 9-30, and 30-31 become overloaded and they are tripped in the next stage. After tripping them, they are no other overloaded lines. They are remarked by colors in Fig. 4-3.

By comparing Figs. 4-2 and 4-3, we can know that the propagation path of outages has been changed after performing active islanding. This strategy is effective if the cascading outage risk of Fig. 4-3 is smaller than that of Fig. 4-2.

Then two problems need to be answered. First, for one scenario of outages, should active islanding be performed? Second, if the answer is yes, which stage to perform active islanding?

In this chapter, a strategy of critical component-based active islanding is proposed to reduce the cascading outage risk online. The basic idea is to perform active islanding when any critical component whose fail can cause large cascading outage risk is involved in the propagation path. The identification of critical components is based on the interaction graph constructed offline.

4.2.2 Critical Components With Interaction Graph

In [27], the interaction graph comprising by the key links and components is constructed. A link $i \rightarrow j$ is quantified for the criticality to the propagation of cascading outages in terms of amount of load shed, which is remarked by link weight I_{ij}:

$$I_{ij} = \frac{1}{N_{ij}} \sum_{m=1}^{N_{ij}} I_{ij,m}, \quad I_{ij,m} = k_1 \frac{L_{s,m}}{N_{s-1,m} N_{s,m}} \tag{4.1}$$

where $I_{ij,m}$ represents the link weight for the link $i \rightarrow j$ in the m-th cascade; $L_{s,m}$ is the amount of load shed at the generation s of m-th cascade; $N_{s-1,m}$ and $N_{s,m}$ are the numbers of line outages at the generations s-1 and s of the m-th cascade;

N_{ij} is the number of cascades involving the link $i \rightarrow j$; k_1 is the non-negative scaling parameters.

A unique subgraph influenced by the link $i \rightarrow j$ can be extracted from the interaction graph shown by Fig. 4-4.

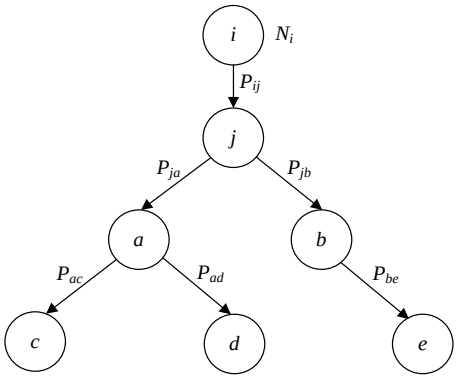

Figure 4-4. Subgraph influenced by the link $i \rightarrow j$.

For the link $i \rightarrow j$, P_{ij} represents the occurrence probability of link $i \rightarrow j$.

$$P_{ij} = \frac{N_{ij}}{N_i} \tag{4.2}$$

where N_i is the number of times of component outage i.

The expected load shed triggered by the link $i \rightarrow j$ and other links in the subgraph is defined as

$$COC_{ij} = \sum_{l \in \eta(ij)} R_l \; ; \; R_l = P_{c_s} P_l I_l \tag{4.3}$$

where $\eta(ij)$ is the set of links in the subgraph influenced by the link $i \rightarrow j$; P_{c_s} is the occurrence probability of the source component outage of link l.

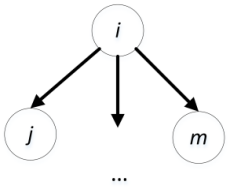

Figure 4-5. Component *i* and involved links.

The links involved in component *i* are shown by Fig. 4.5. The total risk in terms of amount of load shed triggered by the component *i* is defined as:

$$S_i = \sum_{c \in \zeta(i)} COC_{ic} \tag{4.4}$$

where $\zeta(i)$ is the set of components starting from component *i*.

The top ranking components with large S_i can be regarded as critical compoents, remarked by C_b. They are crucial to the cascading outage risk in terms of load shed.

4.2.3 Strategies of Active Islanding

The basic idea of the proposed active islanding can be described: with the propagation of outages, when any component belonging to the set of critical components becomes overloaded which means it is involved in the propagation path of outages, rather than tripping it, active islanding is performed intentionally to change the propagation path of outages. It is named as critical component-based active islanding in this chapter.

As comparison, another non-critical component-based active islanding is proposed. With the propagation of outages, if any component not belonging to the set of critical components becomes overloaded, active islanding will be performed instantaneously.

The effectiveness of the critical component-based active islanding can be verified if the cascading outage risk in those scenarios performing active islanding can be reduced. However, for the strategy of non-critical component-based active islanding, it can increase the cascading outage risk in those scenarios performing active islanding. Based on the above two strategies, two simulation procedures of cascading outages are shown by Figs. 4-6-4-7.

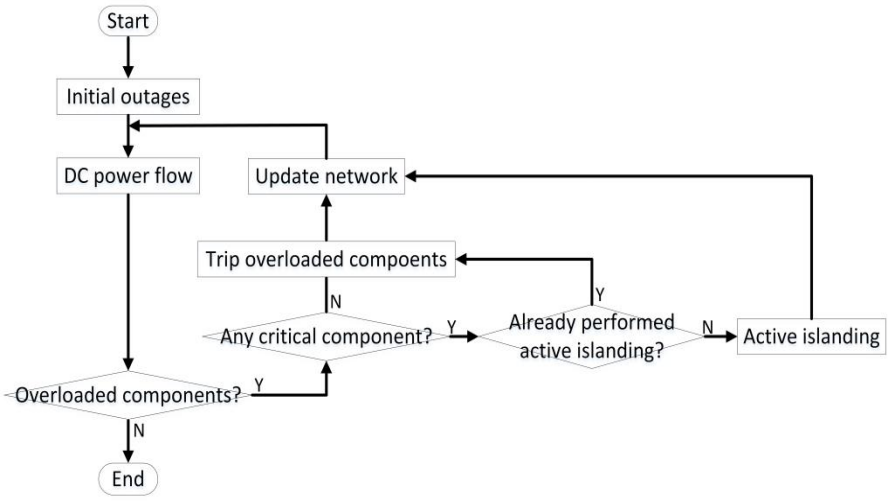

Figure 4-6. Simulation procedure of cascading outages with the strategy of critical component-based active islanding.

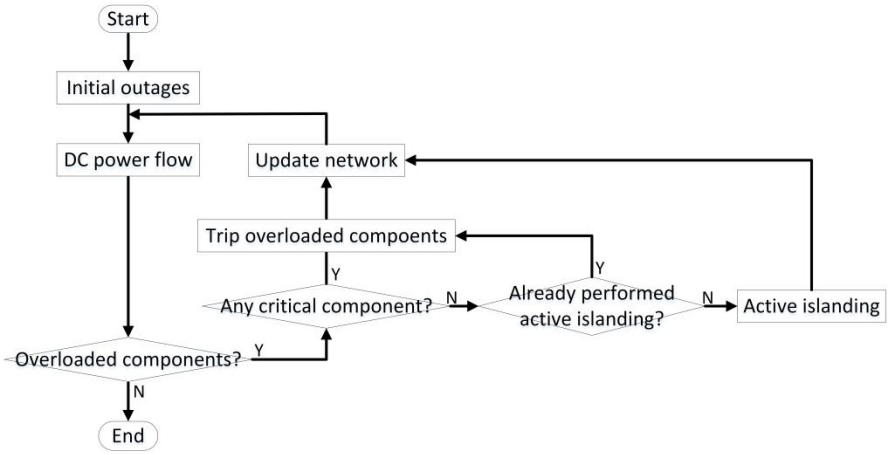

Figure 4-7. Simulation procedure of cascading outages with the strategy of non-critical component-based active islanding.

4.3 Case Studies

The proposed strategies of active islanding are tested and compared on the NPCC power system. For simplicity, it is assumed that the area for isolation is pre-determined that is to isolate ISO New England area. We do not consider isolating other areas in the strategy of active islanding. Then the initial "N-2" component outages located in the ISO New England area are considered. The number is 861.

4.3.1 Different Classes of Cascades

Here seven classes of cascades are simulated, which are remarked by:

Class 1: 861 original cascades without active islanding following the procedure in Fig. 4.1 are simulated.

Classes 2, 3, 4, 5, and 6: 861 cascades with active islanding following the procedure in Fig. 4-6 are simulate in each class. 10, 20, 30, 40, and 50 critical components are used, respectively.

Class 7: 861 cascades with active islanding following the procedure in Fig. 4-7 are simulated.

Remarks:

1) The cascades in Class 1 are also used for identifying the critical components.

2) For each cascade of Class 2, active islanding will be performed instantaneously if any component belonging to the 10 critical components is involved in stage 2 or the later stages.

3) For Classes 3, 4, 5, and 6, the difference when compared with Class 2 is the number of critical components used.

4) For each cascade of Class 7, active islanding will be performed instantaneously if any component rather than 50 critical components is involved in stage 2 or the later stages.

4.3.2 Comparison between Different Classes

For different classes, the number of cascades that performing active islanding is different. It is shown in Fig. 4-8.

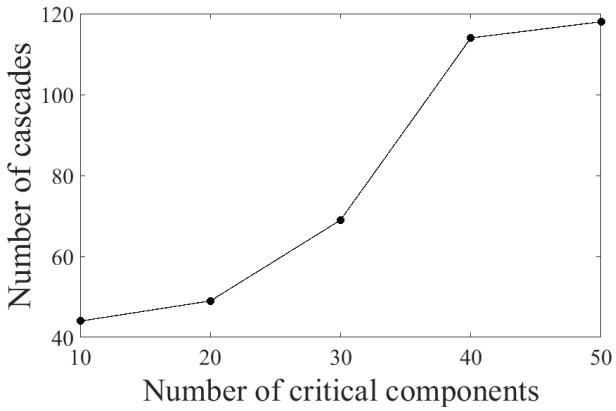

Figure 4-8. Number of cascades performing active islanding.

From Fig. 4-8, we can know that the number of cascades performing active islanding increases with the increased number of critical components.

In order to compare the variation of cascading outage risk, for each cascade that performing active islanding in Classes 2, 3, 4, 5, 6, and 7, the amount of load load is compared with that of the corresponding cascade in Class 1 following the same initial outages. They are shown in Figs. 4-9-4-11.

For Figs. 4-9-4-11, the average amount of load shed between different classes of cascades is compared and listed in Table 4-1. Here we consider six comparisons between different classes.

Comparison 1: Class 1 \& Class 2

Comparison 2: Class 1 \& Class 3

Comparison 3: Class 1 \& Class 4

Comparison 4: Class 1 \& Class 5

Comparison 5: Class 1 \& Class 6

Comparison 6: Class 1 \& Class 7

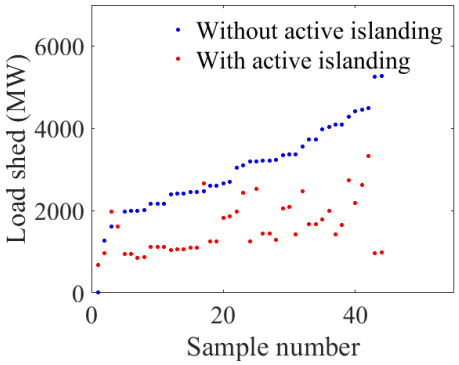

(a) Class 1 and Class 2

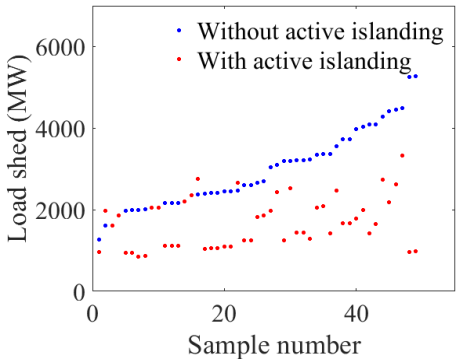

(b) Class 1 and Class 3

Figure 4-9. Comparison of load shed between cascades with and without active islanding for Classes 1, 2, and 3.

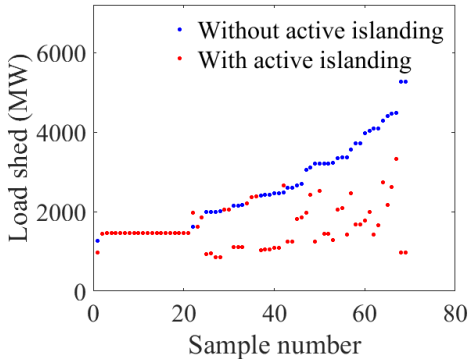

(a) Class 1 and Class 4

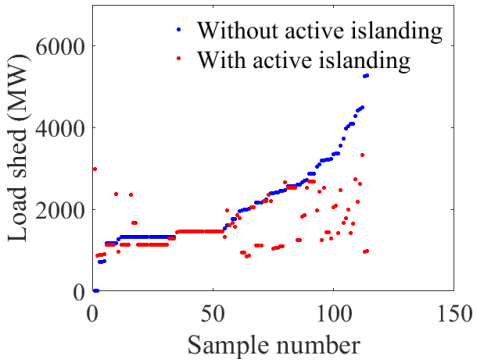

(b) Class 1 and Class 5

Figure 4-10. Comparison of load shed between cascades with and without active islanding for Classes 1, 4, and 5.

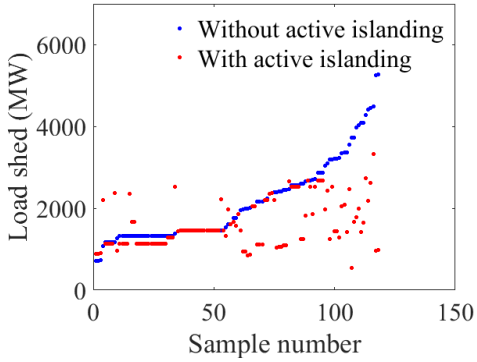

(a) Class 1 and Class 6

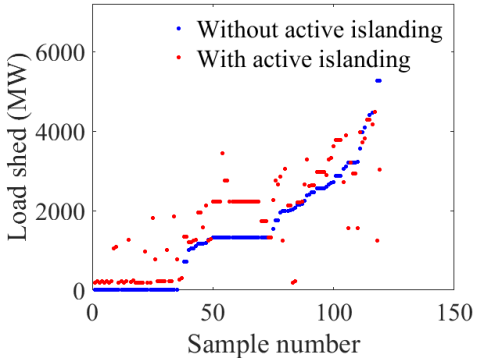

(b) Class 1 and Class 7

Figure 4-11. Comparison of load shed between cascades with and without active islanding for Classes 1, 6, and 7.

Table 4-1. Average Amount of Load Shed

Comparison number	Class 1	Compared Class
1	3064.1MW	1605.3MW
2	2958.9MW	1680.5MW
3	2517.5MW	1608.4MW
4	2098.2MW	1584.9MW
5	2145.1MW	1611.3MW
6	1474.8MW	1823.5MW

From Table 4-1, we can know that the cascading outage risk has decreased for the class (Classes 2, 3, 4, 5, and 6) with critical component-based active islanding when compared with the cascades without active islanding. The cascading outage risk has increased for the class (Class 7) with non-critical component-based active islanding when compared with the cascades without active islanding.

Specifically, active islanding is performed in 43 cascades for Class 2, among these cascades, the amount of load loss for 40 cascades with active islanding is smaller than that of the original cascades without active islanding. The average amount of load loss for 40 cascades with and without active islanding is 1569.6MW and 3151.5MW.

For Class 3, active islanding is performed in 48 cascades, among these cascades, the amount of load loss for 39 cascades with active islanding is smaller than that of the original cascades without active islanding. The average amount of load loss for 39 cascades with and without active islanding is 1578.0MW and 3165.4MW.

For Class 4, active islanding is performed in 69 cascades, among these cascades, the amount of load loss for 40 cascades with active islanding is smaller than that of the original cascades without active islanding. The average amount of load loss for 40 cascades with and without active islanding is 1569.6MW and 3151.5MW.

For Class 5, active islanding is performed in 114 cascades, among these cascades, the amount of load shed for 77 cascades with active islanding is smaller than that of the original cascades without active islanding. The average amount of load shed for 77 cascades with and without active islanding is 1561.6MW and 2423.5MW.

For Class 6, active islanding is performed in 118 cascades, among these cascades, the amount of load shed for the 79 cascades with active islanding is smaller than that of the original cascades without active islanding. The average amount of load shed for 79 cascades with and without active islanding is 1556.8MW and 2243.2MW.

For Class 7, active islanding is performed in 119 cascades, among them, the amount of load loss for 96 cascades is larger than that of the corresponding cascades without active islanding. The average amount of load loss for 96 cascades with and without active islanding is 1725.5MW and 1128.1MW, respectively.

4.3.3 Selection of Number of Critical Components

Here the ratio for the number of cascades with reduced cascading outage risk for different number of critical components is given by Fig. 4-12.

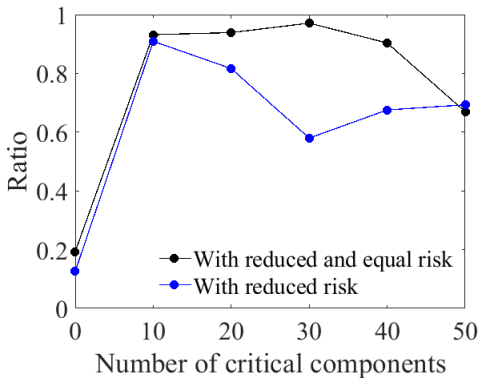

Figure 4-12. Ratio of the number of cascades.
(with reduced and equal risk: consider the cascades with reduced and equal risk; with reduced risk: consider the cascades with reduced risk)

From Fig. 4-12, we can know that the ratio for the strategy of critical component-based active islanding is much higher than that of non-critical component-based active islanding, which verifies the effectiveness and high accuracy of proposed critical component-based active islanding. The larger the ratio is, the better the performance is. With the increasing number of critical components, the performance will change. Considering the cascades with reduced and equal risk, the ratio will increase and then decrease. The strategy with 30 critical components has the best performance. By only considering the cascades with reduced risk, the ratio will decrease and then increase. It suggests that it is better to select 10 critical components in order to have a good performance.

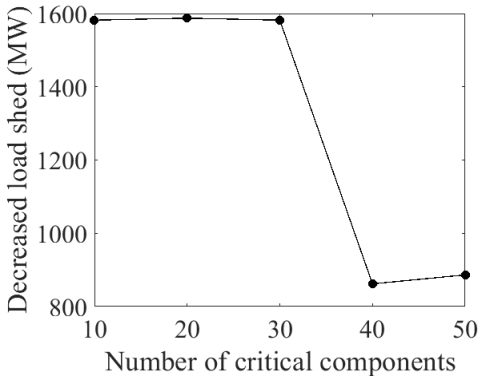

Figure 4-13. Average reduced amount of load shed for those cascades with reduced risk.

Fig. 4-13 gives the average reduced amount of load shed for those cascades not only performing active islanding but also reducing the amount of load shed when compared with the corresponding cascades without active islanding. For 10, 20, and 30 critical components, the performance for reducing the amount of load shed is stable. However, the performance becomes worse when the amount of critical components reaches to 40. This suggests to select 10, 20, or 30 critical components.

Fig. 4-14 gives the ratio of the number of cascades for those cascades not only performing active islanding but also increasing the amount of load shed when compared with the corresponding cascades without active islanding. Fig. 4-

15 gives the average increased amount of load shed. With the increasing number of critical components, the average increased amount of load shed decreases first and then increases. This suggests it is better to select 30 critical components.

By combing the results from Figs. 4-12-4-15, we would like to recommend 10 critical components to be used.

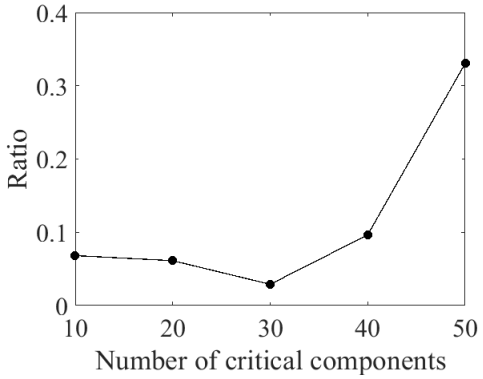

Figure 4-14. Ratio of the number of cascades with increased risk.

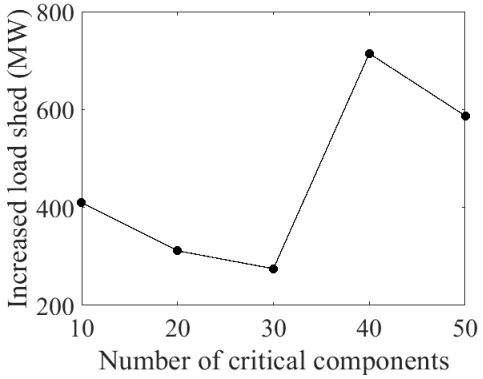

Figure 4-15. Average increased amount of load shed for those cascades with increased risk.

4.4 Conclusion of this Chapter

An online strategy of critical component-based active islanding designed to perform online with the propagation of outages to reduce the cascading outage risk is proposed. Active islanding will be performed instantaneously if any critical

component whose fail can cause large cascading outage in terms of load shed is involved in order to change the propagation path of cascading outage and reduce cascading outage risk. The critical components are identified based on the interaction graph constructed offline. Tests on the NPCC power system validate the proposed strategy of active islanding.

CHAPTER FIVE
SUMMARY AND FUTURE WORKS

5.1 Summary

A test bed based on the Northeastern Power Coordinating Council (NPCC) 48-machine, 140-bus power system model for simulating cascading outages is developed. Then a multi-layer interaction graph on cascading outages of power systems is proposed as an extension of the single-layer interaction model. This multi-layer interaction graph provides a practical framework for prediction of outage propagation and decision making on mitigation actions. It has multiple layers to respectively identify key components and key intra-layer links of components within each layer and key inter-layer links between layers, which contribute the most to outage propagation. Each layer focuses on one of several aspects that are critical for system operators' decision support, such as the number of line outages, the amount of load shedding, and the electrical distance of outage propagation. Besides, the proposed integrated mitigation strategies can limit the propagation of cascading outages by weakening key links.

A novel dynamic load flow (DLF) model for cascading outage simulation considering static power-frequency characteristics (SPFCs) of generators and loads is proposed such that system frequency deviations due to active power imbalance can be calculated during cascading outages. Further, a new AC optimal power flow model considering frequency deviation (AC-OPFf) is proposed to represent remedial control actions when system collapse happens as indicated by power flows divergence. Test results verify that the proposed approach can capture frequency variations under cascading outages and simulate the mechanism of outage propagation more accurately.

A strategy of active islanding designed to perform in real time with the propagation of outages to reduce the potential cascading outage risk is proposed. In order to mitigate cascading outages, active islanding will be performed if critical branches whose fail can cause a huge loss of load are involved. The critical branches are identified based on the interaction graph offline. Tests on the NPCC power system validate the proposed strategy of active islanding.

5.2 Future Works

The future works will be:

1) Integration of the steady-state simulation approach proposed in Chapter 3 and time-domain simulation for an efficient hybrid simulation approach for cascading outages.

2) Investigation of more effective online strategies for reducing the cascading outage risk based on the multi-layer interaction graph.

LIST OF REFERENCES

[1] O. P. Veloza and F. Santamaria, “Analysis of major blackouts from 2003 to 2015: classification of incidents and review of main causes,” *The Electricity Journal*, vol. 29, no. 7, pp. 42-49, 2016.

[2] *Final Report on the August 14, 2003 Blackout in the United States and Canada: Causes and Recommendations*, U.S.-Canada. Power System Outage Task Force, Apr. 2004.

[3] The lessons to be learned from the large disturbance in the European power system on the 4th of November 2006, European Regulators Group for Electricity and Gas, 2007.

[4] PACME Working Group, “Effects of dependent and common mode outages on the reliability of bulk electric system – part II: outage data analysis,” *IEEE Power and Energy Society General Meeting,* Jul. 2014.

[5] M. Vaiman, K. Bell, Y. Chen, B. Chowdhury, I. Dobson, P. Hines, M. Papic, S. Miller, and P. Zhang, “Risk assessment of cascading outages: Methodologies and challenges,” *IEEE Trans. Power Syst*., vol. 27, no. 2, pp. 631–641, May 2012.

[6] M. Papic, K. Bell, Y. Chen, I. Dobson, L. Fonte, E. Haq, P. Hines, D. Kirschen, X. Luo, S. Miller, N. Samaan, M. Vaiman, M. Varghese, and P. Zhang, “Survey of tools for risk assessment of cascading outages,” in *Proc. IEEE Power and Energy Society General Meeting*, Jul. 2011, pp. 1–9.

[7] J. Bialek et al., “Benchmarking and validation of cascading failure analysis tools,” *IEEE Trans. Power Syst*., vol. 31, no. 6, pp. 4887–4900, Nov. 2016.

[8] M. Vaiman, K. Bell, Y. Chen, B. Chowdhury, I. Dobson, P. Hines, M. Papic, S. Miller, and P. Zhang, “Risk assessment of cascading outages: Methodologies and challenges,” *IEEE Trans. Power Syst*., vol. 27, no. 2, pp. 631–641, May 2012.

[9] P. Henneaux, P.-E. Labeau, and J.-C. Maun, “A level-1 probabilistic risk assessment to blackout hazard in transmission power systems,” *Reliab. Eng. Syst. Safety*, vol. 102, no. 0, pp. 41–52, 2012.

[10] J. S. Thorp, A. G. Phadke, S. H. Horowitz, and S. Tamronglak, “Anatomy of power system disturbances: Importance sampling,” Elect. Power Energy Syst., vol. 20, no. 2, pp. 147–152, 1998.

[11] I. Dobson, B. A. Carreras, and D. E. Newman, “A loading-dependent model of probabilistic cascading failure,” *Probab. Eng. Inf. Sci*., vol. 19, no. 1, pp. 15–32, Jan. 2005.

[12] I. Dobson, B. A. Carreras, V. E. Lynch, and D. E. Newman, “Complex systems analysis of series of blackouts: Cascading failure, critical points, and self-organization,” *Chaos: Interdiscipl. J. Nonlin. Sci*., vol. 17, no. 2, p. 026103, 2007.

[13] H. Wu, I. Dobson,“Cascading stall of many induction motors in a simple system,” *IEEE Trans Power Syst.,* vol. 27, no. 4, pp. 2116–2126, Nov. 2012.

[14] H. Wu, I. Dobson, “Analysis of induction motor cascading stall in a simple system based on the CASCADE model,” *IEEE Trans Power Syst.,* vol. 28, no. 3, pp. 3184–3193, 2013.

[15] H. Dong and L. Cui, "System Reliability Under Cascading Failure Models," *IEEE Trans. Reliab*, vol. 65, no. 2, pp. 929 - 940, 2015.

[16] Sankaranarayanan G, “Branching processes and its estimation theory,” Wiley, 1989.

[17] J. Kim and I. Dobson, “Approximating a loading-dependent cascading failure model with a branching process,” *IEEE Trans. Reliab*., vol. 59, no. 4, pp. 691–699, Dec. 2010.

[18] I. Dobson and D. E. Newman, “Cascading blackout overall structure and some implications for sampling and mitigation,” *International Journal of Electrical Power & Energy Systems*, vol. 86, pp. 29–32, 2017.

[19] I. Dobson, “Estimating the propagation and extent of cascading line outages from utility data with a branching process,” *IEEE Trans Power Syst.*, vol. 27, pp. 2146–2155, Nov. 2012.

[20] J. Qi, I. Dobson, and S. Mei, “Towards estimating the statistics of simulated cascades of outages with branching processes,” *IEEE Trans. Power Syst*., vol. 28, no. 4, pp. 3410–3419, Aug. 2013.

[21] I. Dobson, B. A. Carreras, D. E. Newman, and J. M. Reynolds-Barredo, “Obtaining statistics of cascading line outages spreading in an electric transmission network from standard utility data,” *IEEE Trans Power Syst.*, vol. 31, no. 6, pp. 4831–4841, 2016.

[22] B. A. Carreras, D. E. Newman, and I. Dobson, ‘‘North American blackout time series statistics and implications for blackout risk,’’ *IEEE Trans. Power Syst*., vol. 31, no. 6, pp. 4406–4414, Nov. 2016.

[23] J. Kim, K. R. Wierzbicki, I. Dobson, and R. C. Hardiman, “Estimating propagation and distribution of load shed in simulations of cascading blackouts,” *IEEE Syst. J*., vol. 6, no. 3, pp. 548–557, Sep. 2012.

[24] I. Dobson, ‘‘Estimating the propagation and extent of cascading line outages from utility data with a branching process,’’ *IEEE Trans. Power Syst*., vol. 27, no. 4, pp. 2146–2155, Nov. 2012.

[25] I. Dobson, J. Kim, and K. R. Wierzbicki, “Testing branching process estimators of cascading failure with data from a simulation of transmission line outages,” *Risk Anal*., vol. 30, no. 4, pp. 650–662, 2010.

[26] J. Qi, W. Ju, and K. Sun, “Estimating the propagation of interdependent cascading outages with multi-type branching processes”, *IEEE Trans. Power Syst.*, vol. 32, No. 2, pp. 1212-1223, March 2017.

[27] J. Qi, K. Sun, S. Mei, “An interaction model for simulation and mitigation of cascading failures,” *IEEE Trans Power Syst*., vol. 30, no. 2, pp. 804–819, Mar. 2015.

[28] Armitage P, Berry G, Matthews JN, “Statistical methods in medical research,” John Wiley & Sons, 2008.

[29] Z. Wang, A. Scaglione, and R. J. Thomas, “A Markov-transition model for cascading failures in power grids,” *in Proc. 45th Hawaii Int. Conf. Syst*. Sci., 2012.

[30] X. Zhang, C. Zhan, and K. T. Chi, “Modeling the dynamics of cascading failures in power systems,” *IEEE J. Emerg. Sel. Topics Circuits Syst*., vol. 7, no. 2, pp. 192–204, 2017.

[31] C. Zhan, C. K. Tse, and M. Small, “A general stochastic model for studying time evolution of transition networks,” *Physica A Stat. Mech. Appl*., vol. 464, pp. 198–210, Dec. 2016.

[32] R. Yao et al., ‘‘Risk assessment of multi-timescale cascading outages based on Markovian tree search,’’ *IEEE Trans. Power Syst*., vol. 32, no. 4, pp. 2887–2900, Jul. 2017.

[33] M. Rahnamay-Naeini, Z. Wang, N. Ghani, A. Mammoli, and M. Hayat, “Stochastic analysis of cascading-failure dynamics in power grids,” *IEEE Trans. Power Syst*., vol. 29, no. 4, pp. 1767–1779, Jul. 2014.

[34] P. Hines, I. Dobson, and P. Rezaei, “Cascading power outages propagate locally in an influence graph that is not the actual grid topology,” *IEEE Trans. Power Syst.*, vol. 32, no. 2, pp. 958–967, Mar. 2017.

[35] E. Ciapessoni, D. Cirio, and A. Pitto, “Cascading simulation techniques in Europe: The PRACTICE experience,” *in Proc. IEEE PES General Meeting*, Vancouver, BC, Canada, Jul. 2013.

[36] E. Ciapessoni, D. Cirio, and A. Pitto, “Cascadings in large power systems: Benchmarking static vs. time domain simulation,” *in Proc. IEEE PES General Meeting—Conf. Expo*., July 2014, pp. 1–5.

[37] Carreras BA, Lynch VE, Dobson I, Newman DE, “Critical points and transitions in an electric power transmission model for cascading failure blackouts,” *Chaos*, vol. 12, no. 4, pp. 985–994, 2002.

[38] B. A. Carreras, D. E. Newman, I. Dobson, and N. S. Degala, “Validating OPA with WECC data,” *in Proc. 46th Hawaii Int. Conf. System Sciences*, Wailea, HI, Jan. 2013.

[39] S. Mei, F. He, X. Zhang, S. Wu, and G. Wang, “An improved OPA model and blackout risk assessment,” *IEEE Trans. Power Syst*., vol. 24, no. 2, pp. 814–823, May 2009.

[40] S. Mei, Y. N. Weng, G. Wang, and S. Wu, “A study of self-organized criticality of power system under cascading failures based on AC-OPA with voltage stability margin,” *IEEE Trans. Power Syst*., vol. 23, no. 4, pp. 1719–1726, Nov. 2008.

[41] J. Qi, S. Mei, and F. Liu, “Blackout model considering slow process,” *IEEE Trans. Power Syst*., vol. 28, no. 3, pp. 3274–3282, Aug. 2013.

[42] R. Yao, S. Huang, K. Sun, F. Liu, X. Zhang, and S. Mei, ‘‘A multi-timescale quasi-dynamic model for simulation of cascading outages,’’ *IEEE Trans. Power Syst*., vol. 31, no. 4, pp. 3189–3201, Jul. 2016.

[43] Reliability Coordination—Transmission Loading Relief. Standard IRO-006-4. North American Electric Reliability Corporation (NERC). Oct. 2007.

[44] M. A. Rios, D. S. Kirschen, D. Jawayeera, D. P. Nedic, and R. N. Allan, “Value of security: Modeling time-dependent phenomena and weather conditions,” *IEEE Trans Power Syst.*, vol. 17, pp. 543–548, Aug. 2002.

[45] D. P. Nedic, I. Dobson, D. S. Kirschen, B. A. Carreras, and V. E. Lynch, “Criticality in a cascading failure blackout model,” *Int. J. Elect. Power Energy Syst*., vol. 28, pp. 627–633, 2006.

[46] D. Kirschen, D. Jayaweera, D. Nedic, and R. Allan, “A probabilistic indicator of system stress,” *IEEE Trans. Power Syst*., vol. 19, no. 3, pp. 1650–1657, Aug. 2004.

[47] D. S. Kirschen, K. R. W. Bell, D. P. Nedic, D. Jayaweera, and R. N. Allan, “Computing the value of security,” *Proc. Inst. Elect. Eng. Gen. Transm. Distrib.*, vol. 150, no. 6, pp. 673–678, Nov. 2003.

[48] M. Bhavaraju and N. Nour, “TRELSS: A computer program for transmission reliability evaluation of large-scale systems,” *Electr. Power Res. Inst*., Palo Alto, CA, USA, Tech. Rep. EPRI-TR-100566, 1992.

[49] R. C. Hardiman, M. T. Kumbale, and Y. V. Makarov, “An advanced tool for analyzing multiple cascading failures,” in *Proc. 8th Int. Conf. Probability Methods Applied to Power Systems*, Ames, IA, Sep. 2004.

[50] J.-P. Paul and K. R. W. Bell, “A flexible and comprehensive approach to the assessment of large-scale power system security under uncertainty,” *Int. J. Elect. Power Energy Syst.*, vol. 26, no. 4, pp. 265–272, 2004.

[51] Van Cutsem T, Jacquemart Y, Marquet JN, Pruvot P, “A comprehensive analysis of mid-term voltage stability,” *IEEE Trans Power Syst*., vol.10, no.3, pp: 1173–1182, 1995.

[52] Blanchon G, Boukir K, Fliscounakis S, “Active-Reactive OPF using an interior point method. Application to the network management in a deregulated environment,” in *Proc. 13th CEPSI*, Oct. 2000.

[53] S. Henry, E. Bréda-Séyès, H. Lefebvre, V. Sermanson, and M. Béna, “Probabilistic study of the collapse modes of an area of the French network,” in *Proc. 9th. Int. Conf. PMAPS*, Stockholm, Sweden, Jun. 2006.

[54] P. Henneaux, P.-E. Labeau, J.-C. Maun, and L. Haarla, “A two-level probabilistic risk assessment of cascading outages,” *IEEE Trans. Power Syst*., vol. 31, no. 3, pp. 2393–2403, May 2016.

[55] P. Henneaux, J. Song, and E. Cotilla-Sanchez, “Enhancing test power systems for dynamic cascading outage simulations,” in *Proc. IEEE Conf. Technol. for Sustainability*, July 2014, pp. 107–114.

[56] J. Song, E. Cotilla-Sanchez, G. Ghanavati, and P. D. H. Hines, “Dynamic modeling of cascading failure in power systems,” *IEEE Trans. Power Syst*., vol. 31, no. 2, pp. 1360–1368, Mar. 2016.

[57] J. Song, E. Cotilla-Sanchez, and T. Brekken, “Load modeling methodologies for cascading outage simulation considering power system stability,” in *Proc. 1st IEEE Conf. Technol. Sustainability*, 2013, pp. 78–85.

[58] PowerWorld [Online]. Available: http://www.powerworld.com.

[59] M.E.J. Newman, “The structure and function of complex networks”, *SIAM Review*, vol. 45, no. 2, 2003, pp.167-256.

[60] S. Boccaletti, V. Latora, Y. Moreno, M. Chavez, D-U. Hwanga, “Complex networks: structure and dynamics,” *Physics Reports*, vol. 424, pp.175-308, 2006.

[61] S. H. Strogatz, “Exploring complex networks,” *Nature*, vol. 410, pp. 268-276, 2001.

[62] D. J. Watts, “A simple model of global cascades on random networks,” *Proc. Nat. Acad. Sci*., vol. 99, no. 9, pp. 5766–5771, 2002.

[63] A. E. Motter and Y.-C. Lai, “Cascade-based attacks on complex networks,” *Phys. Rev. E*, vol. 66, p. 065102, Dec. 2002.

[64] P. Crucitti, V. Latora, and M. Marchiori, “Model for cascading failures in complex networks,” *Phys. Rev. E*, vol. 69, p. 045104(R), 2004.

[65] D. J. Watts, Small Worlds: The Dynamics of Networks between Order and Randomness. Princeton, NJ: Princeton Univ. Press, 1999.

[66] P. Hines and S. Blumsack, “A centrality measure for electrical networks,” in *Proc. 41st Hawaii Int. Conf. Syst. Sci*., Waikoloa, HI, Jan. 2008, pp. 185–192.

[67] B. Lesieutre, S. Roy, V. Donde, and A. Pinar, “Power system extreme event screening using graph partitioning,” in *Proc. 38th North Amer. Power Symp*., 2006.

[68] S. Roy, C. Asavathiratham, B. C. Lesieutre, and G. C. Verghese, “Network models: Growth, dynamics, and failure,” in *Proc. 34th Hawaii Int. Conf. System Sciences*, Maui, HI, Jan. 2001.

[69] D. L. Pepyne, C. G. Panayiotou, C. G. Cassandras, and Y.-C. Ho, “Vulnerability assessment and allocation of protection resources in power systems,” in *Proc. Amer. Control Conf*., vol. 6, 2001, pp. 4705–4710.

[70] L. M. Shekhtman, M. M. Danziger, and S. Havlin, “Recent advances on failure and recovery in networks of networks,” *Chaos, Solitons & Fractals*, vol. 90, pp. 28–36, 2016.

[71] K. Tazi, F. Abdi and M. F. Abbou, "Review on cyber-physical security of the smart grid: Attacks and defense mechanisms," *2015 3rd International Renewable and Sustainable Energy Conference* (*IRSEC*), Marrakech, 2015, pp. 1-6.

[72] R. M. Lee, M. J. Assante, and T. Conway, “Analysis of the cyber attack on the ukrainian power grid,” in *SANS ICS and Electricity Information Sharing and Analysis Center*. Washington, DC, USA: SANS, 2016.

[73] F. Pasqualetti, F. Dörfler, and F. Bullo, “Cyber-physical attacks in power networks: Models, fundamental limitations and monitor design,” in *Proc. IEEE Conf. Decision Control and Eur. Control Conf*., Orlando, FL, USA, Dec. 2011, pp. 2195–2201.

[74] S. Sridhar, A. Hahn, and M. Govindarasu, “Cyber-physical system security for the electric power grid,” *Proc. IEEE*, vol. 99, no. 1, pp. 1–15, Jan. 2012.

[75] P. Dong, Y. Han, X. Guo, and F. Xie, “A systematic review of studies on cyber physical system security,” *International Journal of Security and Its Applications*, vol. 9, no. 1, pp. 155–164, 2015.

[76] F. Hu et al., “Robust cyber-physical systems: Concept, models, and implementation,” *Future Gener. Comput. Syst*., vol. 56, pp. 449–475, 2016.

[77] H. He and J. Yan, “Cyber-physical attacks and defences in the smart grid: A survey,” *IET Cyber-Physical Syst. Theory Appl*., vol. 1, no. 1, pp. 13–27, 2016.

[78] Rinaldi, S., J. Peerenboom, and T. Kelly, “Identifying, Understanding, and Analyzing Critical Infrastructure Interdependencies,” *IEEE Control Systems Magazine*, IEEE, December 2001, pp. 11-25.

[79] J. Gao, S. V. Buldyrev, H. E. Stanley, and S. Havlin, “Networks formed from interdependent networks,” *Nature Phys*., vol. 8, no. 1, pp. 40–48, 2011.

[80] V. Rosato, L. Issacharoff, F. Tiriticco, S. Meloni, S. Porcellinis, and R. Setola, “Modelling interdependent infrastructures using interacting dynamical models,” *International Journal of Critical Infrastructures*, vol. 4, no. 1, pp. 63–79, 2008.

[81] Buldyrev SV, Parshani R, Paul G, Stanley HE, Havlin S, “Catastrophic cascade of failures in interdependent networks,” *Nature*, vol.464, pp.1025–1028, 2010.

[82] J. Shao, S. Buldyrev, S. Havlin, and H. Stanley, “Cascade of failures in coupled network systems with multiple support-dependence relations,” *Phys. Rev. E*, vol. 83, no. 3, p. 036116, 2011.

[83] C. M. Schneider, N. A. M. Araujo, S. Havlin, and H. J. Herrmann, “Towards designing robust coupled networks,” *Minerva*, pp. 1–7, 2011.

[84] M. Parandehgheibi and E. Modiano, “Robustness of interdependent networks: The case of communication networks and the power grid,” *arXiv preprint arXiv:1304.0356*, 2013.

[85] M. Parandehgheibi, E. Modiano, and D. Hay, “Mitigating cascading failures in interdependent power grids and communication networks,” in *Proc. IEEE Int. Conf. Smart Grid Commun*., Nov. 2014, pp. 242–247.

[86] Y Wang, Z Lin, X Liang, et al, “On modeling of electrical cyber-physical systems considering cyber security,” *Frontiers of Information Technology & Electronic Engineering*, vol.17, no.5, pp.465-478, 2016.

[87] J. Wei, D. Kundur, T. Zourntos, and K. Butler-Purry, “A flocking-based dynamical systems paradigm for smart power system analysis,” in *Proc. IEEE Power Energy Soc. Gen. Meeting*, San Diego, CA, USA, Jul. 2012.

[88] W. Jin, D. Kundur, T. Zourntos, and K. L. Butler-Purry, “A Flocking Based Paradigm for Hierarchical Cyber-Physical Smart Grid Modeling and Control,” *IEEE Trans. Smart Grid*, vol. 5, no. 6, pp. 2687- 2700, 2014.

[89] M. Rahnamay-Naeini and M. M. Hayat, “Cascading failures in interdependent infrastructures: An interdependent Markov-chain approach,” *IEEE Trans. Smart Grid*, vol. 7, no. 4, pp. 1997–2006, Jul. 2016.

[90] N. Bhatt et al., “Assessing vulnerability to cascading outages,” in *Proc*. *IEEE PES Power Syst. Conf*. *Expo*., Mar. 2009, pp. 1–9.

[91] M.K. Koenig, P. Duggan, J. Wong, M.Y. Vaiman, M.M. Vaiman, M. Povolotskiy, "Prevention of Cascading Outages in Con Edison’s Network", *IEEE T & D Conference*, Apr.2010.

[92] Bajrektarevic E, Kang SW, Kotecha V, Kolluri S, Nagle M, Datta S, Papic M, Useldinger J, Patro PC, Hopkins L, Le D, “Identifying optimal remedial

actions for mitigating violations and increasing available transfer capability in planning and operations environments," *CIGRE Session*, C2–213. 2006.

[93] J. Chen, J. S. Thorp, and I. Dobson, "Cascading dynamics and mitigation assessment in power system disturbances via a hidden failure model," *Int. J. Elect. Power Energy Syst*., vol. 27, no. 4, pp. 318–326, May 2005.

[94] D. N. Kosterev, C. W. Taylor, and W. A. Mittelstadt, "Model validation for the August 10, 1996 WSCC system outage," *IEEE Trans. Power Syst*., vol. 14, no. 3, pp. 967–979, Aug. 1999.

[95] H. Guo, C. Zheng, H. H. C. Iu, and T. Fernando, "A critical review of cascading failure analysis and modeling of power system," *Renewable and Sustainable Energy Reviews*, vol. 80, pp. 9–22, 2017.

[96] P. D. Hines, I. Dobson, E. Cotilla-Sanchez, and M. Eppstein, "'Dual graph' and 'random chemistry' methods for cascading failure analysis," in *Proc. 46th HICSS*, Wailea, HI, USA, Jan. 2013, pp. 2141–2150.

[97] W. Ju, J. Qi, and K. Sun, "Simulation and analysis of cascading failures on an NPCC power system test bed", *IEEE Power and Energy Society General Meeting,* Denver CO, Jul. 2015.

[98] W. Ju, K. Sun, and J. Qi, "Multi-layer interaction graph for analysis and mitigation of cascading outages", *IEEE J. Emerg. Sel. Topics Circuits Syst*., vol. 7, No. 2, pp. 239-249, June 2017.

[99] K. Sun, K. Hur, P. Zhang, "A New Unified Scheme for Controlled Power System Separation Using Synchronized Phasor Measurements", *IEEE Trans. Power Systems*, vol. 26, pp. 1544-1554, Aug. 2011.

[100] H. Ren, I. Dobson, B. A. Carreras, "Long-term effect of the n-1 criterion on cascading line outages in an evolving power transmission grid," *IEEE Trans. Power Systems*, vol. 23, pp. 1217–1225, Aug. 2008.

[101] J. Chow, G. Rogers, "User Manual for Power System Toolbox, Version 3.0," 1991–2008.

[102] J. Shortle, S. Rebennack, and F. Glover, “Transmission-capacity expansion for minimizing blackout probabilities,” *IEEE Trans. Power Systems*, vol. 29, no. 1, pp. 43–52, Jan 2014.

[103] E. Bompard, R. Napoli, and F. Xue, “Extended topological approach for the assessment of structural vulnerability in transmission networks,” *IET Generat., Transmis. Distribut*., vol. 4, no. 6, pp. 716–724, Jun. 2010.

[104] 1996 System Disturbances, NERC, Princeton, NJ, USA, 2002.

[105] Q. Shi, F. Li, Q. Hu, Z. Wang, “Dynamic demand control for system frequency regulation: concept review, algorithm comparison, and future vision,” *Electr. Power Syst. Res*., vol. 154, pp. 75-87, Jan. 2018.

[106] H. Pulgar-Painemal, Y. Wang, H. Silva-Saravia, “On inertia distribution, inter-area oscillations and location of electronically-interfaced resources,” *IEEE Trans. Power Syst*., vol. 33, no. 1, pp. 995-1003, 2018.

[107] G. Andersson, P. Donalek, R. Farmer, et al, “Causes of the 2003 Major Grid Blackouts in North America and Europe, and Recommended Means to Improve System Dynamic Performance,” *IEEE Trans. Power Syst*., vol. 20, no. 4, pp. 1922-1928, 2005.

[108] M. Okamura, S. Hayashi, K. Uemura, et al, “A new power flow model and solution method including load and generator characteristics and effects of system control devices,” *IEEE Trans. Power Apparatus and Systems*, vol. 94, pp. 1042-1050, 1975.

[109] R. Ramanathan, “Dynamic load flow technique for power system simulators,” *IEEE Trans. Power Syst*., vol. 1, no. 3, pp.25-30, 1986.

[110] I. Roytelman, S.M. Shahidehpour, “A comprehensive long term dynamic simulation for power system recovery,” *IEEE Trans. Power Syst*., vol. 9, no. 3, pp.1427–1433, 1994.

[111] M. S. Ćalović, V. C. Strezoski, “Calculation of steady-state load flows incorporating system control effects and consumer self-regulation characteristics,” *Int. J. Elect. Power Energy Syst*., vol. 3, pp. 65-74, 1981.

[112] Y. Ping, “A fast load flow model for a dispatcher training simulator considering frequency deviation effects,” *Electr. Power Energy Syst*., vol. 20, no.3, pp.177-182, 1998.

[113] Y. Q. Hai, X. Wei, W. X. Fen, “The improvement of dynamic power flow calculation in dispatcher training simulator,” *Autom. Elect. Power Syst*., vol. 23, no. 23, pp. 20–22, 1999.

[114] D. P. Popović, “An efficient methodology for steady-state security assessment of power systems,” *Int*. *J. Elect. Power Energy Syst*., vol. 10, pp. 110-116, 1988.

[115] Y. Duan, B. Zhang, “Security risk assessment using fast probabilistic power flow considering static power-frequency characteristics of power systems”, *Electr. Power Syst. Res.*, vol. 60, pp. 53-58, 2014.

[116] X. Ye, W. Zhong, X. Song, et al, “Power system risk assessment method based on dynamic power flow,” *International Conference on Probabilistic Methods Applied to Power Systems,* 2016.

[117] P. Bei, B. Zhang, H. Li, et al, “Probabilistic dynamic load flow algorithm considering static security risk of the power system,” *International Conference on Electric Utility Deregulation and Restructuring and Power Technologies*, Changsha, China, 2015.

[118] Y. H. Liu, Z. Q. Wu, S. J. Lin, et al, “Application of the power flow calculation method to islanding microgrids,” *International Conference on Sustainable Power Generation and Supply*, Nanjing China, 2009.

[119] L. Rese, A. S. Costa, A. S. e Silva, “A modified load flow algorithm for microgrids operating in islanded mode,” *IEEE PES Conference on Innovative Smart Grid Technologies,* DC Washington, 2013.

[120] Y. Duan, B. Zhang, “An improved fast decoupled power flow model considering static power–frequency characteristic of power systems with large-scale wind power,” *IEEE Trans. Electr. Electron. Eng.*, vol. 9, no. 2, pp.151-157, 2014.

[121] S. Li, W. Zhang, Z. Wang, “Improved dynamic power flow model with DFIGs participating in frequency regulation”, *IEEE Trans. Electr. Energy Syst.,* vol. 27, pp.1-13, 2017.

[122] O.A. Mousavi, et al, “Blackouts risk evaluation by Monte Carlo Simulation regarding cascading outages and system frequency deviation”, *Electr. Power Syst. Res.*, vol. 89, pp. 157–164, 2012.

[123] O.A. Mousavi, et al, “Inter-area frequency control reserve assessment regarding dynamics of cascading outages and blackouts,” *Electr. Power Syst. Res.*, vol. 107, pp. 144–152, 2014.

[124] W. Ju, K. Sun, and R. Yao, “Simulation of cascading outages considering frequency using a dynamic power flow model”, *IEEE Access*, vol. 6 No. 1, pp. 37784-37795, Dec. 2018.

[125] M. Okamura et al., “A new power flow model and solution method—Including load and generator characteristics and effects of system control devices,” *IEEE Trans. Power App. Syst*., vol. PAS-94, no. 3, pp. 1042–1050, Nov. 1975.

[126] I. Dobson, B. A. Carreras, V. E. Lynch, and D. E. Newman, ‘‘An initial model for complex dynamics in electric power system blackouts,’’ in *Proc. 34th HICSS*, Maui, HI, USA, 2001, pp. 710–718.

[127] Automatic Underfrequency Load Shedding, Standard PRC-006-NPCC1, Feb. 2012. [Online]. Available: http://www.nerc.com/files/PRC-006- NPCC-1.pdf

[128] S. Imai and T. Yasuda, “UFLS program to ensure stable island operation,” in *Proc. IEEE PES Power Syst. Conf. Expo*., Oct. 2004, pp. 283–288.

[129] IEEE Guide for Abnormal Frequency Protection for Power Generating Plants, Standard C37.106-2003, 2004.

[130] A. G. Exposito, J. L. M. Ramos, and J. R. Santos, “Slack bus selection to minimize the system power imbalance in load-flow studies,” *IEEE Trans. Power Syst*., vol. 19, no. 2, pp. 987–995, May 2004.

[131] P. Kundur, Power System Stability and Control. New York, NY, USA: McGraw-Hill, 1994.

[132] M. Variani, S. Wang, and K. Tomsovic, ‘‘Study of flatness-based automatic generation control approach on an NPCC system model,’’ in *Proc. IEEE Power Energy Soc. General Meeting*, Denver, CO, USA, Jul. 2015, pp. 1–5.

[133] P. M. Anderson and M. Mirheydar, ‘‘A low-order system frequency response model,’’ *IEEE Trans. Power Syst*., vol. 5, no. 3, pp. 720–729, Aug. 1990.

[134] PSS/E V32 User Manual, Siemens Power Transmiss. & Distrib. Inc., Heber Springs, AR, USA, Dec. 2007.

[135] A. Melman, ‘‘Geometry and convergence of Euler’s and Halley’s methods,’’ *SIAM Rev*., vol. 39, no. 4, pp. 728–735, 1997.

[136] I. Shames, F. Farokhi, and M. Cantoni, ‘‘Guaranteed maximum power point tracking by scalar iterations with quadratic convergence rate,’’ in *Proc. IEEE 55th Conf. Decis. Control*, Las Vegas, NV, USA, Dec. 2016, pp. 2840–2845.

[137] H. Song and M. Kezunovic, “A new analysis method for early detection and prevention of cascading events,” *Electric Power Syst. Res*., vol. 77, no. 2, pp. 1132–1142, 2007.

[138] R. Baldick, B. Chowdhury, I. Dobson, Z. Dong, B. Gou, D. Hawkins, H. Huang, M. Joung, D. Kirschen, F. Li, J. Li, Z. Li, C.-C. Liu, L. Mili, S. Miller, R. Podmore, K. Schneider, K. Sun, D. Wang, Z. Wu, P. Zhang, W. Zhang, and X. Zhang, “Initial review of methods for cascading failure analysis in electric power transmission systems IEEE PES CAMS task force on understanding, prediction, mitigation and restoration of cascading failures,” in *Proc. 2008 IEEE Power and Energy Society General Meeting—* Conversion and Delivery of Electrical Energy in the 21st Century, 2008, pp. 1–8.

[139] G. Andersson, P. Donalek, R. Farmer, and N. Hatziargyriou, “Causes of the 2003 major grid blackouts in North America and Europe, and recommended

means to improve system dynamic performance," *IEEE Trans. Power Syst*., vol. 20, no. 4, pp. 1922–1928, Nov. 2005.

[140] P. Kundur, C. Taylor, "Blackout experiences and lessons, best practices for system dynamic performance, and the role of new technologies," IEEE Task Force Report, 2007.

[141] V. E. Henner, "A network separation scheme for emergency control," *Int. J. Elect. Power Energy Syst*., vol. 2, no. 2, pp. 109–114, 1980.

[142] M. M. Adibi et al., "On power system controlled separation," *IEEE Trans. Power Syst*., vol. 21, no. 4, pp. 1894–1902, Nov. 2006.

[143] H. You, V. Vittal, and Z. Yang, "Self-healing in power systems: An approach using islanding and rate of frequency decline based load shedding," *IEEE Trans. Power Syst*., vol. 18, no. 1, pp. 174–181, Feb. 2003.

[144] K. Sun, D. Zheng, and Q. Lu, "Splitting strategies for islanding operation of large-scale power systems using OBDD-based methods," *IEEE Trans. Power Syst*., vol. 18, no. 2, pp. 912–922, May 2003.

[145] Q. Zhao et al., "A study of system splitting strategies for island operation of power system: A two-phase method based on OBDDs," *IEEE Trans. Power Syst*., vol. 18, no. 4, pp. 1556–1565, Nov. 2003.

[146] H. You, V. Vittal, and X. Wang, "Slow coherency based islanding," *IEEE Trans. Power Syst*., vol. 19, no. 1, pp. 483–491, Feb. 2004.

[147] G. Xu and V. Vittal, "Slow coherency based cutset determination algorithm for large power systems," *IEEE Trans. Power Syst*., vol. 25, no. 2, pp. 877–884, May 2010.

[148] C. Wang, B. Zhang, Z. Hao, J. Shu, P. Li, and Z. Bo, "A novel real-time searching method for power system splitting boundary," *IEEE Trans. Power Syst*., vol. 25, no. 4, pp. 1902–1909, Nov. 2010.

[149] K. Sun, D. Zheng, and Q. Lu, "A simulation study of OBDD-based proper splitting strategies for power systems under consideration of transient stability," *IEEE Trans. Power Syst*., vol. 20, no. 1, pp. 389–399, Feb. 2005.

[150] L. Hao, G. W. Rosenwald, J. Jung, C. C. Liu, "Strategic Power Infrastructure Defense," *Proceedings of the IEEE*, vol. 93, no.5, pp. 918-933, May 2005.

[151] L. Ding, F. M. Gonzalez-Longatt, P. Wall, and V. Terzija, “Two-step spectral clustering controlled islanding algorithm,” *IEEE Trans. Power Syst*., vol. 28, no. 1, pp. 75–84, Feb. 2013.

[152] J.Machowski, J.W. Bialek, J.R. Bumby, “Power system dynamics stability and control,” John Wiley & Sons, 2008.

[153] A. Peiravi and R. Ildarabadi, “Comparison of computational requirements for spectral and kernel k-means bisection of power system,” *Australian J. Basic Appl. Sci*., vol. 3, no. 3, pp. 2366–2388, 2009.

[154] T. Leighton, S. Rao, “Multicommodity max-flow min-cut theorems and their use in designing approximation algorithms,” *J. ACM*, vol.46, no.6, pp. 787-832,1999,

[155] J. Hartmanis, “Computers and intractability: A guide to the theory of NP-completeness, book review,” *SIAM Rev*., vol. 24, no. 1, pp. 90–91, 1982.

[156] U. von Luxburg, “A Tutorial on Spectral Clustering,” *Statistics and Computing*, vol. 17, pp. 395-416, 2007.

APPENDIX

Publications during Ph.D. Study

Journey Papers

[J1] **W. Ju**, K. Sun, “Critical component-based active islanding for reducing cascading outage risk”, in progress.

[J2] **W. Ju**, K. Sun, “Review on modeling and simulation of cascading outages”, in progress.

[J3] **W. Ju**, K. Sun, and R. Yao, “Simulation of cascading outages considering frequency using a dynamic power flow model”, *IEEE Access*, vol. 6 No. 1, pp. 37784-37795, Dec. 2018.

[J4] **W. Ju**, K. Sun, and J. Qi, “Multi-layer interaction graph for analysis and mitigation of cascading outages”, *IEEE J. Emerg. Sel. Topics Circuits Syst*., vol. 7, No. 2, pp. 239-249, June 2017.

[J5] J. Qi, **W. Ju**, and K. Sun, “Estimating the propagation of interdependent cascading outages with multi-type branching processes”, *IEEE Trans. Power Systems*, vol. 32, No. 2, pp. 1212-1223, March 2017.

[J6] C Liu, K. Sun, B. Wang, **W. Ju**, “Probabilistic power flow analysis using multi-dimensional holomorphic embedding and generalized cumulants,” *IEEE Transactions on Power Systems*, in press.

[J7] Q. Shi, H. Cui, F. Li, Y. Liu, **W. Ju**, and Y. Sun, “A hybrid dynamic demand control strategy for power system frequency regulation,” *CSEE J. Power Energy Syst*., vol. 3, no. 2, pp. 176-185, Jun. 2017.

Conference Papers

[C1] **W. Ju**, B. Wang, and K. Sun, “Can nonlinear electromechanical oscillation be analyzed using an equivalent SMIB system?”, *IEEE Power and Energy Society General Meeting*, Chicago, Jul. 2017.

[C2] **W. Ju**, J. Qi, and K. Sun, “Simulation and analysis of cascading failures on an NPCC power system test bed”, *IEEE Power and Energy Society General Meeting,* Denver CO, Jul. 2015.

[C3] **W. Ju**, Y. Wang, A. D. Rosso, “Average wavelet energy-based method for fault classification in transmission lines”, *IEEE Innovative Smart Grid Technology*, Washington D.C, 2019, submitted.

VITA

Wenyun Ju, was born in Wuhu, Anhui Province in China on Dec. 28th, 1988. He received his B.S. degree and M.S. degree in Electrical Engineering from Sichuan University, Chengdu, China in Jun. 2010 and Huazhong University of Science and Technology, Wuhan, China in Mar. 2013. He is currently working toward his Ph.D in the Department of EECS at the University of Tennessee, Knoxville. His research interest is modeling and simulation of cascading outages in power systems.